VOLUME 30 NOVEMBER 1952 NUMBER 6

Canadian Journal of Physics

Editor: G. M. VOLKOFF

Published by THE NATIONAL RESEARCH COUNCIL
OTTAWA CANADA

CANADIAN JOURNAL OF PHYSICS

(*Formerly Section A, Canadian Journal of Research*)

The CANADIAN JOURNAL OF PHYSICS is published bimonthly by the National Research Council of Canada under the authority of the Chairman of the Committee of the Privy Council on Scientific and Industrial Research. Matters of general policy are the responsibility of a joint Editorial Board consisting of members of the National Research Council of Canada and the Royal Society of Canada.

The National Research Council of Canada publishes also: *Canadian Journal of Botany, Canadian Journal of Chemistry, Canadian Journal of Medical Sciences, Canadian Journal of Technology, Canadian Journal of Zoology.*

EDITORIAL BOARD

Representing
NATIONAL RESEARCH COUNCIL

DR. J. H. L. JOHNSTONE (*Chairman*),
Professor of Physics,
Dalhousie University,
Halifax, N.S.

DR. OTTO MAASS,
Macdonald Professor of
Physical Chemistry,
McGill University,
Montreal, P.Q.

DR. CHARLES W. ARGUE,
Dean of Science,
University of New Brunswick,
Fredericton, N.B.

DR. A. G. MCCALLA,
Dean, Faculty of Agriculture,
University of Alberta,
Edmonton, Alta.

Representing
ROYAL SOCIETY OF CANADA

DR. G. M. VOLKOFF,
Professor of Physics,
University of British Columbia,
Vancouver, B.C.

DR. T. THORVALDSON,
Dean Emeritus of Graduate
Studies,
University of Saskatchewan,
Saskatoon, Sask.

Section III

DR. D. L. BAILEY,
Department of Botany,
University of Toronto,
Toronto, Ont.

DR. E. HORNE CRAIGIE,
Department of Zoology,
University of Toronto,
Toronto, Ont.

Section V

Ex officio

DR. LÉO MARION, *Editor-in-Chief*,
Director, Division of Pure Chemistry,
National Research Laboratories,
Ottawa.

DR. H. H. SAUNDERSON,
Director, Division of Information Services,
National Research Council,
Ottawa.

Representing
THE CHEMICAL INSTITUTE OF CANADA

DR. H. G. THODE,
Department of Chemistry,
McMaster University,
Hamilton, Ont.

THE CANADIAN ASSOCIATION OF PHYSICISTS

DR. G. M. VOLKOFF,
Professor of Physics,
University of British Columbia,
Vancouver, B.C.

Manuscripts should be addressed to:

DR. LÉO MARION,
Editor-in-Chief,
Canadian Journal of Physics,
National Research Council,
Ottawa, Canada.

Each manuscript should be typewritten, double-spaced, and the original and one extra copy submitted (see **Notice to Contributors**, inside of back cover).

Subscription, renewals, and orders for back numbers should be addressed to:

Administrative Services,
National Research Council,
Ottawa, Canada.

Subscription rate: $3.00 a year; single numbers: 50 cents. Special rates can be obtained for subscriptions to more than one of the Journals published by the National Research Council.

Canadian Journal of Physics

Issued by THE NATIONAL RESEARCH COUNCIL OF CANADA

VOLUME 30 NOVEMBER, 1952 NUMBER 6

MODIFIED BRIDGE METHOD FOR ABSOLUTE DETERMINATION OF OHM[1]

BY M. ROMANOWSKI

ABSTRACT

The principal characteristics of Campbell's original bridge for the determination of the ohm (in terms of mutual inductance and time) and of Picard's modification to the bridge are examined. Two other networks for the same measurement are found possible by rearranging components. One arrangement in particular offers advantages over previous methods and was built in an experimental form. In it all important circuit elements are constructed of manganin, rendering the bridge less subject to temperature effects, and no determination of self-inductance is necessary. The new bridge does require a mutual inductance equal to twice the value of the standard. A brief outline of the method for resolving this point is given as part of a more general work under way on the scale of inductance.

While the theory of electrical units was gradually being formulated by the physicists of the previous century, a great number of experimental methods were proposed for the absolute determination of the unit of resistance (2). Most of them are of purely historical interest. Four are considered as satisfactory from a high precision standpoint. Our present knowledge of the ohm is based on these four methods (3). The contribution of Albert Campbell in the field of absolute measurements was particularly important. He proposed a bridge by means of which resistance is expressed in terms of mutual inductance and time, and he also designed a type of mutual inductor (1) which, after several decades of experimentation in different countries, is now considered as the most precise type of standard of inductance, the value of which is deducible from its dimensions.

M. Picard, in 1929, proposed a modification (6) which eliminates the resistance of a copper circuit from the equations of the bridge, but introduces into the sequence of experimental operations the difficulty of directly comparing a mutual and a self-inductance. The Picard bridge was used by the Laboratoire Central d'Electricité in 1938 and is an interesting step towards the improvement of the original method (5). A re-examination of both methods was made last year as a part of the program of the work of the Electricity laboratory in the field of absolute units. It showed that two other arrangements of conductors are possible, which circumvent the troublesome points encountered by previous experimenters, but require two different values of mutual inductance. This question had already been examined and the building of several secondaries for

[1]*Manuscript received May 28, 1952.*
Contribution from the Division of Physics, National Research Council, Ottawa, Canada. Issued as N.R.C. No. 2842.

the same primary had been considered for the purpose of solving the problem of scaling of inductances.

The original Campbell network is represented in Fig. 1 where R_3 is the total resistance and L the self-inductance of the closed circuit composed of R_1 and the two windings, S_1 and P_2, in series with R_1. For zero current in the galvanometer (note p. 636)

$$R_2R_3 = \omega^2 M_1M_2, \tag{1a}$$

$$L\,R_2 = M_1R_1. \tag{1b}$$

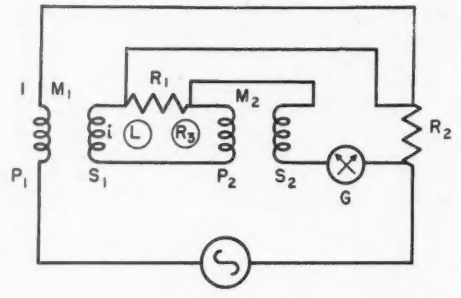

FIG. 1.

It is obvious that M_1 and M_2 can be made equal, which simplifies the practical features of the network.

As the resistance R_3 must be kept very low, it was found impossible to construct it entirely of manganin and, in the National Physical Laboratory's bridge, an important part of this resistance has been made of copper (3 *b*, p. 442). Special precautions have to be taken to maintain R_3 at a constant temperature, but it is difficult to obtain the conditions corresponding to the required precision, the temperature coefficient of copper being about 4×10^{-3}, while for manganin it rarely exceeds 20×10^{-6}.

Picard eliminated R_3, by transferring the galvanometer into the copper circuit as shown in Fig. 2. The balance conditions for this network are:

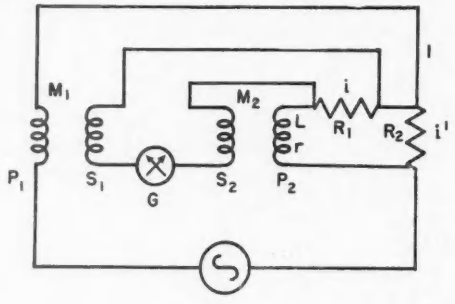

FIG. 2.

$$R_1R_2 = -\omega^2 M_1 L, \tag{2a}$$

$$(R_1 + R_2 + r)\, M_1 = -M_2R_2. \tag{2b}$$

The working equation (2*a*) contains only two resistances R_1 and R_2 which, in the Laboratoire Central d'Electricité bridge, were of the four-terminal standard resistor type made of manganin. The self-inductance L of the primary P_2 (in equation 2*a*) has to be determined by one of the elaborate methods used for comparing a self with a mutual inductance. These methods have also been considered in the Electricity laboratory and eventually it is hoped to extend the scale of mutual inductances into the field of self-inductance using the Maxwell method, rather than the method of Rowland which was preferred by the Laboratoire Central d'Electricité physicists. These methods are almost equivalent and are both very delicate operations.

As may be seen from Fig. 3, the electromotive forces E_1 and E_2, induced in M_1 and M_2 respectively, are not exactly opposed to one another owing to the

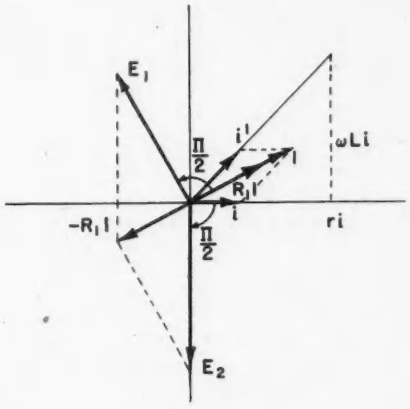

FIG. 3.

angle between the vectors i and I. The sum $E_1 + E_2$ has to be counterbalanced by a vector which may be produced by any of the three currents: i (as used by Picard); i'; or I. The latter cases, which are herein investigated, are shown in Fig. 4 and Fig. 5. The bridge utilizing I (Fig. 3 and Fig. 4) was selected for an experimental realization. The balance equations of this bridge are:

$$R_1 (R_2 + r) = -\omega^2 M_1 L, \tag{3a}$$

$$R_1 L - R_2(M_1 + M_2) - r M_1 = 0. \tag{3b}$$

They differ from (1) and (2) by the fact that L is contained in both of them. It may therefore be eliminated, thus avoiding the delicate experimental operation mentioned above.

The bridge using i' (Fig. 5) leads to the same type of equations.

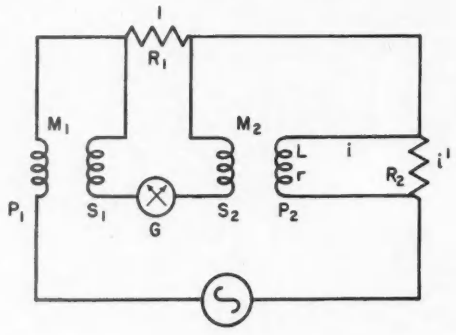

FIG. 4.

The equations (3*a*,*b*) show that M_1 is negative, and that M_2 has to be positive and arithmetically greater than M_1. If we realize the nominal relation

$$M_2 = -2M_1, \tag{4}$$

then

$$R_1^2 \frac{R_2 + r}{R_2 - r} = \omega^2 M_1^2, \tag{5}$$

$$L = \frac{-M_1}{R_1}(R_2 - r). \tag{6}$$

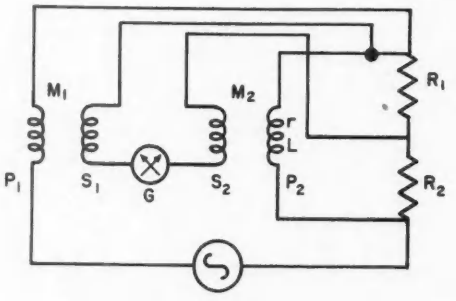

FIG. 5.

The problem which remains is that of determining the exact ratio M_2/M_1. This is accomplished by building two interchangeable secondaries to be used with the same primary of the standard inductor: one of 457 turns and one of 914 turns. The corresponding values of calculated mutual inductance are 10 and 20 mH. (nominal values).

The magnitude of the components being more or less arbitrary, it is possible to give them certain convenient experimental values. In the bridge now under construction, R_1 is a one ohm resistor and will be considered as the "resistor

under test." M_1 is a 10 mH. inductor and M_2 is a 20 mH. inductor. They are calibrated against the corresponding calculated values of the standard.

The frequency of the alternating current of 100 cycles per second, which has been considered as suitable by previous experimenters, will also be adopted for this bridge.

When all these numerical data are taken into account, the equations of the bridge become

$$R_2 = 1.052\, r, \tag{7a}$$

$$\mathrm{L} = 0.00052\, r. \tag{7b}$$

The practical problem is to satisfy equation (7*b*) by an actual coil; preliminary calculations showed that it may be done by using No. 12 B.S. gauge manganin wire. Making r equal to 25 ohms, and using Maxwell's design (Glazebrook Dict. II, p. 417), we find by (7*b*) that L should be equal to 13 mH., the total length of the manganin wire being then 556 ft.

Before the final coil was made of manganin wire (which is not as easily obtainable as copper wire), an experimental coil, of the same gauge copper wire, was wound on a wooden form. The length of the wire was 470 ft. The remaining 86 ft. were used to wind two small coils which, in series with the main coil, brought the total inductance to the required value of 13 mH. The axis of the small coils was perpendicular to the axis of the main coil which is also the axis of the secondary M_2. The mutual inductance between the small coils provided a fine control of L, with almost no effect on M_2. L is considered as one of the adjustable components of the bridge, the other (resistive) is R_2, made adjustable by means of a shunt.

A secondary was then wound over the primary and, by means of a coaxial movable coil, made adjustable to 20 mH.

Using resistance boxes for R_1 and R_2, an experimental model of the Campbell Inductor for M_1, the described inductor for M_2, it was easy to form a bridge, with an oscilloscope as detector (G). The bridge was a check of the method and of the order of magnitude of the components of the network when balance conditions are obtained. It also verified the computed values for the arms of a Wagner ground, without which an alternating current bridge loses most of its high precision characteristics.

The manganin inductor M_2, which was recently completed and checked with the same bridge, is very similar to the experimental copper inductor. It is wound on bakelite forms and kept in a temperature controlled oil bath.

It was mentioned above that the building of a 20 mH. standard inductor, against which M_2 will be compared, is considered as a part of a more general work on the scale of inductances. The calculated 20 mH. value may be checked experimentally against the calculated 10 mH. This check is made by means of a marble replica of the standard inductor equipped with two equal secondaries of intermediate number of turns (722). These secondaries are placed on either side of the plane of the neutral circle and their position is adjusted until the

actual mutual inductance between the primary and each of them is equal to the value of the standard equipped with the smaller secondary (457). Then they are connected in series and measured against the standard equipped with the larger secondary (914). This procedure is being extended by means of a specially built instrument to give complete decades of mutual inductance.

The bridge described in this paper is being used to determine the absolute value of the ohm in terms of our primary standard of mutual inductance and frequency, and the results will be published later.

NOTE

The convention regarding sign of the mutual inductance is given by

$$E = -j\omega M I$$

as used in many standard texts (4). M is then taken as positive if E lags by $\pi/2$ behind I and negative if E is leading by $\pi/2$.

REFERENCES

1. CAMPBELL, A. Proc. Roy. Soc. (London), A, 79: 428. 1907.
2. CURTIS, H. L. (*a*) Electrical measurements. McGraw-Hill Book Company, Inc., New York and London. 1937. p. 171.
   (*b*) J. Wash. Acad. Sci. 32 (No. 2): 40. 1942.
3. (*a*) CURTIS, H. L., MOON, C., and SPARKS, C. M. J. Research Natl. Bur. Standards, 21: 375. 1938. (Method of Grüneisen and Giebe.)
   (*b*) HARTSHORN, L. and ASTBURY, N. F. Trans. Roy. Soc. (London), A, 236: 423. 1937. (Method of A. Campbell.)
   (*c*) VIGOUREUX, P. Natl. Phys. Lab. Collected Researches, 24: 209. 1936. (Method of Lorenz.)
   (*d*) THOMAS, J. L., PETERSON, C., COOTER, I. L., and KOTTER, F. R. J. Research Natl. Bur. Standards, 43: 291. 1949. (Method of Wenner.)
4. HAGUE, A. Alternating current bridge methods. 5th ed. Pitman Publishing Corporation, New York. 1930. p. 414.
5. JOUAUST, R., PICARD, M., and HÉROU, R. Bull. soc. franç. élec., 5th Series, t. VIII, No. 91. 1938.
6. PICARD, M. Compt. rend. 189: 125. 1929.

A MASS SPECTROGRAPHIC DETERMINATION OF THE DECAY ENERGIES OF Rh^{102} AND Rh^{104} [1]

BY BENJAMIN G. HOGG[2] AND HENRY E. DUCKWORTH

ABSTRACT

Mass spectrographic measurements are reported of the following mass differences: $\frac{1}{2}Pb^{204}$–Ru^{102}, $\frac{1}{2}Pb^{204}$–Pd^{102}, $\frac{1}{2}Pb^{206}$–Rh^{103}, $\frac{1}{2}Pb^{208}$–Ru^{104}, and $\frac{1}{2}Pb^{208}$–Pd^{104}. These results are combined with existing transmutation data to obtain the energies available for the disintegrations $Rh^{102} \rightarrow Ru^{102}$, $Rh^{102} \rightarrow Pd^{102}$, $Rh^{104} \rightarrow Pd^{104}$, and $Rh^{104} \rightarrow Ru^{104}$. In the first three cases the energy values are in substantial agreement with those found by beta-ray spectroscopy. The final disintegration, namely, $Rh^{104} \rightarrow Ru^{104}$, is found to possess enough energy for appreciable K-capture and a lesser degree of positron activity. These activities have not yet been observed. Atomic masses are given for Ru^{102}, Pd^{102}, Rh^{103}, Ru^{104}, and Pd^{104}.

I. INTRODUCTION

It is possible by supplementing transmutation data with mass spectrographic mass comparisons to obtain the energies available for the decay of certain radioactive nuclides. This paper will describe mass spectrographic work of this type which leads to values for the total decay energies of Rh^{102} and Rh^{104}.

II. EXPERIMENTAL

The scheme of the experiment is shown in Fig. 1. Here the central character is the single stable isotope of rhodium, Rh^{103}. Since the Q of the $Rh^{103}(d,p)$

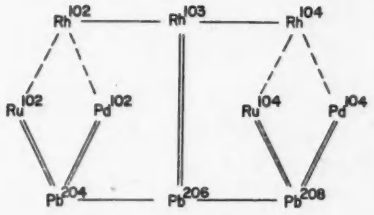

FIG. 1. Scheme of this experiment. The single solid lines represent mass differences known from transmutation studies. The double solid lines indicate mass spectrographic mass comparisons reported in this paper. The dotted lines show decay energies which have been computed on the basis of the transmutation and mass spectrographic data.

Rh^{104} (4) and the threshold of the $Rh^{103}(\gamma,n)Rh^{102}$ reactions (11) have been measured, one knows the Rh^{103}–Rh^{102} and Rh^{104}–Rh^{103} mass differences. Furthermore, as a result of the special interest in reaction energies in the region of the 126-neutron shell, the Pb^{206}–Pb^{204} and Pb^{208}–Pb^{206} mass differences are known to high accuracy (4, 8, 10, 14). Mass spectroscopy can contribute to the

[1] *Manuscript received June 23, 1952.*
Contribution from the Department of Physics, McMaster University, Hamilton, Ont.
[2] *Holder of a National Research Council of Canada Fellowship.*

picture by photographing the five doublets* Pb^{204}–Ru^{102}, Pb^{204}–Pd^{102}, Pb^{206}–Rh^{103}, Pb^{208}–Ru^{104}, and Pb^{208}–Pd^{104}. From these photographs the doublet spacings can be measured and the corresponding mass differences computed. The Rh^{102} and Rh^{104} decay energies then follow directly and can be compared with those obtained by beta-ray spectroscopy.

The mass comparisons described in this paper were made using a Dempster-type double-focusing mass spectrograph (2) with a resolving power of one part in 7000. The ion source consisted of a high-frequency vacuum spark between metallic electrodes, the electrodes consisting in part of the nuclides to be mass-compared. Such a source produces not only singly-charged, but also an abundant supply of multiply-charged ions and is, therefore, very useful in the study of mass spectrographic doublets.

In these experiments one electrode was a hollow brass cylinder while the second was a coaxial thin-walled nickel tube which fitted within the cylinder with a clearance of a few thousandths of an inch. The spark occurred across this narrow gap. The metals required for any particular doublet were mixed in powdered form and packed into the nickel tube, where they became active elements of the electrode as the thin wall of the nickel tube was eaten away in the spark. The two members of the doublet were matched in intensity by adjusting the composition of the mixture.

III. MASS DIFFERENCES

The mass differences obtained for the five doublets are tabulated in Table I. The precision of the first two measurements leaves something to be desired. The lack of accuracy was caused in part by the low abundance of Pb^{204}(1.4%) and Pd^{102}(0.8%), resulting in the need for longer exposures and wider collimating slits.

TABLE I

MASS SPECTROGRAPHICALLY MEASURED MASS DIFFERENCES

Nuclides	Mass difference in mMU
$\frac{1}{2}Pb^{204}$–Ru^{102}	82.44 ± 30
$\frac{1}{2}Pb^{204}$–Pd^{102}	81.03 ± 40
$\frac{1}{2}Pb^{206}$–Rh^{103}	81.76 ± 10
$\frac{1}{2}Pb^{208}$–Ru^{104}	82.83 ± 15
$\frac{1}{2}Pb^{208}$–Pd^{104}	83.77 ± 10

IV. DECAY ENERGIES FOR Rh^{102}

The $\frac{1}{2}Pb^{204}$–Ru^{102}, $\frac{1}{2}Pb^{204}$–Pd^{102}, and $\frac{1}{2}Pb^{206}$–Rh^{103} mass differences have been combined with the $Rh^{103}(\gamma,n)Rh^{102}$ threshold (11) and the known Pb^{206}–Pb^{204}

**A doublet, it will be recalled, is a pair of mass spectral lines produced by two species of ions whose e/m values are almost, but not quite, equal. Thus, for example, a doubly-charged ion, which appears on a mass spectrum at a position corresponding to one-half its mass, will frequently form a doublet with a lighter singly-charged ion.*

mass difference (14), as shown in Fig. 2, to obtain the energies available for the decay of Rh^{102}. The values so obtained are 2.57 ± 0.4 Mev. (0.00276 ± 38 AMU) for the $Rh^{102} \rightarrow Ru^{102}$ decay, and 1.26 ± 0.45 Mev. (0.00135 ± 46 AMU) for the $Rh^{102} \rightarrow Pd^{102}$ decay.

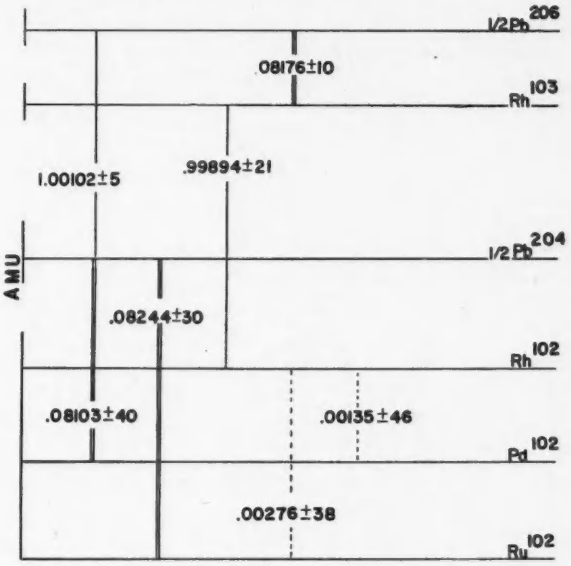

FIG. 2. Energetics at mass number 102. Single solid lines represent transmutation data, double solid lines represent mass spectrographic data, and dotted lines show computed decay energies for Rh^{102}.

The Rh^{102}–Ru^{102} energy difference has been found from beta-ray spectroscopy to be 2.32 Mev. and 2.15 Mev. by Sullivan, Sleight, and Gladrow (13), and by Hole (6), respectively. These two values yield an average of 2.24 Mev., which is 0.33 Mev. lower than that calculated from the combination of mass spectrographic and transmutation data.

The $Rh^{102} \rightarrow Pd^{102}$ decay has also been studied by Hole (6) who found a total decay energy of 1.04 Mev., a figure 0.22 lower than the deduced one.

We feel that it is significant that both deduced decay energies are larger, by roughly the same amount, than the directly measured values. This we regard as a basis for assuming that the $\frac{1}{2}Pb^{204}$–Ru^{102} and $\frac{1}{2}Pb^{204}$–Pd^{102} mass differences, despite their rather large error, are substantially correct, and that there is an error of 0.25–0.30 Mev. elsewhere in the cycle shown in Fig. 2, in particular, in the $\frac{1}{2}Pb^{206}$–Rh^{103} measurement, or in the determination of the $Rh^{103}(\gamma,n)Rh^{102}$ threshold. If it is the former value which is in error, the measured value is too small, while if the latter is the culprit, the measured threshold is too large. An argument will be given below which suggests that the blame can be laid to the threshold measurement.

V. DECAY ENERGIES FOR Rh^{104}

The energy diagram at mass number 104 is shown in Fig. 3. The energies deduced for the $Rh^{104} \rightarrow Ru^{104}$ and $Rh^{104} \rightarrow Pd^{104}$ decays are 1.24 ± 0.3 Mev. (0.00133 ± 29 AMU) and 2.11 ± 0.2 Mev. (0.00227 ± 25 AMU), respectively. No activity corresponding to the former transition has been observed. The latter figure is to be compared with directly determined values of 2.58 Mev., 2.46 Mev., and 2.3 Mev. obtained by Hole (7), Moore (9), and Crittenden (1), respectively. These values average to 2.45 Mev., which is 0.34 larger than the figure deduced from mass spectrographic and transmutation data.

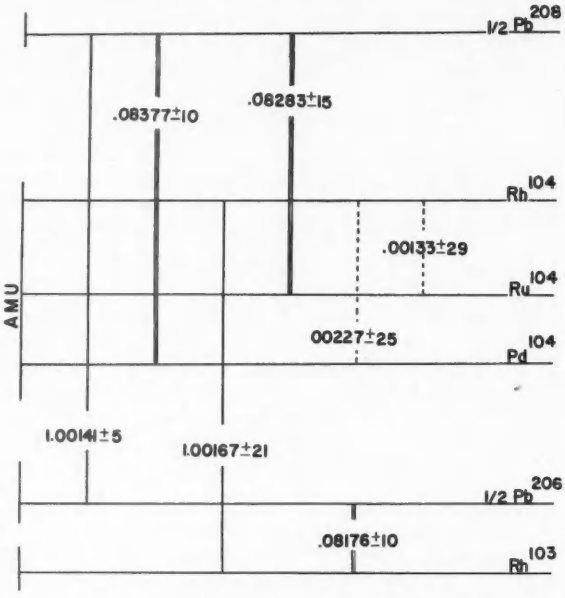

FIG. 3. Energetics at mass number 104. Single solid lines represent transmutation data, double solid lines represent mass spectrographic data, and dotted lines show computed decay energies for Rh^{104}.

If we assume, as was done at mass number 102, that the discrepancy is caused by an error in either the $\frac{1}{2}Pb^{206}$–Rh^{103} mass difference, or in the determination of the Q of the $Rh^{103}(d,p)Rh^{104}$ reaction, this requires that the measured value for the one or the other be too large by 0.34 Mev. Since the $\frac{1}{2}Pb^{206}$–Rh^{103} mass difference was required to be 0.28 Mev. *too small* in order to remove the discrepancy at mass 102, and *too large* by 0.34 Mev. to remove the discrepancy at mass 102, we conclude that it is substantially correct, as is. In this way the onus is laid, by default, on the $Rh^{103}(\gamma,n,)$ and $Rh^{103}(d,p)$ measurements.

We have discussed the $Rh^{103}(d,p)$ work with Dr. J. A. Harvey, who performed it, and he has commented that the rhodium target which he used in his experi-

ment was rather thick, with the result that the ground state peak was not well resolved from excited levels. He feels that it is quite possible (5) that the Q could be 0.2–0.3 Mev. lower than his published value of 4.58 ± 0.2 Mev.

The third alternative which could remove the 0.34 Mev. discrepancy at mass number 104 is that the $\frac{1}{2}Pb^{208}$–Pd^{104} mass difference is in error. We feel that this is the least likely of the three alternatives. It will be noted that we assume throughout that the Pb^{208}–Pb^{206} and the Pb^{206}–Pb^{204} mass differences are above suspicion.

Since a correction of approximately 0.3 Mev. (corresponding to the postulated error in the $Rh^{103}(d,p)Rh^{104}$) must be added to the deduced figure of 2.11 Mev. for the $Rh^{104} \rightarrow Pd^{104}$ decay energy, it must similarly be added to the value of 1.3 Mev. deduced for the $Rh^{104} \rightarrow Ru^{104}$ transition. This gives $\backsim$ 1.6 Mev. available for the latter mode of decay and suggests, according to the curves of Feenberg and Trigg (3), that Rh^{104} should decay as follows: β^-(95%), K-capture (4%), and β^+(1%). As mentioned above, these latter two modes of decay have not yet been observed and, apparently, no serious search has been made for them.

VI. MASS VALUES

The mass of Pb^{208} has recently been determined in this laboratory. Using this value (12), plus the values in Table I and the proper Pb^{208}–Pb^{206} and Pb^{206}–Pb^{204} mass differences, masses have been computed for Ru^{102}, Pd^{102}, Rh^{103}, Ru^{104}, and Pd^{104}. These are shown in Table II.

TABLE II

NEW ATOMIC MASS VALUES

	Atomic mass value in AMU
Ru^{102}	101.9359 ± 6
Pd^{102}	101.9373 ± 6
Rh^{103}	102.9376 ± 5
Ru^{104}	103.9380 ± 5
Pd^{104}	103.9370 ± 5

VII. SUMMARY

The results of this investigation are summarized as follows:

(*a*) The $Rh^{103}(\gamma,n)Rh^{102}$ threshold and the Q of the $Rh^{103}(d,p)Rh^{104}$ reaction are likely both too high by 0.2–0.3 Mev.

(*b*) The known β^+ and β^- groups (that is, with end points of 1.24 Mev. and 1.04 Mev., respectively) represent the total energies available for the two modes of decay of Rh^{102}.

(*c*) The known β^- group (end point $\backsim$ 2.45 Mev.) represents the total Rh^{104} – Pd^{104} energy difference.

(*d*) There is a strong likelihood that Rh^{104} decays to Ru^{104} by both *K*-capture and positron-emission, the former being several times more probable than the latter.

VIII. ACKNOWLEDGMENTS

We have been helped during the course of these experiments by communications from Dr. J. A. Harvey, Dr. N. Hole, Dr. L. G. Elliott, and Dr. B. B. Kinsey. We have also enjoyed many enlightening discussions with Dr. M. W. Johns.

It is a pleasure to acknowledge the generous support of this work by the National Research Council of Canada and the Research Council of Ontario.

REFERENCES

1. CRITTENDEN, E. C. Phys. Rev. 56: 709. 1939.
2. DUCKWORTH, H. E. Rev. Sci. Instruments, 21: 54. 1950.
3. FEENBERG, E. and TRIGG, G. Revs. Modern Phys. 22: 399. 1950.
4. HARVEY, J. A. Phys. Rev. 81: 353. 1951.
5. HARVEY, J. A. Private communication, March 7, 1952.
6. HOLE, N. Arkiv Mat. Astron. Fysik, 32A, No. 3: 1. 1945.
7. HOLE, N. Arkiv Mat. Astron. Fysik, 34B, No. 5: 1. 1947.
8. KINSEY, B. B., BARTHOLOMEW, G. A., and WALKER, W. H. Phys. Rev. 82: 380. 1951.
9. MOORE, B. L. Phys. Rev. 57: 355. 1940.
10. PALEVSKY, H. and HANSON, A. O. Phys. Rev. 79: 242. 1950.
11. SHER, R., HALPERN, J., and MANN, A. K. Phys. Rev. 84: 387. 1951.
12. STANFORD, G. S., DUCKWORTH, H. E., HOGG, B. G., and GEIGER, J. S. Phys. Rev. 85: 1039. 1952.
13. SULLIVAN, W. H., SLEIGHT, N. R., and GLADROW, E. M. *Quoted in* Nuclear data: Circular of the National Bureau of Standards 499, September 1, 1950.
14. WAY, K. and WOOD, M. Phys. Rev. 86: 608. 1952.

THE NEW RADIOACTIVE ISOTOPES VANADIUM 46, MANGANESE 50, COBALT 54[1]

By W. M. Martin[2] and S. W. Breckon

ABSTRACT

Three new positron activities assigned to V^{46} (0.40 sec.; $E_{max} > 6.0$ Mev.), Mn^{50} (0.28 sec.; $E_{max} > 6.3$ Mev.), and Co^{54} (0.18 sec.; $E_{max} > 7.4$ Mev.) have been induced by (p,n) reactions which take place in the McGill cyclotron at thresholds less than 12.5 Mev. The assignments are based on the thresholds and on the approximate *ft* values of the transitions.

After a brief period of bombardment, controlled through the oscillator, the targets are shot back by a pneumatic extractor to a position of minimum magnetic field near the cyclotron where a suitably shielded anthracene counter system sends pulses to the main laboratory. Finally, the output of a counting-rate meter is displayed against time on an oscilloscope. This visual display reveals immediately new periods in decays, which are then photographed for later analysis.

INTRODUCTION

As part of the isotope research program instituted by Professor Foster at the Radiation Laboratory, it was initially intended to develop only a survey method for the easy detection of new isotopes of very short life. Having in mind the possibility of extending the series of odd–even positron emitters known from N^{13} to Sc^{41}, it was decided through extrapolation that the method should handle the particular range of half-lives from 0.2–10 sec. Through attention to details, the ultimate display of counting-rate meter output on a cathode-ray tube has in practice yielded somewhat more precise information than was at first expected, and has permitted not only the detection but also the accurate measurement of periods and the highly probable assignment of the new isotopes. Incidentally, these do not in fact represent an extension of the above series, but are odd–odd positron emitters each containing one neutron more than the corresponding members in the proposed extension.

EXPERIMENTAL METHOD

In this work it is essential to induce in the target an activity which, at the beginning of the counting interval, is as intense and as pure as possible. To this end, a scintillation counter, a wide-band amplifier, and a high-resolution prescaler have been used in order to handle intense activities satisfactorily. To reduce to one-quarter second the delay between bombardment and counting, a pneumatic target extractor is employed. Backgrounds are kept low by carefully controlling the bombardment time (which should not exceed three half-lives), and by using fresh targets as long-lived background builds up. Matthey "H.S." Brand materials are used to keep the activities as pure as possible.

A direct and immediate indication of the short activities is afforded by a counting-rate meter which in this respect has some advantages over representative

[1] *Manuscript received July 11, 1952.*

The material in this paper was taken in part from two theses, one by each author, submitted to McGill University in partial fulfillment of the requirements for the degree of Doctor of Philosophy.

The method and results of this work were also presented as paper No. 114, Section III, to the Royal Society of Canada at the June meeting, 1951, held at McGill University, Montreal.

[2] *Now at Queen's University, Kingston, Ontario.*

earlier methods used for a similar purpose by Elliot and King (4), Alvarez (1), Schelberg, Sampson, and Mitchell (15), and more recently by Boley and Zaffarano (3). In the meter itself a time constant is selected which suits the period under study. The amplified output of the rate meter is displayed against time on a cathode-ray oscilloscope the trace of which is brightened by pulses of preset frequency from a signal generator. The screen thus displays a series of dots which represent the decay curve with negligible distortion provided the time constant of the meter is less than one-tenth of the period under investigation (16). One must, of course, ignore the points plotted before the meter comes into transient equilibrium with the radioactivity. This display on a 5JP11A screen is photographed on 35 mm. film and subsequently is enlarged for graphical analysis. Such photographs include, as zero reference, a base-line sweep made immediately before activation.

While the above method is found to give rather accurate periods of decay, additional information is required for identification of the new activities. Most important for this purpose are the threshold energies, since the low values obtained are the strongest indication that the isotopes with new periods are formed in (p,n) reactions.

Under the conditions of the experiment, one may consider it highly probable that the new activities arise from positrons of high energy. That the radiations consist mainly of positrons is shown by the rapid drop in counts with absorbers which were eventually arranged to stop 10 Mev. β particles. On the other hand, the charge is determined through differential curves taken by the same counter through the heavy absorber. These closely resemble the curve produced under similar conditions by annihilation radiation from the known positron emitter Si^{27}.

Rough estimates of the maximum energies of the β particles are obtained from integral bias curves. The anthracene crystal was calibrated for this purpose by plotting integral bias curves for several simple positron emitters of known energies. The calibration was then realized by plotting against positron energy the bias corresponding to a specific attenuation of the integral count.

In the absence of a channel analyzer, only one point on an integral bias curve can be obtained from each activation. In order to normalize successive runs, two independent discriminators are employed. The count through one discriminator is expressed as a percentage of the count through the second discriminator, which is kept at a low fixed bias. The two counts thus taken over the decay of the primary activity are first corrected for background.

APPARATUS

The complete assembly of the target extractor unit including the probe with inserted counter unit is shown in Figs. 1*a* and 1*b*. This assembly is run along the standard probe track and is secured in a position such that the counter unit is in minimum magnetic field. Under this condition the stainless steel probe projects into the cyclotron chamber. Inside the probe, the light aluminum target holder runs on a track and is operated by the pneumatic cylinder of Fig. 1*b*. An enlarged view of the target holder is given in Fig. 1*c*. The slow forward and quick return motion of the target is accomplished by remote control of solenoid valves. The

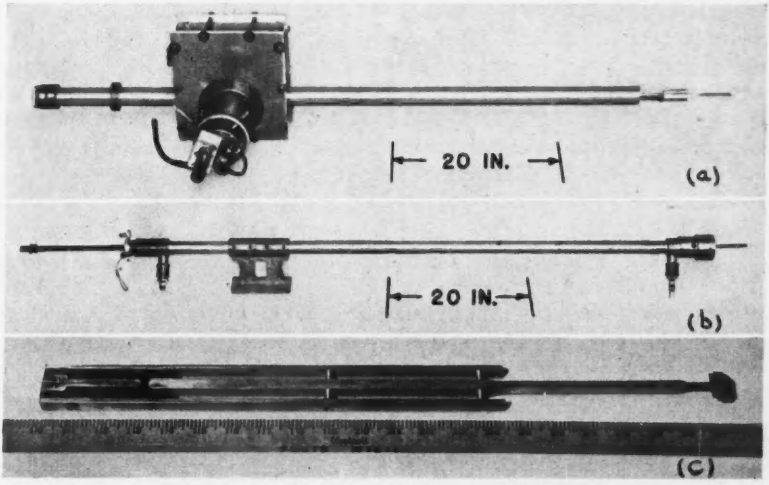

FIG. 1. Photographs of the target-extractor unit: (*a*) counter unit and probe, (*b*) pneumatic cylinder, (*c*) target holder.

target position of desired bombarding energy and the position of the target opposite the counter are set by adjustable stops. The return motion of the target is air-cushioned to minimize shock.

We now turn to Fig. 2 which is a schematic diagram of the principal units of the counting and recording equipment. The counter system at the cyclotron

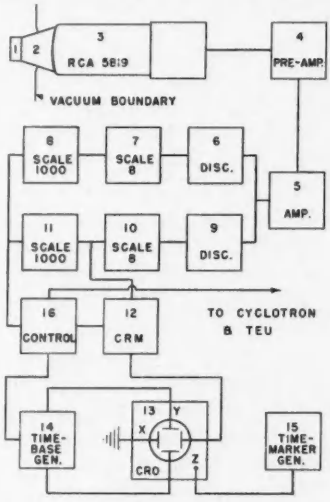

FIG. 2. Schematic diagram of experimental arrangement. The target extractor unit (TEU) is not shown.

consists of an anthracene crystal, a short Lucite pipe, an RCA type 5819 photomultiplier, and a preamplifier. The Lucite pipe serves the usual purpose of adapting the scintillator to the photomultiplier, and, in addition, since it passes through an O-ring vacuum seal, obviates at once the necessity for either placing a window between the source and the detector or having the photomultiplier with its high voltage and signal connections in the vacuum proper. The photomultiplier is adequately shielded by concentric cylinders of mild steel and mu-metal. The preamplifier contains an inverting stage and a cathode follower consisting of two 6AG7's in parallel.

Pulses from the preamplifier are transmitted through an RG8/U cable to an Atomic Instrument Co. wide-band amplifier in the main laboratory. The cable is terminated at the transmitting end by the transconductance of the cathode follower and at the receiving end by a carbon resistor of 56 ohms. The wide-band amplifier drives two channels each consisting of a discriminator, a high resolution scale of eight, and a Berkeley decimal scaler. The scale-of-eight units are similar in design to the scale of four described by Fitch (8).

The counting-rate meter, which follows one of the scale-of-eight units, consists simply of a pulse-shaping circuit (pulse width approximately 7 μsec.), the integrating circuit, and a d-c. amplifier stage of gain approximately 140. This device of using fast scaling circuits leaves one free to design the counting-rate meter for minimum statistical fluctuations (consistent with radioactive decay periods) without incurring undue counting losses. These losses, according to a nomograph due to Elmore (5), would arise almost entirely in the discriminator, and there would be no appreciable contribution from circuits following the scale of eight even at intensities of 50,000 per sec.

To obtain the best counting statistics with a specific decay period, several time constants are provided in the counting-rate meter. Various ranges of sensitivity are also incorporated in order to achieve the largest deflection, due to a given source, within the linear range of the apparatus. The highest counting rate which can be handled satisfactorily is 50,000 per sec., corresponding to counting losses of 10%, and the minimum half-life is about one-fifth second, corresponding to the target-extraction time of one-quarter second.

The output of the rate meter is applied to the X-plates of a Du Mont Oscilloscope, Type 241. A variable scale on the time base is provided by a unit which consists of a motor-driven General Radio potentiometer modified for continuous rotation. The time-marker generator, which is a relaxation oscillator with pulse-shaping circuits, supplies brightening signals at either 2 or 20 per sec. to the Z-axis of the oscilloscope.

A control system consisting of cams, microswitches, and relays ensures rapid and accurate sequence of bombardment, extraction, and recording. The counting intervals on the scalers are thus initiated automatically; their duration is determined by an electronic stopwatch arrangement. The bombardment interval is set by a gating circuit which controls the cyclotron-pulsing equipment described by Henry and Keys (11).

A Du Mont Record Camera, Type 314A, is used to photograph the display on the oscilloscope. The photographs are enlarged to 5 in. × 7 in. Over-all calibration of the prints is done simply by photographing the response to known counting rates of various intensities. The response is linear within 3% over the usable part of the cathode-ray tube. During each series of runs, the time scale is carefully checked by calibration against mains frequency which, by comparison with signals from station WWV, has been found to be remarkably constant.

EXPERIMENTAL RESULTS

(*a*) *Preliminary Experiments*

(1) Counting losses for the equipment were determined by the two-source method (12) using Co^{60} γ rays. Assuming for the relationship between true and observed counting rates

$$N_{\text{true}} = N_{\text{obs.}} + \alpha N_{\text{obs.}}^2,$$

values of α were obtained for widely different counting rates. These values showed close agreement, and their mean, $\alpha = 2.3 \times 10^{-6}$ sec. per count, has been used in computing counting loss corrections. To check the validity of these corrections, a decay curve of C^{11} was taken. A graphite target of spectrographic purity was bombarded for $1\frac{1}{2}$ min. at 30 Mev. After waiting $2\frac{1}{2}$ hr. to allow for the decay of undesired activities, such as the 10.1 min. period due to the reaction $C^{13}(p,n)N^{13}$, counting was begun at an initial rate of 60,000 counts per sec., and the decay was followed over 12 half-lives of C^{11}. A further delay of $1\frac{1}{2}$ hr. was observed before taking measurements of the background. After the background had been subtracted, and the computed corrections applied, a semilogarithmic graph was obtained which is linear over the entire range of counting rates. This linearity indicates that the corrections are valid. The period obtained from the graph for C^{11} is 20.25 min.

(2) As an over-all check on the method of measuring short periods, photographs of the decay of Sc^{41} and Cu^{58} were taken. A calcium target was bombarded at 30 Mev., and a nickel foil at 15 Mev. Analysis of the photographs gave the mean values 0.873 sec. and 3.04 sec. respectively for the half-lives of Sc^{41} and Cu^{58}. These compare favorably with published figures of 0.87 ± .03 sec. and 3 sec. (4, 13).

(3) Energy calibration of the counter for positrons. The positron activities of Mg^{23}, Si^{27}, A^{35}, and Sc^{41} were induced with less than 1% background. This was accomplished by bombarding sodium, aluminum, chlorine, and calcium at energies which were only slightly above the thresholds for the desired reactions. The activation time was adjusted to keep the initial counting rate below 20,000 counts per sec. The targets were: aluminum (spectrographic purity), and calcium (chemical purity) which required no backing material; sodium hydroxide and lead chloride (both of chemical purity) which were fused on niobium. The C^{11} activity which was induced in B^{11} at 18 Mev. was also used for calibration. In this case, decay curves were obtained at 14, 20, 22, 24, and 26 volts bias, and the C^{11} activity was isolated. The target for this experiment was boron powder (chemical

purity) in 0.0015 in. wall aluminum tubing. Ample time was allowed for the decay of the short period activities due to C^{10} and Si^{27}.

After subtraction of background where necessary, the count recorded in the variable channel was taken as a percentage of the count obtained simultaneously

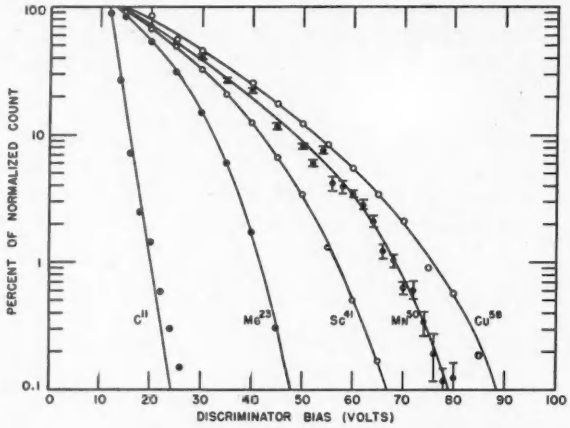

FIG. 3. Integral bias curves normalized to 100% at the fixed bias (approximately 14 volts) of the normalizing channel.

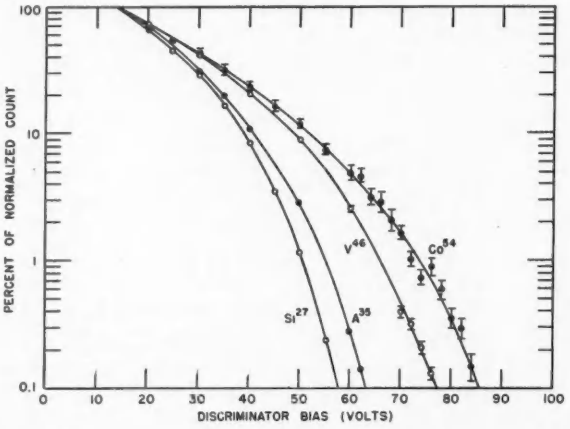

FIG. 4. Integral bias curves normalized to 100% at the fixed bias (approximately 14 volts) of the normalizing channel.

in the fixed channel. This percentage was plotted on a semilogarithmic graph against the variable bias, to give curves both for calibrating activities and for new isotopes, as shown in Figs. 3 and 4. It will be noted that with the exception of C^{11}, the curves all converge at 100% of the normalized count, indicating the relative stability of the bias levels in the two discriminators.

In Fig. 5, two calibration curves give as a function of energy, the bias at which the count in the variable channel was reduced to 0.2% and 0.1% respectively

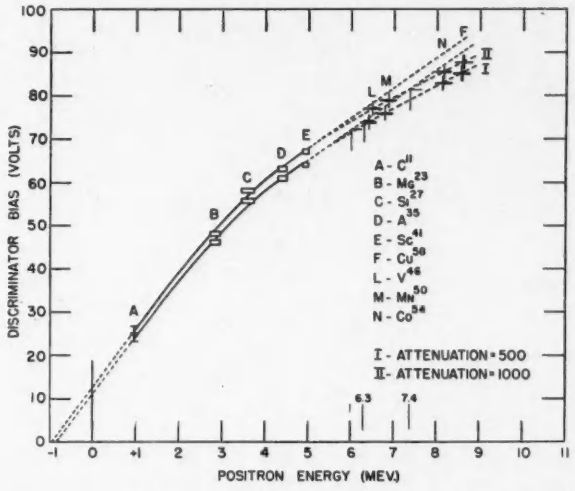

FIG. 5. Positron energy calibration curves. Lower limits to the maximum energies of the new positron emitters are indicated.

(attenuations of 500 and 1000). Each point is represented by a small rectangle which indicates the uncertainty in reading the bias from the integral curves, and also the limits of accuracy to which the positron energy is known (13).

Extrapolation of the curves leads to negative intercepts on the axis of energy. The poor energy resolution of the system undoubtedly contributes appreciably to these negative values. However, a partial explanation of a complex situation may also be found in pulses which arise from absorption in the crystal of a positron and its annihilation quanta. The fixed bias of the normalizing channel is a considerable fraction of the maximum amplitude of pulses from C^{11} positrons. Thus for a value of the variable bias which gives an attenuation of 1000 in the normalized count, a much smaller fraction of the total distribution of pulses from the crystal is recorded. This fraction lies in the high energy region where relatively rare absorption events become evident (i.e., high energy positron plus contributions from the annihilation quanta).

As the fixed bias becomes lower, relative to the maximum pulse amplitude, as for example in the case of Sc^{41} positrons, an attenuation of 1000 in the count approaches a value which is 0.001 of the pulse distribution from the crystal. Indeed, this may be in part the reason for nonlinearity of the curves. However, the chief reason is thought to be the small size of the crystal, preventing complete absorption of all particles entering it.

Tangents have been drawn to the curves at the point Sc^{41} to give a lower limit for energies lying in the upper extrapolated region. The extrapolated curve,

however, gives the correct energy (as calculated from the mass formula) for positrons of Cu^{58}.

(*b*) *The New Isotopes*

Titanium, chromium, and iron targets were bombarded in the proton beam of the McGill cyclotron. In each case, as a result of at least 100 activations, a new short-lived activity has been observed and enough information has been obtained to make an assignment. Ten photographs of each activity have been analyzed. The bombarding energy, the initial activity, and the half-life of the new isotopes formed in each of these runs are listed in Table I, as well as the mean value of

TABLE I

HALF-LIFE MEASUREMENTS

Titanium			Chromium			Iron		
E_p, Mev.	Initial activity, counts/sec.	τ, sec.	E_p, Mev.	Initial activity, counts/sec.	τ, sec.	E_p, Mev.	Initial activity, counts/sec.	τ, sec.
22	57,000	0.387	22	4,100	0.304	17	6,800	0.184
22	29,000	0.405	22	8,800	0.257	17	9,500	0.181
22	25,000	0.393	17	15,000	0.256	17	7,000	0.206
17	12,000	0.398	17	10,000	0.269	17	12,000	0.195
17	14,000	0.419	17	11,000	0.281	17	13,000	0.178
15	23,400	0.405	17	12,000	0.303	17	9,000	0.186
15	26,000	0.397	17	18,000	0.305	17	11,500	0.169
15	24,500	0.392	17	10,200	0.307	17	12,800	0.176
22	42,000	0.385	17	13,000	0.269	19	3,800	0.173
22	14,000	0.395	17	15,500	0.280	19	5,180	0.178
Mean value		0.40 ± 0.01			0.28 ± 0.02			0.18 ± 0.01

the half-life obtained for each of the three activities from the 30 runs analyzed. The standard deviation from the mean is also given. It should be emphasized that the results given in Table I were obtained over a period of several months during which widely differing operating conditions were encountered and in which various circuits and techniques were employed.

The background in the titanium and iron targets was in general of the order of 1% or less, while in chromium the background ranged from 10% to 35%. This large background was principally due to the 21 min. γ rays (13) from the reaction $Cr^{52}(p,n)Mn^{52}$, and was particularly troublesome owing to the abundance of Cr^{52} (83.7%). A photograph taken in a selected run for each target element is reproduced in Fig. 6 and the graphical analysis of these runs is shown in Fig. 7.

Targets of spectrographic purity were first used in these experiments. When it had been established that the activity of interest was in fact due to a specific element, advantage was then taken of commercial grade materials which were more suitable for mounting. The targets were in the form of foils (0.002–0.005 in. thick), small beads or wire (0.010 in. diameter). The foils and wire were directly mounted on the aluminum target holder but the beads were spot-welded to niobium foil. In all cases, the target itself or the niobium foil was of sufficient

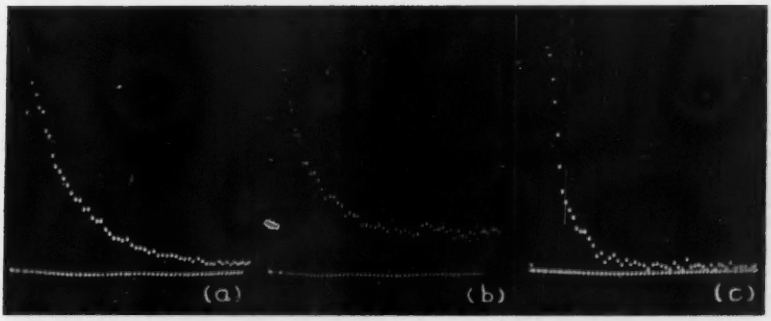

FIG. 6. Photographs of the short-period decays: (*a*) V^{46} from a titanium target, (*b*) Mn^{50} from a chromium target, (*c*) Co^{54} from an iron target.

extent to prevent protons in the beam from falling on the aluminum holder. The target thickness was dictated by the material available and by the rigidity necessary for mounting in the extraction mechanism. Careful experiments have shown that with such targets, only about 10 counts per sec. can be attributed to the 4.9 sec. activity (13) produced in the reaction $Al^{27}(p,n)Si^{27}$, even when the target has been bombarded for 1 sec. Moreover it has been proved experimentally

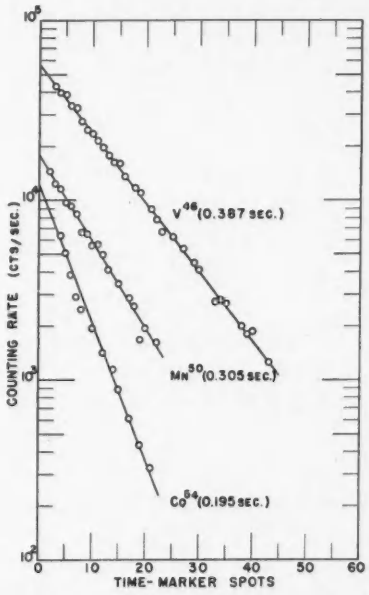

FIG. 7. Representative decay curves for V^{46}, Mn^{50}, and Co^{54}. In each case background activity has been subtracted and corrections made for counting losses. Each curve has a slightly different time factor with respect to the time markers (approximately 20 per sec.).

that the new activities found are not interfered with by any activity in the niobium which has been separately bombarded by itself. Most of the work on each of the three targets, titanium, chromium, and iron, was carried out with no niobium present.

All of the elements listed as impurities in the spectrographic analysis of the Matthey "H.S." Brand materials, and many other elements as well, some of which may have been present to the extent of 1% in the targets of commercial grade, were mounted in target form and studied individually. These targets were bombarded at 17–22 Mev. for as long as 1 sec., and no short-lived activities were observed which could be confused with those reported in this paper. During these experiments, the cyclotron beam current was normal and the sensitivity range of the counting-rate meter was such that at least half-scale deflection would be obtained from the titanium, chromium, and iron targets. The list of elements so studied includes: lithium, beryllium, carbon, oxygen, sodium, magnesium, aluminum, silicon, sulphur, chlorine, calcium, copper, silver, vanadium, and lead.

(*c*) *The Thresholds*

The targets were bombarded for 0.5 sec. at various energies in the range 10–20 Mev., several runs being done at each energy. An accurately timed count

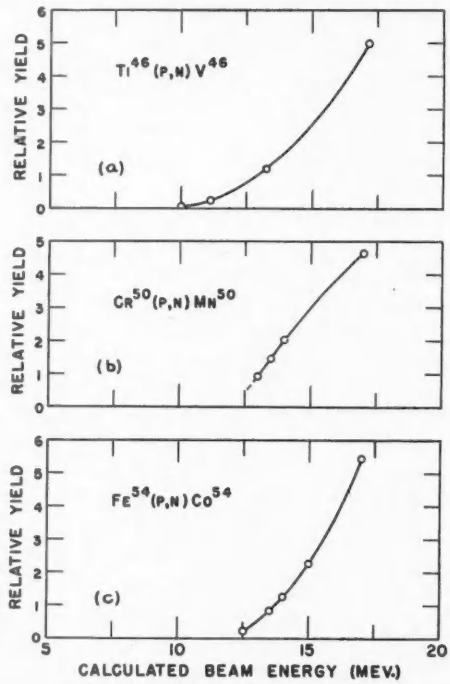

FIG. 8. Relative yield of each new activity as a function of calculated proton energy. The ordinates of each graph bear no simple relation to each other except as noted in the text.

lasting for 2 sec. was taken during the decay of the primary activity. A second count of suitable duration was taken 15 sec. later to determine the background. The corrected count is then proportional to the number of atoms formed, and the mean of several runs at each energy is plotted against the calculated energy to give the curves of Fig. 8. The yields from the three targets are in arbitrary units and are not relative to one another. Photographs taken of each run showed that the short-lived activity of interest was present. From Fig. 8*a*, for example, one reads that the threshold is approximately 10 Mev. (probably correct to within ± 2 Mev.) on the basis of calculated proton energy. In view of beam measurements, described in a later paragraph, this value is more likely to err on the high side than on the low. For similar reasons the thresholds from Figs. 8*b* and 8*c* will be less than 12.5 Mev.

There are two principal sources of error in these experiments: (i) the variation of the beam current in successive activations, and (ii) the proton energy. Galvanometer measurements of the beam current stopped in the beam-monitoring copper block showed that, in the energy range, the current is independent of the energy. Further, over a short series of activations such as is required for threshold determination, it is found, when the activity is large enough to be accurately measured, that it can be reproduced to within ± 10% approximately.

The proton energy in the cyclotron is not sharply defined, nor is its value accurately known. The energies quoted are obtained from the relativistic formula

$$E = 938.3\left[[1 + (0.8115 \times 10^{-6}\, BR)^2]^{\frac{1}{2}} - 1 \right] \text{Mev.}$$

where B = magnetic induction (gauss),

R = target radius (inches).

This formula is based on an oversimplified mode of cyclotron action.

In the course of his investigations of the proton beam, Henry (10) exposed a nuclear plate, covered with graded thicknesses of absorber, to a short burst of protons whose calculated energy was 9 Mev. By measuring the length of proton tracks in the plate, he found a distribution in energy with a broad peak at about 7 Mev. Of 700 tracks measured, none were found to correspond to a proton energy of more than 9 Mev. A similar experiment has been performed at 13 Mev. with the result that less than 0.01% of the protons in the beam had energy greater than 13.7 Mev., and an estimated 5% in the range 12–13.7 Mev. It is significant that in this latter experiment, the nuclear plate was mounted in the target-extractor unit and its radius in the cyclotron was measured in precisely the same way as were the target radii in the experiments on the short-period activities. In view of these results, the threshold measurements can set only an upper limit.

A series of experiments, taken at 17 Mev., during which the proton current was periodically monitored, permit a rough estimate of the relative yields of the short activities from the titanium, chromium, and iron targets. Approximately, the activities at saturation bombardment per proton per target nucleus are in the proportion 4:1:2.

(d) Integral Bias Curves

Data for the integral bias curves (Figs. 3 and 4) were obtained by bombarding at 17 Mev. and increasing the bias in the variable channel in successive runs, first by 5-volt steps and, near the end point, in 2-volt steps. To ensure correct subtraction of background, photographs were taken over a 16 sec. interval immediately following the primary decay. Since, within the errors of measurement, these showed no further decay, the background in each run was taken 15 sec. after activation. The standard deviation in the corrected count in each channel and the resulting standard deviation in the ratio of the two corrected counts have been calculated and are indicated on some of the curves. The bias voltages corresponding to an attenuation in the integral count of 500 and 1000 respectively are transferred to the calibration curves of Fig. 5. Lower limits for the energy are thereby found to be 6, 6.3, and 7.4 Mev. respectively for the activities from the titanium, chromium, and iron targets.

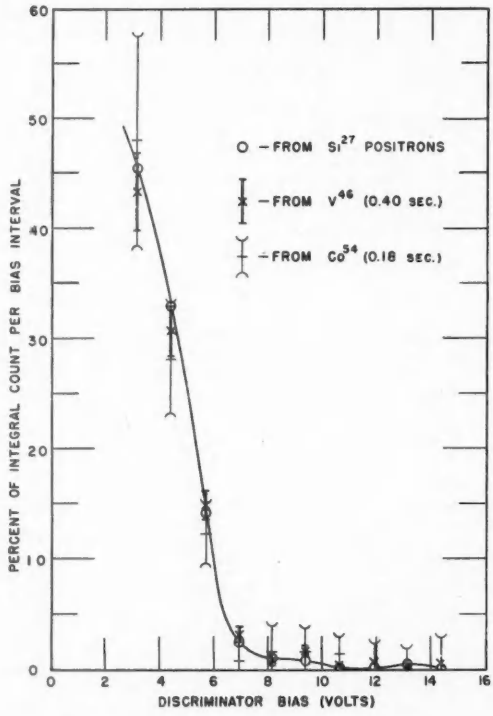

FIG. 9. Differential bias curve of the radiation from Si^{27} positrons stopped in a 10 Mev. thick copper absorber, together with points from two of the short-period activities. The bias interval is $1\frac{1}{4}$ volts. The integral bias curves were normalized to 100% count at $2\frac{1}{2}$ volts bias, the ordinate being expressed as a per cent of the total count above this bias.

(*e*) *Identification of Positrons*

A copper absorber, 10 Mev. thick for β rays, was placed in front of the anthracene crystal, and integral bias curves were obtained for Si^{27} and for the radiations from the titanium and iron targets. The differential curves were calculated and plotted in Fig. 9. It will be seen that, within experimental error, the three curves are superimposed. Since no particles can be counted through the absorber, the curves must be those of γ-radiation, and the fact that the curves are similar strongly suggests that the γ rays are principally the quanta of positron annihilation. Further, photographs show that the half-life is, in each case, qualitatively the same as that obtained without the absorber. An attempt was made, using an aluminum absorber, to find a similar result for the chromium activity, but on the first activation, the long-lived γ-ray background arising mainly from Mn^{52} amounted to 150% of the short-period activity, and it was, therefore, considered impracticable to proceed with the experiment. However, counts taken at 15 volts bias showed that the short-period intensity was reduced at least 100-fold when the absorber was inserted. This reduction is much greater than can be accounted for on the basis of nuclear γ rays. It is concluded, therefore, that, as with the titanium and iron experiments, the activity induced in chromium is largely, if not entirely, due to positron emission.

DISCUSSION OF RESULTS

Three new and distinct short-lived positron activities have been found which are due to proton reactions on isotopes of titanium, chromium, and iron respectively. Owing to the low bombarding energies at which the activities appeared, no reactions save (p,γ), (p,n), $(p,2n)$, (p,pn), and (p,α) need be considered, and of these, only (p,n) and $(p,2n)$ reactions can lead to isotopes not already known to be stable or relatively long-lived. While it is true that Mn^{53}, which might result from the reactions $Cr^{53}(p,n)Mn^{53}$, $Cr^{54}(p,2n)Mn^{53}$, or $Fe^{56}(p,\alpha)Mn^{53}$, is not known, yet, since it is adjacent to the stable line on the nuclear chart, its period must indeed be very much longer than any of the new periods which have been found. With the elimination of Mn^{53}, it follows that only the lowest mass isotopes, viz. Ti^{46}, Cr^{50}, and Fe^{54}, can take part in the reactions. The problem of making an assignment is now reduced to deciding between (p,n) and $(p,2n)$ reactions on these isotopes. This decision can be made by comparing the measured threshold and decay energy with the expected values calculated from the semiempirical mass formula (17, 2, 7). The bearing of *ft* products on the matter will also be discussed.

The accuracy to be expected of the mass formula in the neighborhood of chromium may be judged from a comparison of calculated neutron binding energies with observed (γ,n) thresholds. From such a comparison made by Harvey (9), one can say that the mass formula is accurate within one Mev. The *ft* products, based on the measured periods and on the calculated positron energy, have been obtained using curves published by Feenberg and Trigg (6). Because the *ft* product is sensitive to positron energy, it was considered preferable to use the calculated energy rather than our measured value which is only a lower limit.

In Table II the observed and calculated data are summarized for each of the target nuclei listed in column 1. The product nuclei for (p,n) and $(p,2n)$ reactions are listed in columns 5 and 9 respectively. In the table, τ represents the half-life,

TABLE II

ENERGIES AND *ft* VALUES

Observed				Calculated							
				(p,n) Reactions				$(p,2n)$ Reactions			
(1)	(2) τ, sec.	(3) E_0, Mev.	(4) T, Mev.	(5)	(6) E_0, Mev.	(7) T, Mev.	(8) *ft*	(9)	(10) E_0, Mev.	(11) T, Mev.	(12) *ft*
Ti^{46}	0.40	> 6	~ 10	V^{46}	7.7	9.6	8400	V^{45}	5.6	20.6	1930
Cr^{50}	0.28	> 6.3	< 12.5	Mn^{50}	7.9	10.0	6200	Mn^{49}	6.0	21.2	1850
Fe^{54}	0.18	> 7.4	< 12.5	Co^{54}	8.3	10.3	5400	Co^{53}	6.5	21.6	1800

E_0 the positron end point, and T the threshold. It will be seen at once that, on the basis of threshold energy alone, the $(p,2n)$ reactions, and consequently the assignments of column 9, can no longer be considered. The discrepancy between calculated and observed thresholds is far greater than can be accounted for by combined uncertainties of measurement and calculation. There is also a slight discrepancy as regards positron energy, but this point is not decisive. On the other hand, if one turns to the (p,n) reactions, one finds qualitative agreement both for positron energy and threshold energy. Further, if one takes the positron energies from the extrapolated calibration curve rather than from the tangent curves, the agreement between measured and calculated positron energies is improved in the case of (p,n) reactions, whereas the discrepancy in the case of $(p,2n)$ reactions is increased.

It is of interest to note that all of the *ft* products of columns 8 and 12 are small enough to be classed as superallowed. This is to be expected certainly for the $(p,2n)$ reactions since the residual nuclei form "mirror" pairs with their daughter nuclei (7). However, according to Wigner's theory of supermultiplets (18, 19, 14), such transitions also fit in with the (p,n) scheme, since the nuclei of columns 1 and 5 belong to a series characterized as follows:

$$A = k(2 \text{ protons} + 2 \text{ neutrons}) + 2$$

$$\text{where } k = 1, 2, 3, \ldots .$$

The transitions take place between nuclei with $N = Z$ (column 5) and $N = Z + 2$ (column 1).

One is thus led to assign the 0.40, 0.28, and 0.18 sec. activities to the isotopes V^{46}, Mn^{50}, and Co^{54} respectively.

It is apparent that the discovery of these odd–odd isotopes has resulted from an attempt to extend the series of odd–even positron emitters now terminating in Sc^{41}. However, the occurrence of short periods in the former series introduces experimental difficulties in the quantitative study of the latter which are the

product nuclei of $(p,2n)$ reactions. Moreover, the decay energies in the two series are similar. Thus, when the bombarding energy is increased in order to bring in the $(p,2n)$ reactions, one can expect only to find an apparent modification of the decay period. This was indeed found to be so in the case of titanium where bombardment at 40 Mev. showed a distinct retardation in gross decay owing to the admixture of a slightly longer-lived activity.

These experimental difficulties are not present to the same extent when nickel is the target. In this case, Cu^{58}, the next member of the odd–odd series, is produced in the reaction $Ni^{58}(p,n)Cu^{58}$ (13). The evidence excludes a superallowed transition in Cu^{58}. In fact, the half-life (3 sec.) is long enough to permit observation of a new period of approximately 0.14 sec. superimposed on the 3 sec. background. This new activity is known to have a threshold of production below 33 Mev. Further work on this problem is being undertaken.

ACKNOWLEDGMENTS

The authors wish to express their thanks to Professor Foster, Director of the Radiation Laboratory, for his continued interest and for the guidance and advice he has given in all phases of this work. Thanks are also due to Dr. A. L. Thompson and Prof. J. P. Ogilvie for their assistance in the preparation of targets, and to Dr. J. D. Jackson for valuable discussions. The assistance of Mr. R. H. Mills in the experimental work is gratefully acknowledged.

REFERENCES

1. ALVAREZ, LUIS W. Phys. Rev. 80: 519. 1950.
2. BOHR, N. and WHEELER, J. A. Phys. Rev. 56: 426. 1939.
3. BOLEY, F. I. and ZAFFARANO, D. J. Phys. Rev. 84: 1059. 1951.
4. ELLIOT, D. R. and KING, L. D. P. Phys. Rev. 60: 489. 1941.
5. ELMORE, W. C. Nucleonics, 6(No. 1): 26. 1950.
6. FEENBERG, E. and TRIGG, G. Revs. Modern Phys. 22: 399. 1950.
7. FERMI, E. Nuclear physics. Revised edition. The University of Chicago Press, Chicago. 1950.
8. FITCH, V. Rev. Sci. Instruments, 20: 942. 1949.
9. HARVEY, J. A. Phys. Rev. 81: 353. 1951.
10. HENRY, W. H. Private communication. 1951.
11. HENRY, W. H. and KEYS, J. D. Can. J. Phys., 29: 137. 1951.
12. KOHMAN, T. P. MDDC-905. U.S. Atomic Energy Commission, Oak Ridge National Laboratory, Oak Ridge, Tenn. 1945.
13. National Bureau of Standards (U.S.). Nuclear data. Circ. 499. N.B.S., Washington. 1950.
14. ROSENFELD, L. Nuclear forces. Interscience Publishers, Inc., New York. 1948.
15. SCHELBERG, A. D., SAMPSON, M. B., and MITCHELL, ALLAN C. G. Rev. Sci. Instruments, 19: 458. 1948.
16. SCHIFF, L. I. and EVANS, R. D. Rev. Sci. Instruments, 7: 456. 1936.
17. v. WEIZACKER, C. F. Z. Physik, 96: 431. 1935.
18. WIGNER, E. Phys. Rev. 51: 106. 1937.
19. WIGNER, E. Phys. Rev. 56: 519. 1939.

A SIMPLE ACTIVATION FOR BeCu MULTIPLIERS[1]

By F. J. Fitz Osborne[2]

ABSTRACT

A consideration of previous methods used in activating BeCu electron multiplier plates has resulted in the development of a simple inert gas treatment using a minimum of apparatus and resulting in a total multiplication factor comparable to that obtained by other treatments.

Use of BeCu plates as the active surfaces in secondary emission multipliers requires that the plates be sensitized before they exhibit high multiplication or yield. Allen (1) in using BeCu plates used a heat treatment involving the heating of the plates in vacuum of 10^{-5} mm. to a temperature of 650°C.

This procedure is difficult, since the initial heavy degassing of the plates requires a large pumping capacity. In addition the vacuum limits the methods by which the heating may be carried out. The most satisfactory method is by radio-frequency heating and thus a large amount of auxiliary apparatus is required for the sensitization.

Dare and Rowen (2) attempted to use the Allen treatment and found it difficult. Therefore they developed a treatment in a hydrogen atmosphere, again heating the plates to about 650°C. This achieved an activation comparable to that of Allen. However this method involves the use of a dangerous gas at high temperatures and thus great care must be taken to avoid leaks in the system and to protect the user.

Consideration of the effects of the two methods of sensitization suggests that a successful activation requires two conditions for the production of the thin oxide film on the plate surfaces. First, heating to about 600–650°C. is required. Secondly, a low partial pressure of oxygen is required to keep the rate of oxide formation low enough to be easily controlled by the length of the treatment. In Allen's treatment the oxygen comes from the atmosphere and from the oxygen in and on the plates themselves. For the Dare and Rowen treatment, the only oxygen source is the plates, while the hydrogen tends partially to reduce the oxygen and thus to slow the rate of oxidation.

A simple method of achieving a low partial pressure during the heating is to carry out the sensitization in an inert gas, preferably by a continuous flow method. To try such a method, a small oven capable of being heated to about 650° and having an inlet for an inert gas such as argon was constructed. This oven was not airtight but the argon was used at such a rate as to allow the escaping gas to prevent the entrance of the air. A conventional nichrome coil of 30 ohms wound around the oven and connected to a 5 amp. variac provided enough heat at 600 watts. A thermocouple inside the oven indicated

[1] *Manuscript received June 10, 1952.*
Contribution from the Department of Physics, Laval University, Quebec, Que.
[2] *Holder of a grant from the Scientific Research Bureau, Province of Quebec.*

the atmosphere's temperature, while the plates themselves were in a glass carrying tube to keep them from touching the walls of the tube and also for simplicity in insertion and removal.

For a heat treatment, the plates are first cleaned with fine emery paper. They are then placed in the oven and the heating started. As the temperature begins to rise, the flow of argon is started, with the flow sufficient to ensure flushing of the air from the furnace. The furnace constructed takes about 20 min. to heat to the required temperature, at which time the plates are removed for cooling. Cooling takes about one minute after which the multiplier may be assembled. The total time required from the start of activation until the multiplier is under vacuum is of the order of 40 min.

Multiplication achieved by this method of heat treatment is of the same order as that of the other methods developed with the advantage of simplicity and speed of sensitization with no complicated apparatus.

This method of treatment was developed as part of a project aided by the Scientific Research Bureau of the Province of Quebec.

REFERENCES

1. ALLEN, J. S. Rev. Sci. Instruments, 18: 739. 1947.
2. DARE, J. A. and ROWEN, W. H. Tech. Rept. No. 6, Laboratory for Nuclear Science and Engineering, M.I.T. 1947.

NOMOGRAM OF LIFETIME–ENERGY–SPIN FOR GAMMA-RAY TRANSITIONS[1]

By R. Montalbetti

ABSTRACT

A nomogram of the recent Weisskopf formula relating the mean life for gamma-ray transitions to the energy and spin change has been constructed. The nomogram is useful in that it allows rapid computations and shows at a glance the dependence of mean lifetime upon the variables involved.

Several attempts have been made to relate the mean life for gamma-ray transitions to the energy and spin change (2, 5). The earlier attempts met with only moderate success.

Axel and Dancoff (1) developed a theoretical formula for the lifetime which gave satisfactory agreement with experimental results after the latter were corrected for internal conversion.

Recently, Weisskopf (4) obtained an improved formula which gives good agreement with experimental data in spite of the crude estimates used in its derivation.

We have had several occasions, in this laboratory, to use the Weisskopf formula and for convenience have constructed a nomogram of it. It was felt that the nomogram would be of use to others and it is given in the accompanying figures.

The lifetime for gamma-ray transitions, written in the form used by Goldhaber and Sunyar (3), is

$$\tau_\gamma \text{ (sec.)} = \frac{\Delta I[1 \cdot 3 \cdot \ldots \cdot (2\Delta I + 1)]^2}{2(\Delta I + 1)} \frac{(\Delta I + 3)^2}{3^2} \frac{1}{\rho^{2\Delta I}} \left(\frac{137}{W}\right)^{2\Delta I + 1} \frac{\hbar}{mc^2}$$

where ΔI = spin change,

$\rho = 0.532\, A^{1/3}$,

W = transition energy in units of $mc^2 = E/mc^2$,

E = transition energy in ev.,

A = mass number.

Also

$$(\tau_\gamma)_{\Delta I,\text{mag}} = (\tau_\gamma)_{\Delta I,\text{el}}\, 5.11 A^{2/3}.$$

To illustrate the use of the nomogram, consider a specific case where $A = 40$, $E = 3 \times 10^6$ ev., $\Delta I = 1$. The line joining $A = 40$ and $E = 3 \times 10^6$ cuts the axis for $\Delta I = 1$ at 3×10^{-15}. Thus the mean life for the electric dipole transition is then 3×10^{-15} sec. This value is transferred to the axis labeled $\tau_{\gamma,\text{el}} \times 10^n$ sec., and a line is drawn between this value and $A = 40$. The mean life for a magnetic dipole transition is then read as 180×10^{-15} sec.

[1] *Manuscript received August 3, 1952.*
Contribution from the Department of Physics, University of Saskatchewan, Saskatoon, Sask.

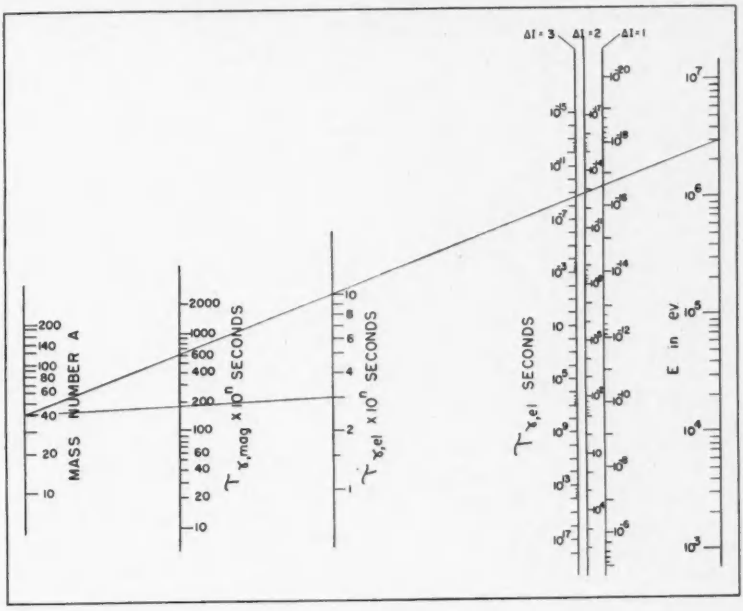
MASS NUMBER A
200
140
100
80
60
40
20
10
$\tau_{\gamma,mag} \times 10^n$ SECONDS
2000
1000
600
400
200
100
60
40
20
10
$\tau_{\gamma,el} \times 10^n$ SECONDS
10
8
6
4
2
1
$\tau_{\gamma,el}$ SECONDS
ΔI = 3
ΔI = 2
ΔI = 1
E in eV

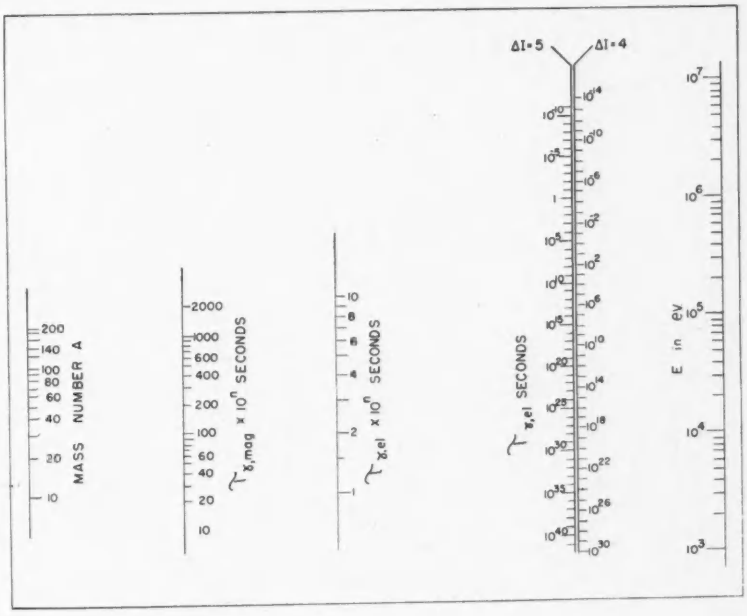
MASS NUMBER A
200
140
100
80
60
40
20
10
$\tau_{\gamma,mag} \times 10^n$ SECONDS
2000
1000
600
400
200
100
60
40
20
10
$\tau_{\gamma,el} \times 10^n$ SECONDS
10
8
6
4
2
1
$\tau_{\gamma,el}$ SECONDS
ΔI = 5
ΔI = 4
E in eV

The author wishes to express his thanks to Prof. L. Katz who suggested the usefulness of such a nomogram and carefully checked it.

REFERENCES

1. AXEL, P. and DANCOFF, S. M. Phys. Rev. 76: 892. 1949.
2. FLÜGGE, S. Physik. Z. 42: 221. 1941.
3. GOLDHABER, M. and SUNYAR, A. W. Phys. Rev. 83: 906. 1951.
4. WEISSKOPF, V. F. Phys. Rev. 83: 1073. 1951.
5. WEIZSÄCKER, C. F. v. Naturwissenschaften, 24: 813. 1936.

DIELECTRIC PROPERTIES OF SOME SOLID PROTEINS AT WAVE LENGTHS 1.7 METERS AND 3.2 CENTIMETERS[1]

By Elizabeth R. Laird

ABSTRACT

Measurements have been made of the dielectric constant and the attenuation coefficient of casein, egg albumin, lactalbumin, and zein, in powder form at λ 1.7 meters and λ 3.2 cm., and of horn keratin, at stages in drying, at λ 3.2 cm. The Böttcher formula was used to reduce the observed value of the dielectric constant of a powder to that of the solid. It was tested on cane sugar in granulated and powder forms with satisfactory results. The attenuation coefficients of the powders were found to be roughly inversely proportional to the wave lengths. The values at λ 3.2 cm. were in the range 0.03 to 0.04 cm.$^{-1}$ and did not suggest resonance absorption. The dielectric constants found for the albumins at both wave lengths were close to 3.6. ϵ for zein increased from 3.7 at λ 3.2 cm. to 4.0 at λ1.7 meters, for casein from 4.0 to a possible 4.2. ϵ for keratin increased from 3.6 when dry to 4.4 with 6.5% moisture, and α increased from 0.05 to 0.14 cm.$^{-1}$

The possibility of resonance absorption at centimeter wave lengths in proteins, especially in those that occur in animal tissue, is of general interest. It is not considered probable (6) that such resonance would occur at wave lengths as long as 3.2 cm., but a study of the dielectric properties of a few readily obtainable proteins was undertaken to determine whether the methods previously used (8) would yield useful information. The materials used were casein, lactalbumin, egg albumin, zein, and horn keratin. Measurements were made at wave lengths 1.7 meters and 3.2 cm.

METHOD AND EQUIPMENT

The general equipment was the same as that described earlier (8). At λ 1.7 meters the method was essentially that of Cooledge (3). It uses a container for the material placed across a pair of Lecher wires at a point between a movable and a fixed bridge. A thermocouple is attached to the fixed bridge, and the movable bridge is set for maximum thermocouple response. From the position of the bridges and container and the thermocouple response, the dielectric constants of the material may be found if the constants of the line and container are known. The container was restandardized by using air and benzene as contents.

At λ 3.2 cm. the method was that described by Roberts and von Hippel (10). The previous wave guide arrangement of source, attenuator, frequency meter, slotted line, right angle section, and cup was slightly altered. The right angle section was omitted and the cup was changed to make it possible to insert a half wave plate of polystyrene just above the material being used. This was done to prevent error due to slight changes in the flexible part, to reduce the absorption of moisture from the air during a test, and to simplify the measurement of the depth of the material used. The standing wave ratio in the slotted line, the

[1] *Manuscript received June 6, 1952.*
Contribution from the Department of Physics, the University of Western Ontario, London, Ont. This work was supported in part by the Ontario Cancer Treatment and Research Foundation.

distance of a minimum from the surface of the sample in the cup, the thickness of the sample, together with the wave length in the wave guide, serve to determine the dielectric constants.

Except for keratin the materials were in powder form. The zein and lactalbumin were obtained from the Nutritional Biochemicals Corporation. Sample analyses supplied gave nitrogen 15.8% for zein and 12.0–12.5% for the lactalbumin. The casein was from Difco Laboratories, and the egg albumin as scales from Eimer and Amend, and powdered in a mortar. The keratin was from an old buffalo horn supplied by the Department of Biology. A piece was cut approximately $2.84 \times 1.25 \times 0.9$ cm. so that the electric field would be across the grain. In order to determine the properties of the solid material from observations on the powders it was necessary to know the density of the solid, as well as the apparent density of the powder as used. A specific gravity bottle method was first tried, but the lack of temperature control and uncertainty as to whether the mixture was free from air led to the choice of the flotation method as more accurate for finding the density of the solids. Mixtures of dichloroethylene, N-butylbromide, dichlorobenzene, and bromotoluene were used as needed. The values adopted as a result of such tests were zein 1.27, casein 1.30, lactalbumin 1.305, egg albumin 1.315 gm. per cc. The error should not be greater than $\frac{1}{2}\%$.

A few early experiments showed the need for the drying of the materials to get consistent results. For the measurements at λ 1.7 meters the powders were dried over calcium chloride for periods varying from one day to one month. The final observations at λ 3.2 cm. were made on material dried for at least three months over magnesium perchlorate. No changes greater than the experimental error were found in the constants of the powders after six weeks' drying. The horn was still losing weight after drying for three and a half months at room temperature. It was then dried for a total period of 30 days in oven space having a temperature range of 10° C. and mean temperature initially 75° C., then 80° C., and finally 93° C. The horn was removed a number of times, cooled, weighed, and measured. As the horn dried it shrank and the value of the dielectric constant found, ϵ, was corrected by use of the formula (9)

$$\epsilon_1 = (\epsilon - 1)b'/b + 1$$

where b' is the breadth of the wave guide and b of the sample.

PRELIMINARY TESTS

Preliminary experiments were made at λ 3.2 cm. on cane sugar in fine powder and granulated forms in order to find whether scattering at this wave length in the equipment used would have an appreciable effect on the apparent absorption. It was found that any absorption was at the very limit of observation, and it was concluded that scattering could be neglected. These experiments were made by A. R. Abercrombie, now of the R.C.A.F., who also did some exploratory work in the measurements on proteins.

These measurements on sugar were used also to test the formula given by Böttcher (2) for computing the dielectric constant of a solid, ϵ_1, from that of a

powder, ϵ, when the partial volume, δ_1, is known. In the case of a powder in air the formula becomes

$$(\epsilon - 1)/3\epsilon = \delta_1(\epsilon_1 - 1)/(\epsilon_1 + 2\epsilon) .$$

The value computed thus for cane sugar from observations on the granulated form was 3.14 ± 0.02 and from those on the fine powder form 3.19 ± 0.07. In the trials, two for each form, the apparent density varied from 0.75 to 0.906 gm. per cc. The agreement in the results was considered very satisfactory. Values are given in I.C.T. for cane sugar at a frequency 3×10^8 c.p.s., namely 3.16 and 3.49 in directions parallel to the principal axes and 3.32 in the direction parallel to the macrocrystallographic axis. At the higher frequency used here it might be expected that the value would be somewhat smaller, and as a result of these tests the Böttcher formula has been used throughout in computing the dielectric constants of the materials used in powder form, and the absorption has been taken to be proportional to the apparent density.

RESULTS AND DISCUSSION

At λ 1.7 meters the attenuation coefficient found for lactalbumin and zein was within the limits 0.0005 ± 0.0002 cm.$^{-1}$, and for casein and egg albumin 0.001 ± 0.0005 cm.$^{-1}$ A drift of the power supply was a factor in making the uncertainty large. Under the circumstances it was not certain that there is any real difference in the absorption by the different powders. The egg albumin was dried for a shorter time than the others, and the values found for casein on three different days varied widely. It was thought that possibly the fine powder was not distributed evenly through the small container.

The results on absorption at λ 3.2 cm. and on the dielectric constant at λ 1.7 meters and 3.2 cm. for the powders are shown in Table I, and the results

TABLE I

	Dielectric constant		Attenuation coefficient (cm.$^{-1}$) at 3.2 cm.
	1.72 m.	3.2 cm.	
Casein	4.2	4.01	0.041
Lactalbumin	3.72	3.61	0.041
Lactalbumin with 5.6% moisture		3.84	0.074
Egg albumin	3.65	3.66	0.0295
Zein	3.97	3.72	0.038

for keratin at λ 3.2 cm. in the graphs of Fig. 1. The over-all accuracy in the attenuation coefficient is considered to be about 5%. The dielectric constants at λ 3.2 cm. could be measured to an accuracy of 1% but at λ 1.7 meters the initial uncertainty was as great as 2% and the possible error in the apparent density added to this makes the over-all accuracy not better than 4%, and again the variation in the observed values for casein was greater than for the others.

It will be seen that the attenuation coefficients for the powders are much larger at λ 3.2 cm. than at λ 1.7 meters; but if the results were expressed in terms of the loss factor, tan δ at λ 3.2 cm. would lie within the limits for λ 1.7

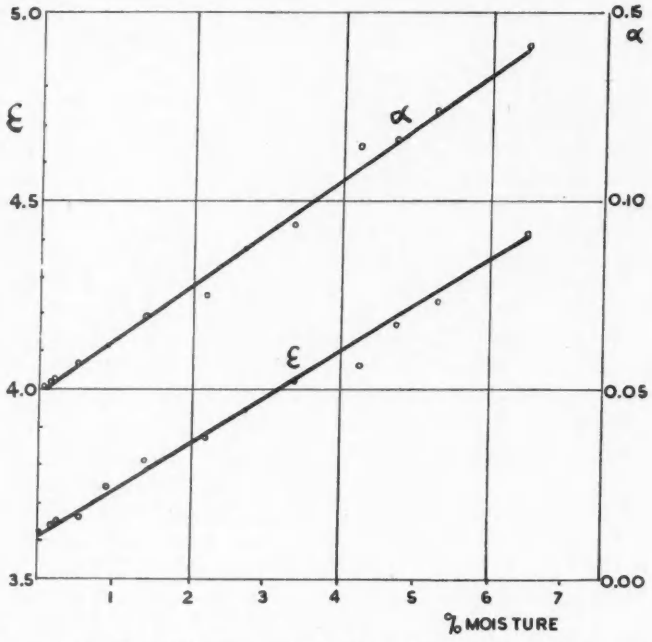

FIG. 1. Variation of dielectric constant and attenuation coefficient of horn keratin with water content at λ 3.2 cm.

meters. The dielectric constants for lactalbumin and egg albumin were found to be the same at the two wave lengths within the experimental error. The internal consistency of the sets of measurements on zein at both wave lengths was good, and the increase in the dielectric constant at the longer wave length is considered real. For casein the difference is doubtful because of the large uncertainty in the measurements at the longer wave length.

The differences found in the attenuation coefficients of the materials at λ 3.2 cm. are greater than can be accounted for by error in measurement. From the graph it will be seen that dry horn keratin was found to have a somewhat larger attenuation coefficient than any of the powders. Differences were also found in the dielectric constants, though the results for lactalbumin, egg albumin, and keratin were the same within the limits of error.

A source of error in any comparison of the properties of the different materials lies in the possible water content. The casein absorbed water rapidly during handling, and during a test gained about 0.9% in weight. The gains in weight of egg albumin and zein in handling were of the order of 0.2% or less, of lactalbumin 0.4%, and of the horn 0.03%. Information on the effect of moisture on the absorption is given by the measurements on lactalbumin and keratin. The lactalbumin was tested before and after drying. The change in weight

indicated a moisture content of 5.6% in air at a relative humidity of about 25%. This amount of moisture produced an increase in the attenuation coefficient of 0.033 cm.$^{-1}$, and in the dielectric constant of 0.23. From the graph it is seen that the change in the constants of keratin for the same increase in moisture is more than double that for lactalbumin. Some measurements were made on the other powders before they were dried, but not as exact data were kept on the change in weight. The estimates indicate that the constants for egg albumin and casein change in the same degree as lactalbumin and that for zein the change is somewhat greater but not as great as for keratin. If one corrects the values of the constants for casein on the supposition that the measurements were made on material having 1% moisture, it would make ϵ 3.97 and α 0.035 for dry casein; these values are still considerably larger than for egg albumin. Effect of moisture in the other cases would be less than the experimental error.

The effect of moisture on the dielectric constant of keratin has been studied by King (7) at lower frequencies. Fig. 2, line (*a*), shows his results on dry horn

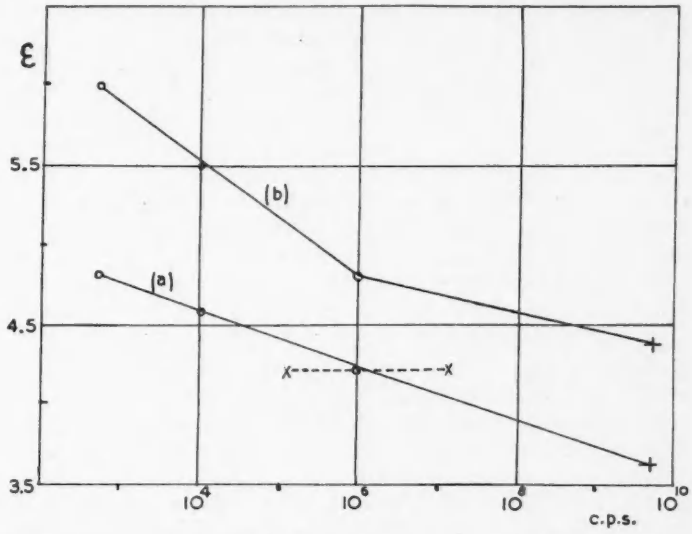

FIG. 2. Dielectric constant of keratin over a frequency range (*a*) material dry, (*b*) material with 7.2% moisture.
o Data from King (7).
× · · · × Data from Errera and Sack (4).
\+ Present data.

as read from a graph, together with the value obtained here at 9.8×10^9 c.p.s. and a line indicating the value found by Errera and Sack (4) for wool fiber in the region from 120 kc. to 13 Mc. per sec. The points show a nearly linear relationship between dielectric constant and frequency. Both earlier authors refer to Fox and Finsh (5) as having measured the optical refractive index as

$n^2 = 2.4$. The dielectric constant near 10^{10} c.p.s. is still considerably larger than this square of the index of refraction and there is no indication of a sudden change. Fig. 2 shows also, line (*b*), the relation of the present measurement at 6.5% moisture content to King's measurements at 7.2% moisture content at the lower frequencies. The effect of moisture appears larger at 10^{10} c.p.s. than at 10^6 c.p.s. and about the same as at 10^4 c.p.s. During the last two weeks of drying, about half in the oven and half at room temperature, the horn weight did not change by more than 0.05%, and it is improbable that further attempts at drying would change the picture. The horn had lost 4.2% of dry weight before the first test was made. King estimated the relative contributions of the mobile water, bound water, and rotation in the keratin lattice induced by the water to the dielectric constant. If the increased effect of water at 10^{10} c.p.s. is real, it suggests a change in the relative magnitude of these contributions or the presence of a new factor.

A study of the dielectric properties of various solid crystalline proteins over a wide frequency range has been reported recently by Bayley (1). The proteins were used in powder form, for the most part not dried, and no data are given on the partial volume occupied. For these reasons it is difficult to compare his results with the present ones. Taking from a graph the values 1.7 and 1.9, for the dielectric constants of bovine serum albumin at 7.3 cm., the shortest wave length used, and in the meter region, and assuming a partial volume of about 0.36, one finds 3.7 and 4.7 as the corresponding values for the solid. This is a greater difference than for any of the materials measured here in this range of frequencies. The corresponding tan δ, about 0.034, is nearly the same as that measured here for zein and lactalbumin powders as used and not dried. Bayley made some measurements mostly at low frequencies on materials kept *in vacuo* several hours and observed much lower values in the constants, and says that it is not certain to what extent the dispersion found in the centimeter regions is to be attributed to sorbed water.

A few observations were made here on zein with the frequency varied over a range of 60 c.p.s. No reproducible differences were found over this short range. In general, while some differences were found in the absorption of the proteins tested at λ 3.2 cm. the results do not indicate any marked selective absorption in this region, and show the marked effect of any moisture present. On the other hand it may be questioned whether the dried material reacts to the radiation in the same way as the proteins in their natural setting. It would probably be possible to greatly increase the accuracy at λ 1.7 meters by changes in the form of container and bridge, and by use of a highly stabilized power supply, to make it comparable with that at λ 3.2 cm. It might then be possible by measurements on powders of the same material but of different sizes, held in suspension, to test whether resonance absorption of an electromechanical nature may play a role in the effect produced by radiation. Schereschewsky (11) in 1926 reported such a suggestion made to him by Prof. G. W. Pierce as a possible cause of observed differential action of radiation on mice and used a formula given by Lamb for the frequency of vibration of an elastic sphere to estimate the diameter of body

cells that would respond to the frequencies used by him, but uses the term speculation in the discussion. In some search of references no report of a direct test of the magnitude of such an effect has been found.

ACKNOWLEDGMENTS

The writer is indebted to Dr. R. C. Dearle for general support of the project, to Mr. N. J. Abbott of the Ontario Research Foundation for advising the use of the flotation method in the density determination, to Dr. J. K. Watson for suggestions about the type of liquids to use and for other help, and to Dr. Helen Battle for directing attention to horn and for information about it.

REFERENCES

1. BAYLEY, S. T. Trans. Faraday Soc. 47: 509. 1951.
2. BÖTTCHER, C. J. F. Rec. trav. chim. 64: 47. 1945.
3. COOLEDGE, W. D. Ann. Physik, 69: 125. 1899.
4. ERRERA, J. and SACK, H. S. Ind. Eng. Chem. 35: 712. 1943.
5. FOX, K. R. and FINSH, R. B. Textile Research, 11: 62. 1940.
6. FRÖHLICH, H. Trans. Faraday Soc. 42 A: 3. 1946.
7. KING, G. Trans. Faraday Soc. 43: 601. 1947.
8. LAIRD, E. R. and FERGUSON, K. Can. J. Research, A, 27: 218. 1949.
9. MONTGOMERY, C. Technique of microwave measurements. Radiation Laboratory Series Vol. 11. McGraw Hill Book Company Inc., New York and London. 1947. p. 576.
10. ROBERTS, S. and VON HIPPEL, A. J. Applied Phys. 17: 610. 1946.
11. SCHERESCHEWSKY, J. W. Pub. Health Repts. 41: 1939. 1926.

THE ENERGY SPECTRUM OF THE X RAYS FROM A 70-MEV. SYNCHROTRON[1]

By I. B. McDiarmid

ABSTRACT

The spectrum of the X rays produced in the forward direction by 70-Mev. electrons striking a very thick target has been measured. The scattering method has been used to determine the energies of about 650 electron pairs produced by the X rays in G-5 emulsions and from this the spectrum has been deduced. The number of photons found below 25 Mev. is considerably less than that expected from the Bethe–Heitler–Schiff theory. No satisfactory explanation of this has been found but the measured spectrum is in agreement with "yield" measurements done in this laboratory.

INTRODUCTION

The energy spectra of X rays produced by high energy electrons striking thin targets have been measured by a number of investigators (10, 15, 2, 19). In these experiments cloud chambers and a magnetic pair spectrometer have been used to determine the energies of suitably produced electron pairs and the spectra obtained agree reasonably well with the Bethe–Heitler theory (1). However, Lasich and Riddiford (11) have measured the spectrum from a 2.8-Mev. betatron by examining recoil (Compton) electrons produced by the X rays in a cloud chamber. In this experiment the X rays were produced in a 0.02 in. thick tungsten target which cannot be considered thin for electrons of this energy. The spectrum obtained by these authors differs greatly from the Bethe–Heitler theory.

In the Queen's synchrotron the target consists of a tungsten rod about $\frac{1}{4}$ in. in diameter. For the interpretation of other experiments it is necessary to determine the spectrum coming from this target. Presumably the X rays are produced by what one might call glancing blows of the electrons on the target and hence the effective target thickness cannot be determined directly.

To measure the spectrum we have examined a large number of electron pairs produced by the X rays in Ilford G-5 emulsions. This method of using emulsions as a pair spectrometer has been reported previously by King (9) and Voyvodic and Pickup (20). It has the advantage of involving relatively simple equipment and it is generally straightforward. It has the disadvantage, however, of being quite slow; consequently considerable time is required to accumulate sufficient data to ensure statistical accuracy.

THEORY

Schiff (18) has obtained the distribution in energy and angle of photons produced by fast electrons in a thin target, by integrating the differential bremsstrahlung cross section of Bethe and Heitler (1) over the angles of the scattered electron. The differential distribution obtained in this way is also integrated

[1] *Manuscript received May 22, 1952.*
Contribution from the Synchrotron Laboratory, Queen's University, Kingston, Ont.

over the angles of the outgoing photon to give the total or integrated energy spectrum. The calculations assume the Thomas–Fermi model of the atom and are dependent on the Born approximation. Since Parzen (14) has shown that the errors in the energy distribution caused by the Born approximation are appreciable only at large angles, there should be little error in the integrated spectrum as obtained by Schiff since this is due mainly to the radiation in the forward direction.

The radiation from a thick target is altered by several factors not included in the above theory. The electrons are multiply scattered in passing through the target and Schiff (17) has shown that to a good approximation, the distribution in energy at all angles is that given by the integrated cross section. Therefore, in the present experiment, in which the spectrum is measured only in the forward direction, the results are compared with the integrated rather than the differential spectrum in the forward direction. Schiff's expression for the integrated cross section giving the relative number of photons with fractional energies between v and $v + dv$ is

$$\phi(E_0, v)\,dv = \frac{dv}{v}\left\{(1.33 - 1.33\,v + v^2)\left(\ln M + 1 - \frac{2}{b}\tan^{-1}b\right)\right.$$
$$+ (1 - v)\left[\frac{2}{b^2}\ln(1 + b^2) + \frac{2.67 - 1.33b^2}{b^3}\tan^{-1}b\right.$$
$$\left.\left. - \frac{2.67}{b^2} + .222\right]\right\} \tag{1}$$

where

$$\frac{1}{M} = \left(\frac{\mu K}{2E_0E}\right)^2 + \left(\frac{Z^{\frac{1}{3}}}{c}\right)^2, \qquad b = \frac{2E_0EZ^{\frac{1}{3}}}{c\mu K},$$

E_0 = energy of incident electron,
E = energy of scattered electron,
K = energy of photon,
v = K/E_0,
μ = rest energy of electron,
c = 111,
Z = atomic number.

The quantity $v\phi(E_0, v)$ which is proportional to the X-ray intensity is shown plotted for $E = 70$ Mev. and $Z = 74$ in Fig. 1, curve 1.

For further calculations the thickness of the target should be known. In the Queen's synchrotron the effective target thickness is not known accurately, however measurements by Holloway and Janzen of the angular width of the beam indicate a target thickness of the order of 0.05 to 0.1 cm. (obtained by comparing the measured shape with theoretical curves given by Schiff (17)). The spectrum is appreciably affected by a target this thick in two ways, self-absorption of the X rays and a double radiation process. The ionization loss of the electrons in the target can be neglected since this is only of the order of 1 to

3 Mev. The self-absorption can be calculated in the usual way, the relative number of photons with fractional energy between v and $v + dv$ after absorption being approximately

$$\phi(E_0, v)\, dv\, t_0 - \tfrac{1}{2}\phi(E_0, v)\, dv\, t_0^2\, \lambda(K) \tag{2}$$

where $\lambda(K)$ is the total absorption coefficient for photons of energy K and t_0 is the target thickness.

The nature of the double radiation process referred to above can be stated as follows: an electron of energy E_0 radiates a photon of energy K, the electron still has energy $E_0 - K$ and can radiate another photon further on in the target. The effect of this process can be calculated approximately as follows. We want the contribution to the photons of energy between K and $K + dK$ produced by electrons that have already radiated once. The number of these electrons with energy between E and $E + dE$ at a thickness t will be equal to the number of photons that have been radiated in the thickness t with energy between $(E_0 - E)$ and $(E_0 - E) - d(E_0 - E)$ and this number is proportional to

$$t\, \phi\left(E_0, \frac{E_0 - E}{E_0}\right) d\left(\frac{E}{E_0}\right).$$

Therefore the number of photons produced by these electrons in the thickness dt with energies between K and $K + dK$ is

$$t\, dt\, \phi\left(E_0, \frac{E_0 - E}{E_0}\right) d\left(\frac{E}{E_0}\right) \phi\left(E, \frac{K}{E}\right) d\left(\frac{K}{E}\right).$$

Since all of these electrons with energy greater than K will contribute to this, the total effect will be given by

$$\int_0^{t_0} \int_{E=K}^{E_0} \phi\left(E_0, \frac{E_0 - E}{E_0}\right) d\left(\frac{E}{E_0}\right) \phi\left(E, \frac{K}{E}\right) d\left(\frac{K}{E}\right) t\, dt.$$

To evaluate this we make the approximation $\phi(v) = 1/v$ (this being a first approximation for the number of photons of energy v produced per radiation length). Integrating and combining the result with equation (2) taking account of the self-absorption we get approximately that the relative number of photons of fractional energy v coming from a thick target is

$$\phi(E_0, v) - \tfrac{1}{2}\, t_0\, \phi(E_0, v)[\lambda(K) - \ln(1 - v)] \tag{3}$$

where t is in radiation lengths and $\lambda(K)$ is per radiation length. Eyges (5) has obtained an expression similar to this by substituting a power series in t, corresponding to the correct initial conditions, into the shower equations of Rossi and Greisen (16).

Intensity spectra corrected for target thicknesses of 0.05 and 0.1 cm. are given by curves 2 and 3 of Fig. 1. It can be seen that the main effect is a relative lowering of the high energy end. In this experiment the best agreement with theory, above 25 Mev., is obtained if we assume a 0.1 cm. thick target. Therefore, in what follows, the experimental results are compared with the photon distribution obtained from curve 3 of Fig. 1.

The X rays leaving the target pass through the glass wall of the donut and 3 meters of air before reaching the plates. The effect of this is to diminish the intensity almost uniformly above 5 Mev. and hence no correction has been applied for this.

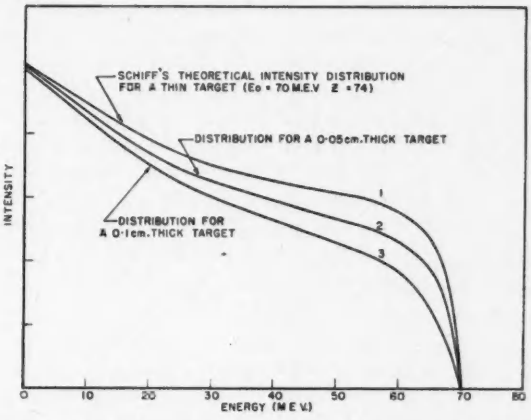

FIG. 1. Integrated intensity spectra for different thicknesses of tungsten targets.

In order to compare the results of this experiment with the above theory a cross section for pair production in the emulsion must be assumed. The quantity $\phi_{(\text{pair})}$ given by Bethe and Heitler (1) is proportional to the pair cross section and is practically independent of Z over the energy range being investigated. Therefore $\phi_{(\text{pair})}$ gives the relative pair cross section for a mixed medium such as an emulsion, provided that it gives the correct relative cross section for the individual elements. That this is the case has been shown by Walker (21), Lawson (12), and others. They find that the measured cross section for pair production in light elements agrees with the Bethe–Heitler theory and that the departures from the theory for elements of high Z are not energy dependent (21). The quantity $\phi_{(\text{pair})}$ taken from Bethe and Heitler's paper has therefore been used to give the relative pair cross section in the emulsion.

PROCEDURE

The Ilford G-5 emulsions were irradiated in an open-end lead box placed in the center of the beam 3 meters from the target. A 4 in. thick lead collimator allowed a cone of X rays of half angle 0.28° to strike the plates which were given approximately 10 milliroentgens of radiation as measured by a thick-walled ionization chamber. The emulsions were then processed using a standard temperature development method to bring out minimum ionization tracks. After they were developed and dried, the plates were searched systematically for electron pairs and the mean angle of scattering measured on each electron in all of the pairs which satisfy certain conditions given below. From the measured mean angle of scattering and Williams (22) multiple scattering theory the

energies of the pairs have been calculated. The method used to measure the scattering and the evaluation of the constants in Williams' theory for G-5 emulsions have been described previously (13).

The probable error in the measured mean deviation and also in the calculated energy is approximately $50/\sqrt{N}\,\%$ (6) where N is the number of independent readings of deviation. The number of readings N that can be obtained from a particular track depends on the length of the track and on the magnitude of the 'spurious scattering' or 'noise level' (7). The 'noise level' of the microscope used in this work has been measured and found to be approximately 0.17μ. In order that the error in the measured mean deviation, due to this 'noise level', should be less than 6% the cell length used in a measurement must be chosen so large that the mean deviation is greater than 0.9μ.

To increase the number of readings of deviation obtained on the shorter tracks, overlapping cells have been used. If we define x to be the degree of overlap, meaning that readings of position are taken a fraction $1/x$ of the cell length apart, then it can be shown approximately that the fraction of the total number of deviations, obtained in this way, that are statistically independent is $2/(x+1)$. This expression has been used to obtain the probable error in an energy determination when overlapping cells have been used.

To ensure that the probable error in the measured energy of an electron is less than a fixed value, only pairs in which both electrons travel at least a given distance in the emulsion are measured. This selection process discriminates against the low energy electrons since they scatter through larger angles and thus have a greater tendency to leave the emulsion before going the given distance. To correct for this energy discrimination, consider a plane through the emulsion perpendicular to its surface and lying in the direction of the X rays. Then the arithmetic mean value $\bar{Y}(E,t)$ of the lateral displacement projected on this plane for an electron of energy E going a distance t is given by the distribution function of Rossi and Greisen (16)

$$\bar{Y}(E,t) = 1/\sqrt{3}\; t\; \bar{\theta}(E,t) \tag{4}$$

where $\bar{\theta}(E,t)$ is the projected arithmetic mean angle of scattering for an electron of energy E and cell length t, which can be calculated from Williams (22) theory for G-5 emulsions. Then if d is the emulsion thickness (400μ here), it is easy to show that the fraction f of electrons of energy E that escape before going a distance t is $\bar{Y}(E,t)/d$. This assumes that the initial direction of the electrons is parallel to the surface of the emulsion, which is very nearly the case. Now suppose we have a number N_T of similar pairs in the emulsion, i.e., pairs in which one electron has energy E_1 and the other E_2, and let f_1 and f_2 be the respective fractions of these electrons that escape before going a distance t. Let N_m be the number in which both electrons travel at least the distance t; i.e., the number measured, then

$$N_T = \frac{N_m}{(1-f_1)(1-f_2)}. \tag{5}$$

Therefore, from the observed number N_m, N_T can be calculated.

These corrections have been applied in two slightly different manners. In the first method we take all the pairs measured in a given energy interval E to $E + \Delta_1 E$ and from these take the pairs in which the energy distribution is the same; i.e., one electron in each pair lies in the interval E_j to $E_j + \Delta_2 E$ and the other in the interval E_k to $E_k + \Delta_2 E$. Let the number of these pairs be N_{jk}; then if f_j and f_k are the average values of the fractions that escape in these energy intervals, the corrected number of pairs with total energy in the interval E to $E + \Delta_1 E$ is

$$N_T = \sum_{jk} \frac{N_{jk}}{(1 - f_j)(1 - f_k)}. \tag{6}$$

The finite width of the interval $\Delta_1 E$ makes the double summation necessary. The intervals $\Delta_1 E$ and $\Delta_2 E$ have been chosen to be 5 Mev.

In the second method the grouping of the electrons into different energy intervals is not the same as above but the final result agrees with that given by equation (6), as it should. Here the energies of both electrons from pairs with total energy in a given 5 Mev. interval are divided by the energy of the pair and a histogram of number of electrons against fractional energy plotted. The corrections to be applied to the electrons at the different fractional energies are obtained from equation (5) taking the pair energy to be the average of all the pairs in the interval. By comparing the corrected distributions obtained in this way with theoretical curves given by Bethe and Heitler (1) for the energy distribution between members of a pair it is possible to check the randomness of the pairs selected, and in particular to ensure that the method does not discriminate against pairs in which the energy division is extremely asymmetric. The theoretical distributions have been verified experimentally by a number of investigators (10, 2, 4). The fact that we cannot distinguish between electrons and positrons offers no difficulty since at these energies the distributions for both are the same. The results of this comparison are discussed below (Fig. 3).

Two different sets of conditions have been used in selecting the pairs to be measured and corresponding corrections for energy discrimination applied. In the first method all the pairs measured can be used but the corrections applied are large, whereas in the second method not all the pairs measured can be used but the corrections to be applied are small.

Method I

Only pairs in which both electrons travel at least 1300μ in the emulsion are measured. The minimum distance apart at which readings are taken is 40μ, the maximum overlap is 2, and the minimum deviation allowed is 0.9μ. These conditions ensure that the probable error in the energy determination is always less than 10%, hence all the pairs measured can be used. The corrections to be applied for pairs not measured are calculated as described above, taking $t = 1300\mu$ which gives $\bar{Y}(E, 1300\mu) = 1630/E$ microns. This along with equations (5) and (6) allows the corrected number of pairs in each energy interval to be calculated by the two methods of grouping the electrons described.

Method II

All pairs in which both electrons travel at least 300μ in the emulsion are measured. Readings are taken at distances along the track such that at least 30 readings are obtained. Not all of these pairs that are measured can be used because the probable error in the energy determination of a high energy electron traveling only 300μ in the emulsion would be very large. Only those pairs are used for which it is possible, for both electrons, to obtain a mean deviation of at least 0.9μ with maximum overlapping of 4. In the worst cases (there are very few of these) the conditions give a maximum probable error of about 15% in the energy determination. The corrections to be applied now are for pairs not measured and for pairs measured but not used. The procedure here is the same as described for method I except that t in the distribution function of equation (4) has no longer a constant value, but depends on the energy of the electrons, being chosen in such a way that all the conditions given above are satisfied. Table I

TABLE I

MAXIMUM ALLOWED ENERGIES FOR THREE TRACK LENGTHS

t,μ	E_{max}, Mev.
300	11
600	32
900	60

gives three values of t and the corresponding maximum energies for which the conditions are just satisfied; i.e., 30 readings of deviation, mean deviation 0.9μ, overlapping of 4.

RESULTS

The energies of 159 pairs have been measured, satisfying the conditions of method I, and the number of these pairs found in the different energy intervals is given by the solid histogram in Fig. 2*a*. Corrections for pairs not satisfying the selection conditions have been applied as described above and the result is given by the broken histogram in Fig. 2*a*. Since the total corrected number of pairs should equal the total number found (those selected plus those discarded) it is possible, from the areas under the two histograms in Fig. 2*a*, to predict the ratio of pairs measured to pairs found; this ratio is 0.45. The ratio can also be measured and from the measurements it is found to be 0.43 which indicates that the corrections applied are of the right order. The randomness of the pairs selected was checked by comparing the measured and theoretical energy distributions of the electrons in the pairs as described above. The results are very similar to those given below for pairs selected by method II except that the corrections applied are much larger.

The corrected number of pairs found in the various energy intervals was divided by the corresponding cross section for pair production giving numbers proportional to the number of photons in the X-ray beam at these energies.

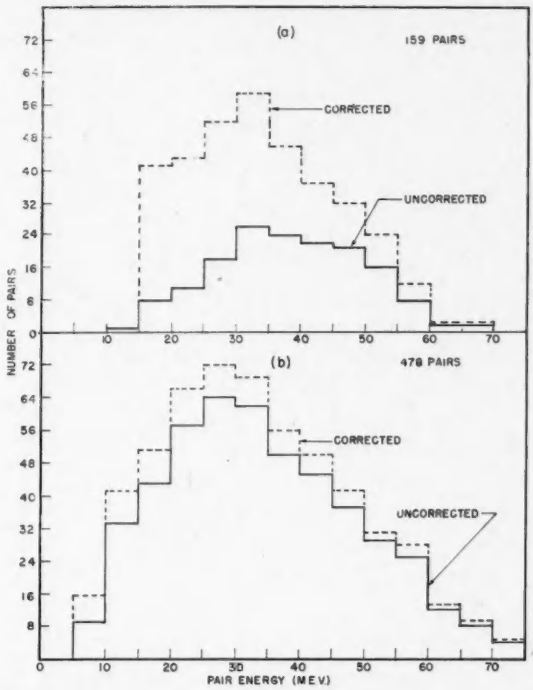

FIG. 2. Electron pair energy spectrum. (*a*) From pairs satisfying conditions of method I. (*b*) From pairs satisfying conditions of method II.

The results of this procedure have been compared with the theoretical photon distribution (the intensity divided by v) by drawing through the experimental points a theoretical curve which gives what appears to be the best fit. To do this and also to aid in comparing the shapes of the theoretical and experimental distributions independently of the normalization, both have been transformed in such a way that the theoretical distribution is a horizontal straight line. This is shown in Fig. 4*a* in which the theoretical curve giving the best fit (the straight line shown) has been drawn through the points. Obviously this is not the best fit curve for the experimental points. Both distributions have been transformed back to their normal shapes and are given in Fig. 5*a*. Figs. 4*a* and 5*a* indicate that the number of photons below 25 Mev. may be less than that predicted by theory; however, nothing definite can be said as the statistics are poor and the points only extend down to 17.5 Mev. The discrepancy above 60 Mev. is not significant as only four pairs were measured, by this method, with energies between 60 and 70 Mev.

The energies of another 478 pairs have been measured satisfying the conditions of method II and the number of these found at the different energies is

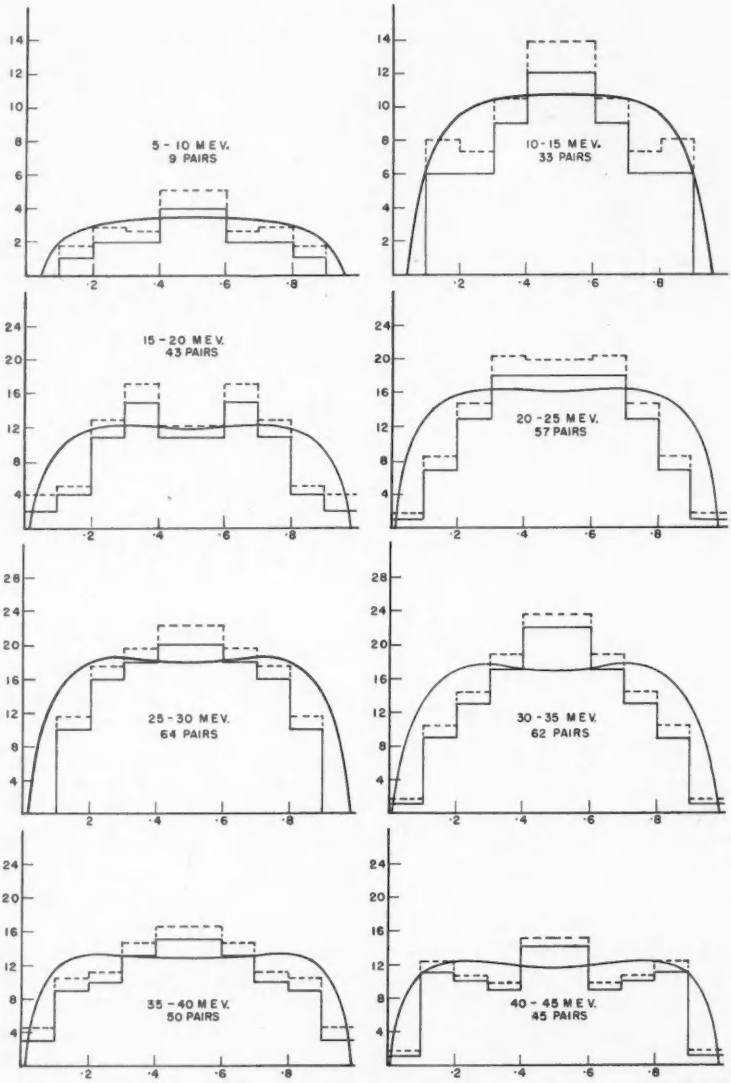

FIG. 3. The energy distribution of pairs. The solid histograms are plots of the number of positive and negative electrons against their fractional energies (i.e., energy of electron divided by the total pair energy) for pairs selected by method II. The broken histograms are the corrected numbers. The smooth curves shown are the theoretical distributions given by Bethe and Heitler.

given by the solid histogram in Fig. 2*b*. Corrections appropriate to this method have been applied as described above and the corrected distribution is also given in Fig. 2*b*. Again from the areas under the two histograms in Fig. 2*b* the ratio of the number of pairs satisfying all the conditions to the number found can be predicted—it is 0.88. The measured ratio is 0.9 and again the agreement is satisfactory.

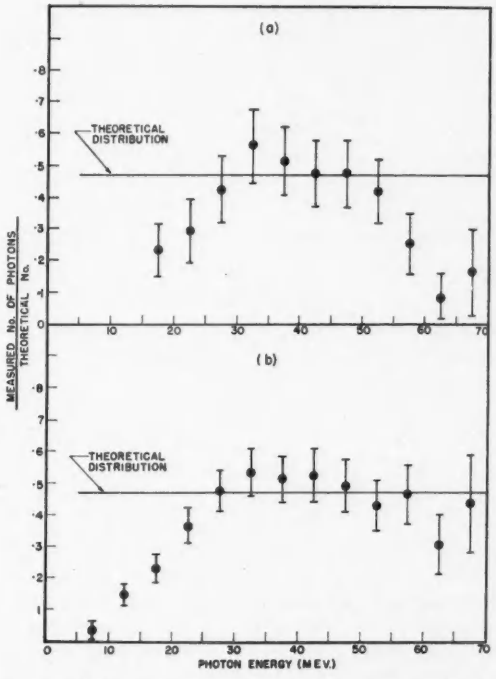

FIG. 4. Experimental and theoretical photon distributions transformed so that the theoretical distribution is a horizontal straight line. (*a*) Method I. (*b*) Method II.

The randomness of the pairs selected by this method has been checked and the results are shown in Fig. 3 which gives plots of the number of electrons, from pairs in the different intervals, against their fractional energy. The smooth curves shown are those given by Bethe and Heitler (1) and these have been normalized to represent the same number of electrons as do the corrected distributions (broken histograms) between the fractional energies 0.1 to 0.9. The agreement is seen to be fair although the measured distributions are in general slightly more peaked. However, in view of the poor statistics it can at least be said that they do not disagree with theory. Certainly any discrepancy that there is between the measurements and theory here is not large enough to account for the shape of the resulting spectrum. In fact, practically the same spectrum is

obtained if we normalize the theoretical curve to the central part of the measured distribution (i.e., between .3 and .7) and take the area under this theoretical curve to give a measure of the number of pairs in this interval.

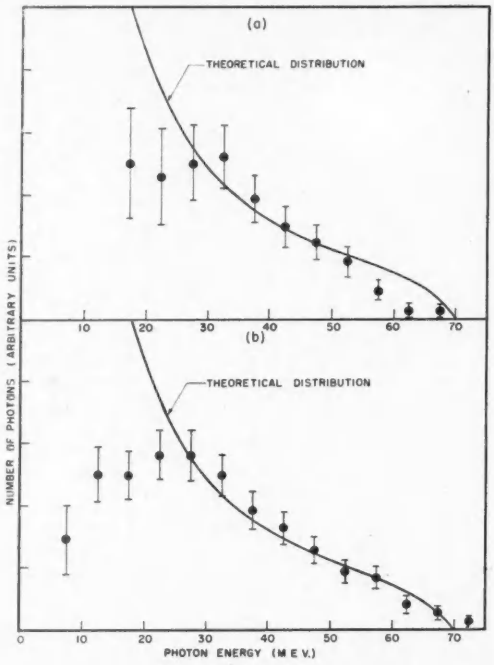

FIG. 5. Number of photons as a function of energy. (*a*) Method I. (*b*) Method II.

The photon distribution has been obtained and compared with the theoretical distribution as described for method I. The distributions have been normalized so that the theoretical curves giving the best fit for the two methods coincide. This is shown in Figs. 4*b* and 5*b* and it can be seen that the spectra obtained by the two methods of selecting the pairs agree reasonably well, although the results of method II are of course the more reliable. Figs. 4*b* and 5*b* indicate that the number of photons below 25 Mev. is considerably less than that predicted by theory.

The photon distributions obtained using both methods have been combined by taking weighted averages of the ordinates of Figs. 5*a* and 5*b* for each energy interval. The weighting factors, for a particular interval, have been taken proportional to the number of pairs measured in that interval by the respective methods. The resulting photon distribution for 637 pairs is shown along with the theoretical distribution for a 0.1 cm. thick target in Fig. 6. The agreement with theory above 25 Mev. is seen to be quite good, if we assume a target this

thick, and the discrepancy below 25 Mev. is again evident. The errors indicated throughout are given by $\pm 100/\sqrt{N}$ % where N is the number of pairs measured in the particular interval.

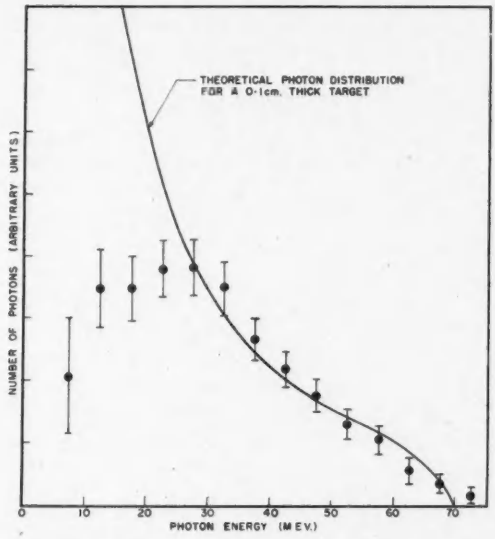

FIG. 6. Number of photons as a function of energy. The theoretical curve is Schiff's integrated distribution corrected for a 0.1 cm. thick target.

The photon spectrum we have found is approximately independent of energy in the region 15 to 25 Mev. and this is in agreement with recent measurements made in this laboratory by L. S. Edwards (to be published). In these experiments metal foils are irradiated in the X-ray beam and the saturation activity, i.e., the activity produced in the foils by an infinitely long irradiation, is measured. From this a 'relative yield' for the reaction is calculated. The 'yield' is defined as the ratio of the saturation activity per milligram atom of the parent isotope to the saturation activity in a given amount of polystyrene. This definition leads to the approximate expression

$$\frac{Y_1}{Y_2} = \frac{N_1}{N_2} \cdot \frac{\int \sigma_1(E)\, dE}{\int \sigma_2(E)\, dE} \tag{7}$$

for the ratio of two 'yields', where Y is the 'yield' measured here, N is the number of photons per Mev. around the average energy producing the reaction, and $\int \sigma(E)\, dE$ is the integrated cross section. If the integrated cross sections are known, then N_1/N_2, the ratio of the number of photons around different energies, can be calculated from equation (7). This has been done, using the 'yields' for several elements, and the results have been compared with the corresponding ratios given by the pair measurements and the theory. Table II gives the data

necessary for the calculation; the integrated cross sections and the average energies producing the reactions are those given by the Saskatchewan group (8), and Diven and Almy (3). Table III gives values of the ratios determined in the three ways and it can be seen that the ratios given by the 'yield' measurements agree roughly with those given by the pair measurements* but certainly do not agree with those predicted by theory.

TABLE II

LATEST 'YIELDS' OF (α,n) REACTIONS IN FIVE ELEMENTS AS MEASURED IN THIS LABORATORY BY L. S. EDWARDS, ALSO INTEGRATED CROSS SECTIONS AND AVERAGE ENERGIES PRODUCING THESE REACTIONS OBTAINED FROM REFERENCES (3) AND (8)

Element	Yield measured here	Average energy of reaction, Mev.	Integrated cross section, Mev-barns
C^{12}	0.10	24	0.046
Mo^{92}	1.74	18.7	0.85
Cu^{65}	1.76	18	1.11
Cu^{63}	1.27	17	0.66
Ag^{109}	2.92	15	1.65

The values of the integrated cross sections quoted are not likely known to better than 20%, but only the ratios of these, which are presumably more accurate, have been used here. However the discrepancy between the ratios given by the 'yields' and the theory in Table III is on the average 85% and hence is significant in any case. Thus the yield measurements do support the pair measurements.

TABLE III

RATIOS OF THE NUMBER OF PHOTONS AROUND ONE ENERGY OF TABLE II TO THAT AROUND ANOTHER

	No. at 18.7 Mev. / No. at 24 Mev.	No. at 18 Mev. / No. at 24 Mev.	No. at 17 Mev. / No. at 24 Mev.	No. at 15 Mev. / No. at 24 Mev.
From yield measurements	0.94	0.73	0.89	0.81
From pair measurements	$\backsim 1$	$\backsim 1$	$\backsim 1$	$\backsim 1$
From Schiff's theory	1.38	1.47	1.59	1.86

DISCUSSION

As only 637 pairs have been measured the statistics are not as good as they might be. However, the large discrepancy at the low energy end is difficult to account for entirely by poor statistics, since in all 163 pairs have been measured with energies between 5 and 25 Mev. Hence, until further experiments can be

* *The ratios given by the yields are on the average 19% lower than those given by the pair measurements. This might be expected since the value 0.046 (used here for the C^{12} integrated cross section) does not include any contribution from energies higher than 30 Mev. (Sagane, R. Phys. Rev. 84: 587. 1951.) while the value 0.10 used for the C^{12} 'yield' does. This would make the ratio of the C^{12} integrated cross section to the 'yield' too small and possibly account for the above difference.*

performed, it has been concluded that the number of photons below 25 Mev., in the central cone of half angle 0.28°, is considerably less than that expected from theory. The 'yield' measurements referred to above appear to support this result.

It should be mentioned that the energy of the electrons in the donut is not known to better than ±4 Mev. One might therefore compare the results with a theoretical curve for 66-Mev. electrons which would make the discrepancy at the lower energies slightly less but would increase it at the higher energies. However, since pairs were found with energies as high as 75 Mev. (with probable error in energy no more than ±8 Mev.) and since the agreement with the theory for 70-Mev. electrons is good above 25 Mev. it is felt that there is no very good reason for choosing any energy other than 70 Mev. The particular way in which the theory has been normalized to the results is of course not unique either, but however this is done it will not alter the large difference in shape of the two distributions below 25 Mev.

This lack of photons at the lower energies is very difficult to explain in the light of the other spectrum determinations mentioned above. It is possible, though, that in the radiation from a circular target nearly $\frac{1}{4}$ in. in diameter the proportion of low energy photons in the center of the beam is less than that at larger angles. We are not suggesting here that the Bethe–Heitler theory for a thin target is incorrect, obviously it is not. However, there does appear to be a need for further investigation of the radiation from very thick targets.

ACKNOWLEDGMENTS

I wish to thank Dr. J. A. Gray for suggesting this problem and for his continued interest and help throughout the course of the work. I am also indebted to Mrs. Stewart and Mrs. Varley for carefully performing many scattering measurements and to Mrs. Laphen for scanning several plates. Finally, I wish to thank the National Research Council of Canada for financial assistance.

REFERENCES

1. BETHE, H. and HEITLER, W. Proc. Roy. Soc. (London), A, 146: 83. 1934.
2. DEWIRE, J. W. and BEACH, L. A. Phys. Rev. 83: 476. 1951.
3. DIVEN, B. C. and ALMY, G. M. Phys. Rev. 80: 407. 1950.
4. EMIGH, C. R. Phys. Rev. 86: 1028. 1952.
5. EYGES, L. Phys. Rev. 81: 981. 1951.
6. GOLDSCHMIDT-CLERMONT, Y., KING, D. T., MUIRHEAD, H., and RITSON, D. M. Proc. Phys. Soc. (London), 61: 183. 1948.
7. GOTTSTEIN, K., MENON, M. G. K., MULVEY, J. H., O'CEALLAIGH, C., and ROCHAT, O. Phil. Mag. 42: 708. 1951.
8. KATZ, L. and CAMERON, A. G. W. Can. J. Phys. 29: 518. 1951, and private communication.
9. KING, D. T. Nature, 165: 526. 1950.
10. KOCH, H. W. and CARTER, R. E. Phys. Rev. 77: 165. 1950.
11. LASICH, W. B. and RIDDIFORD, L. J. Sci. Instruments, 24: 177. 1947.
12. LAWSON, J. L. Phys. Rev. 75: 440. 1949.
13. MCDIARMID, I. B. Phys. Rev. 84: 851. 1951.
14. PARZEN, G. Phys. Rev. 81: 808. 1951.
15. POWELL, W. M., HARTSOUGH, W., and HILL, M. Phys. Rev. 81: 213. 1951.
16. ROSSI, B. and GREISEN, K. Revs. Modern Phys. 13: 241. 1941.
17. SCHIFF, L. I. Phys. Rev. 70: 87. 1946.
18. SCHIFF, L. I. Phys. Rev. 83: 252. 1951.
19. STOKES, R. H. Phys. Rev. 84: 991. 1951.
20. VOYVODIC, L. and PICKUP, E. Phys. Rev. 81: 471. 1951.
21. WALKER, R. L. Phys. Rev. 76: 527, 1440. 1949.
22. WILLIAMS, E. J. Phys. Rev. 58: 292. 1940.

BOUNDARY CONDITIONS IN THE MECHANICS OF FIELDS[1]

By S. M. Neamtan and E. Vogt[2]

ABSTRACT

A variational principle has been set up for the description of relativistic fields with the aid of Lagrangians involving second order derivatives of the field functions. This constitutes a generalization of the usual formulation in that, besides the boundary conditions usually imposed, it admits also linear homogeneous boundary conditions. The formulation has been developed for the complex scalar and complex vector fields. The variational principle then yields not only the wave equations but also the allowed boundary conditions. A Hamiltonian and equations of motion in canonical form can be set up. A symmetric stress–energy tensor and a charge–current vector are defined, yielding the usual conservation equations. For the vector field, π_4 is not identically zero; also the Lorentz condition arises out of the variational principle and does not have to be separately imposed. For the Dirac field an extension to Lagrangians with second order derivatives is not possible, but for this field also the variational principle yields the allowed boundary conditions.

1. INTRODUCTION

The motion of a wave field in a finite spatial region is governed not only by the wave equation to be satisfied by the field but also by conditions imposed at the boundary of the region. In general, in the description of such a field by means of a variational principle, various different Lagrangian densities can be used in setting up the action integral, all of which yield the same wave equation as the Euler–Lagrange equation of the variational problem. The difference in the nature of the physical systems described by two such Lagrangians becomes apparent only when one considers the possible boundary conditions with which they are compatible. In considering a field which satisfies a homogeneous linear equation like the Klein–Gordon equation, we require that the boundary conditions satisfy a superposition principle and be such as can lead to a complete orthonormal set of eigenfunctions in terms of which an arbitrary field function can be expanded. Three such boundary conditions, which we shall refer to henceforth as the "usual boundary conditions", are

$$\text{(1.1)} \qquad \begin{aligned} &1. \quad \psi = 0 \text{ on } S, \\ &2. \quad \frac{\partial \psi}{\partial n} = 0 \text{ on } S, \\ &3. \quad \psi \text{ periodic in } V. \end{aligned}$$

In the above we consider the field enclosed in a spatial volume V, bounded by a fixed surface S. ψ is the field function and $\partial/\partial n$ represents differentiation along

[1] *Manuscript received July 10, 1952.*
Contribution from the Department of Mathematical Physics, University of Manitoba, Winnipeg, Man.
A brief account of this work was presented at the Quebec meeting of the Canadian Association of Physicists on May 29, 1952. This paper is based on a thesis presented to the Faculty of Graduate Studies and Research of the University of Manitoba, by one of the authors (E.V.), in partial fulfillment of the requirements for the degree of Master of Science.
[2] *Holder of an N. R. C. Bursary, 1951-52.*

the outward-drawn normal to S. Another boundary condition which satisfies the requirements is the linear homogeneous boundary condition,

$$\frac{\partial \psi}{\partial n} = \gamma \psi \text{ on } S, \tag{1.2}$$

where γ is a constant.

It will be shown below that, in contrast with the usual boundary conditions, the linear homogeneous boundary condition for the scalar and vector fields is not admitted by a variational principle constructed with the aid of the first order Lagrangians ordinarily employed in the description of these fields. In order to accommodate the linear homogeneous boundary condition as well as the usual boundary conditions it is necessary to use Lagrangians which contain second order derivatives (and not first order derivatives) of the field functions.

The use of Lagrangians with second order derivatives demands a considerable number of modifications in the discussion of the fields, both in regard to setting up canonical equations of motion and conservation theorems, as well as to their physical interpretation in the case of the linear homogeneous boundary conditions.

2. THE REAL SCALAR FIELD AND THE VARIATIONAL PRINCIPLE

The nature of the variational principle and the restrictions to be imposed in the choice of a Lagrangian for the specification of a field both in regard to the wave equation and the boundary conditions to be satisfied can be best illustrated by the simple example of a real scalar field. We consider a real scalar function ψ which is to satisfy the Klein–Gordon equation

$$\partial_\alpha \partial_\alpha \psi = \mu^2 \psi \tag{2.1}$$

where μ is a real constant.* We seek a Lorentz invariant Lagrangian density, a function of ψ and its derivatives, which when used in setting up an action integral whose variation is to vanish will yield (2.1) as the Euler–Lagrange equation. Since equation (2.1) is linear, homogeneous, and of second order, the Lagrangian density must be homogeneous quadratic in ψ and must not contain derivatives of ψ of higher order than the second. We must then take for our Lagrangian density the form

$$\mathscr{L} = \tfrac{1}{2}[A\psi^2 + B(\partial_\alpha \psi)(\partial_\alpha \psi) + C\psi \partial_\alpha \partial_\alpha \psi] \tag{2.2}$$

where A, B, and C are constants whose values are for the moment left unspecified.

We are now interested in the motion of the field in a fixed spatial volume. We therefore assume ψ to be defined in a region τ of space–time bounded by a cylinder with generators parallel to the x_4 axis. The intersection of any plane, $x_4 =$ constant, with τ is a volume, V, in the three-dimensional subspace defined

**The notation used throughout the paper is as follows: x_1, x_2, x_3, and t represent respectively three cartesian coordinates and the time. With the velocity of light set equal to unity, $x_4 = it$. $\partial_\alpha \equiv \partial/\partial x_\alpha$. Greek indices take on the values 1,2,3,4 and Latin indices the values 1,2,3. Except where otherwise indicated, summation is to be understood over repeated indices. An asterisk superscript indicates the complex conjugate.*

by the spatial coordinates x_1, x_2, x_3. The boundary of V is the fixed two-dimensional surface S. We define the action integral

$$I \equiv \int_{x_4^0}^{x_4^1} \int_V \mathscr{L}\, d\tau \tag{2.3}$$

where x_4^0 and x_4^1 are two values of x_4 and $d\tau$ is the four-dimensional element of volume. We now state the variational principle as follows. For arbitrary values of x_4^0 and x_4^1

$$\delta I = 0 \tag{2.4}$$

subject to the following conditions on the variation of ψ. $\delta\psi$ is to be completely arbitrary except at x_4^0 and x_4^1 where it is to vanish together with its first derivatives, $\delta\partial_\alpha\psi$, and on S where it is to be consistent with the boundary conditions. This principle differs from the usual one invoked in this connection in that we do not require $\delta\psi$ to vanish everywhere on the boundary of our space–time region. If for the moment we write

$$\mathscr{L} \equiv \mathscr{L}(\psi, \partial_\alpha\psi, \partial_\alpha\partial_\alpha\psi) \tag{2.5}$$

equation (2.4) reduces after some manipulation and with the aid of the conditions imposed on $\delta\psi$ to the following form:

$$\begin{aligned} 0 = \delta I = \int_{x_4^0}^{x_4^1} \int_S \left\{ \frac{\partial \mathscr{L}}{\partial(\partial_\alpha\psi)}\,\delta\psi + \frac{\partial \mathscr{L}}{\partial(\partial_\gamma\partial_\gamma\psi)}\,\partial_\alpha\delta\psi - \left(\partial_\alpha \frac{\partial \mathscr{L}}{\partial(\partial_\gamma\partial_\gamma\psi)}\right)\delta\psi \right\} n_\alpha\, dS\, dx_4 \\ + \int_{x_4^0}^{x_4^1} \int_V \left\{ \frac{\partial \mathscr{L}}{\partial\psi} - \partial_\alpha \frac{\partial \mathscr{L}}{\partial(\partial_\alpha\psi)} + \partial_\alpha\partial_\alpha \frac{\partial \mathscr{L}}{\partial(\partial_\gamma\partial_\gamma\psi)} \right\}\delta\psi\, d\tau. \end{aligned} \tag{2.6}$$

Here n_α is the unit normal to S.

Because of the arbitrariness of $\delta\psi$ within V, it is clear that the two integrals that appear in equation (2.6) must vanish individually; in fact the coefficient of $\delta\psi$ in the second integral must vanish, and if the equation is to be valid for arbitrary values of x_4^0 and x_4^1 the surface integral that appears in the first integral in (2.6) must be set equal to zero. Thus the variational principle yields the two equations,

$$\frac{\partial \mathscr{L}}{\partial\psi} - \partial_\alpha \frac{\partial \mathscr{L}}{\partial(\partial_\alpha\psi)} + \partial_\alpha\partial_\alpha \frac{\partial \mathscr{L}}{\partial(\partial_\gamma\partial_\gamma\psi)} = 0 \tag{2.7}$$

and

$$\int_S \left\{ \frac{\partial \mathscr{L}}{\partial(\partial_\alpha\psi)}\,\delta\psi + \frac{\partial \mathscr{L}}{\partial(\partial_\gamma\partial_\gamma\psi)}\,\partial_\alpha\delta\psi - \left(\partial_\alpha \frac{\partial \mathscr{L}}{\partial(\partial_\gamma\partial_\gamma\psi)}\right)\delta\psi \right\} n_\alpha\, dS = 0. \tag{2.8}$$

Equation (2.7) is the Euler–Lagrange equation which is to be identified with the wave equation for the field through a suitable choice of the constants that

appear in the Lagrangian (2.2). The requirement that the surface integral in (2.8) shall vanish yields the boundary conditions that are compatible with a particular choice of $\mathscr{L}$.

With the aid of equation (2.2) equations (2.7) and (2.8) can be reduced to the following forms

$$A\psi + (C - B)\partial_\alpha\partial_\alpha\psi = 0, \tag{2.9}$$

$$\int_S \left\{\left(B - \frac{C}{2}\right)(\partial_\alpha\psi)\delta\psi + \frac{C}{2}\psi\partial_\alpha\delta\psi\right\}n_\alpha\, dS = 0. \tag{2.10}$$

Equation (2.9) reduces to the wave equation (2.1) if A, B, and C are chosen such that

$$\frac{A}{B - C} = \mu^2. \tag{2.11}$$

Thus the required equation can be obtained from a Lagrangian containing both first and second derivatives of ψ, and there exist a variety of different Lagrangians all of which lead to the same wave equation. This fact is of course well known. What requires especial emphasis is the fact that through the requirement that equation (2.10) be satisfied, the type of boundary condition which can be imposed on the field is dependent on the specific choice of a Lagrangian from amongst all those which lead to the same wave equation. This does not seem to have been clearly pointed out before.*

Examination of equation (2.10) reveals that it is satisfied by the usual boundary conditions (1.1) for arbitrary values of B and C. If, however, it is to be satisfied also by the linear homogeneous boundary condition (1.2), the constant B must be set equal to zero.** This means that the Lagrangian is to contain derivatives of second order but not of first order. Such a Lagrangian is of a more general nature than one containing first order derivatives in that it accommodates a wider class of boundary conditions.

The above treatment of the real scalar field can be carried over with very little change to the complex scalar and complex vector fields. The results are similar. The variational principle yields not only the wave equations but also the nature of the admissible boundary conditions through the requirement that certain integrals over the boundary S shall vanish. As in the case of the real scalar field it is found that in order to accommodate linear homogeneous boundary conditions as well as the usual boundary conditions Lagrangians must be chosen which contain second order derivatives of the field functions but not their first order derivatives. These results will be assumed in what follows and the appropriate Lagrangians will be set down without carrying through the argument on which their adoption is based.

**See, for example, References 1,2,3,5. These authors carry through a development which requires that the action principle yield the field equations, while the boundary conditions are added to the formalism in an ad hoc manner whenever required. Thus, for example, the boundary integral in (2.10) is dismissed by requiring that $\delta\psi$ vanish on S.*

***It should be borne in mind that our variational principle requires that $\delta\psi$ be consistent with the boundary conditions, that is, $\delta\psi$ must satisfy any boundary conditions imposed on ψ.*

3. THE SCALAR FIELD

The complex scalar field equations are:

$$\partial_\alpha\partial_\alpha\psi = \mu^2\psi, \qquad \partial_\alpha\partial_\alpha\psi^* = \mu^2\psi^*. \tag{3.1}$$

For this field, the generalized Lagrangian density, which allows the use of linear homogeneous boundary conditions, is given by

$$\mathscr{L} = -\mu^2\psi\psi^* + \tfrac{1}{2}(\psi\partial_\alpha\partial_\alpha\psi^* + \psi^*\partial_\alpha\partial_\alpha\psi). \tag{3.2}$$

The results obtained with the use of this Lagrangian density will be compared with those obtained with the use of the Lagrangian density, $\mathscr{L}'$, which is usually employed in the discussion of the complex scalar fields,

$$\mathscr{L}' = -\mu^2\psi\psi^* - (\partial_\alpha\psi)(\partial_\alpha\psi^*).$$

By following a procedure similar to that employed in the preceding discussion of the real scalar field, it can be shown that for all the usual boundary conditions the use of $\mathscr{L}$, in the action principle, is entirely equivalent to the use of $\mathscr{L}'$ in this principle. However, the usual Lagrangian density, $\mathscr{L}'$, does not allow the use of linear homogeneous boundary conditions.

The Lagrangian density for the complex scalar field should lead in a natural manner to the construction of a Hamiltonian function and the expressions for the momentum, angular momentum, and charge densities of the field. These functions should enter into the conservation theorems associated with the motion of the wave field. This aspect of the classical (unquantized) theory will be developed here for the generalized Lagrangian density.

We define the momentum fields π and π^* conjugate to ψ and ψ^* and the Hamiltonian density $\mathscr{H}$, for the complex scalar field, by

$$\pi \equiv \dot{\psi}^*, \qquad \pi^* \equiv \dot{\psi},$$

$$\begin{aligned}\mathscr{H} &\equiv \pi\dot{\psi} + \pi^*\dot{\psi}^* - \psi\psi^* + \mu^2\psi\psi^* - \tfrac{1}{2}(\psi\partial_k\partial_k\psi^* + \psi^*\partial_k\partial_k\psi) \\ &= \pi\pi^* + \mu^2\psi\psi^* - \tfrac{1}{2}(\psi\partial_k\partial_k\psi^* + \psi^*\partial_k\partial_k\psi).\end{aligned} \tag{3.3}$$

It is shown in the Appendix that these are natural definitions in a theory employing the generalized Lagrangian density. The usual definitions of these field quantities following from the usual Lagrangian density, $\mathscr{L}'$, are:

$$\pi' \equiv \frac{\partial\mathscr{L}'}{\partial\dot{\psi}} = \dot{\psi}^*, \qquad \pi^{*\prime} \equiv \frac{\partial\mathscr{L}'}{\partial\dot{\psi}^*} = \dot{\psi},$$
$$\mathscr{H}' \equiv \pi'\dot{\psi} + \pi^{*\prime}\dot{\psi}^* - \mathscr{L}' = \pi'\pi^{*\prime} + \mu^2\psi\psi^* + (\partial_k\psi)(\partial_k\psi^*). \tag{3.4}$$

The canonical Hamilton equations for the complex scalar field may be obtained by replacing $\mathscr{L}$ by $-\mathscr{H} + \pi\pi^*$ in the action principle for this field. In order to write down the results obtained for the generalized Hamiltonian

density, $\mathscr{H}$, we define the functional derivatives $\delta\mathscr{H}/\delta\psi$, $\delta\mathscr{H}/\delta\psi^*$, $\delta\mathscr{H}/\delta\pi$, and $\delta\mathscr{H}/\delta\pi^*$ of $\mathscr{H}$ in the following way:

$$\frac{\delta\mathscr{H}}{\delta\psi} \equiv \frac{\partial\mathscr{H}}{\partial\psi} + \partial_j\partial_j\frac{\partial\mathscr{H}}{\partial(\partial_k\partial_k\psi)} \tag{3.5}$$

with similar definitions for $\delta\mathscr{H}/\delta\psi^*$, $\delta\mathscr{H}/\delta\pi$, and $\delta\mathscr{H}/\delta\pi^*$. Then the canonical equations of motion are

$$\begin{aligned} \dot{\psi} &= \frac{\delta\mathscr{H}}{\delta\pi}, \qquad \dot{\pi} = -\frac{\delta\mathscr{H}}{\delta\psi}, \\ \dot{\psi}^* &= \frac{\delta\mathscr{H}}{\delta\pi^*}, \qquad \dot{\pi}^* = -\frac{\delta\mathscr{H}}{\delta\psi^*} \end{aligned} \tag{3.6}$$

and using the explicit definition of the generalized Hamiltonian density, (3.3), these equations are

$$\dot{\psi} = \frac{\delta\mathscr{H}}{\delta\pi} = \pi^* = \dot{\psi}, \text{ an identity,}$$

and

$$\dot{\pi} = -\frac{\delta\mathscr{H}}{\delta\psi} = -\mu^2\psi^* + \tfrac{1}{2}\partial_k\partial_k\psi^* + \tfrac{1}{2}\partial_k\partial_k\psi^*$$

which is the field equation for ψ^*. Similarly the other two canonical equations yield an identity and

$$\partial_\alpha\partial_\alpha\psi - \mu^2\psi = 0,$$

the other field equation.

In order to identify $\mathscr{H}$ with the energy density for the complex scalar field and in order to obtain some of the other field quantities for the complex scalar field, a stress–energy tensor will be defined. Using the complex scalar field equations the generalized Hamiltonian density, $\mathscr{H}$, (3.3), may be written

$$\mathscr{H} = -(\partial_4\psi)(\partial_4\psi^*) + \tfrac{1}{2}(\psi\partial_4\partial_4\psi^* + \psi^*\partial_4\partial_4\psi). \tag{3.7}$$

It is desired to construct a symmetric tensor, $T_{\mu\nu}$, of second rank whose 4-4 component is the negative of $\mathscr{H}$. That is

$$T_{44} = -\mathscr{H}. \tag{3.8}$$

Such a tensor is obviously

$$T_{\mu\nu} \equiv \tfrac{1}{2}\{(\partial_\mu\psi)(\partial_\nu\psi^*) + (\partial_\nu\psi)(\partial_\mu\psi^*) - \psi\partial_\mu\partial_\nu\psi^* - \psi^*\partial_\mu\partial_\nu\psi\}. \tag{3.9}$$

If this is the correct form of $T_{\mu\nu}$, then we shall expect that the conservation theorems associated with $T_{\mu\nu}$ may be summarized by

$$\partial_\mu T_{\mu\nu} = 0. \tag{3.10}$$

This equation is an immediate consequence of the definition of $T_{\mu\nu}$, (3.9), and of the scalar field equations.

In the formulation of the complex scalar field with the usual Lagrangian density the stress–energy tensor, $T_{\mu\nu}'$, is defined

$$T_{\mu\nu}' = (\partial_\mu\psi)(\partial_\nu\psi^*) + (\partial_\nu\psi)(\partial_\mu\psi^*) + \mathscr{L}'\delta_{\mu\nu} \tag{3.11}$$

where $\delta_{\mu\nu} = 0 \quad \nu \neq \mu,$

$= 1 \quad \nu = \mu.$

This definition of $T_{\mu\nu}'$ is consistent with the definition of the usual Hamiltonian density $\mathscr{H}'$. If we define

$$S_k \equiv -iT_{k4} \tag{3.12}$$

then the time-component ($\nu = 4$) of (3.10) is

$$\frac{\partial \mathscr{H}}{\partial t} + \partial_k S_k = 0 \tag{3.13}$$

which will be shown to be the continuity equation for the energy of the complex scalar field. We shall identify $\mathscr{H}$ with the energy density and S_k with the energy flux density of the complex scalar field. Such an identification is easily effected for a scalar field with any of the usual boundary conditions. For such a field the total energy is given by the usual integrated Hamiltonian, H',

$$H' \equiv \int_V \mathscr{H}'\, dV. \tag{3.14}$$

For the usual boundary conditions this is identical with the generalized integrated Hamiltonian, H,

$$H \equiv \int_V \mathscr{H}\, dV \tag{3.15}$$

since

$$\begin{aligned} H - H' &= -\int_V \{\tfrac{1}{2}(\psi\partial_k\partial_k\psi^* + \psi^*\partial_k\partial_k\psi) + (\partial_k\psi)(\partial_k\psi^*)\}dV \\ &= -\int_S \{\psi\partial_k\psi^* + \psi^*\partial_k\psi\}n_k\, dS \end{aligned} \tag{3.16}$$

which vanishes for all the usual boundary conditions. Therefore for a complex scalar field with these boundary conditions H is the total energy of the field and thus $\mathscr{H}$ may be identified with the energy density of the field.

The identification of the Hamiltonian density with the energy density of the wave field may be extended, using $\mathscr{H}$ (and not $\mathscr{H}'$), to include physical systems consisting of complex scalar fields under linear homogeneous boundary conditions. For such a system the boundary conditions may imply the existence of a boundary energy. We define a surface energy density $\mathscr{E}_B$ by

$$\mathscr{E}_B = -(\psi\partial_k\psi^* + \psi^*\partial_k\psi)n_k \tag{3.17}$$

so that we may write

$$\int_V \mathscr{H}\, dV = \int_V \mathscr{H}'\, dV + \int_S \mathscr{E}_B\, dS. \tag{3.18}$$

Then $\mathscr{H}$ is clearly the energy density not only within V but also for the boundary S. $\mathscr{H}$ is the energy density for the whole system. The energy of the boundary, E_B ($= \int_S \mathscr{E}_B ds$), will not, in general, remain constant in time. That is, an exchange of energy will occur between the field and the boundary. However, the continuity equation for energy holds at every point of the field region. From it

we should expect that the total energy of the system is conserved. The net flux of energy from the combined system of field plus boundary is given by

$$\int_S S_k n_k \, dS = -\frac{i}{2}\int_S \{(\partial_k\psi)(\partial_4\psi^*) + (\partial_k\psi^*)(\partial_4\psi) - \psi\partial_4\partial_k\psi^* - \psi^*\partial_4\partial_k\psi\} n_k \, dS$$

$$= -\frac{1}{2}\int_S \left\{\psi^*\frac{\partial\psi}{\partial n} + \psi\frac{\partial\psi^*}{\partial n} - \psi\frac{\partial}{\partial t}\frac{\partial\psi^*}{\partial n} - \psi^*\frac{\partial}{\partial t}\frac{\partial\psi}{\partial n}\right\} dS$$

$$= 0$$

for all the usual boundary conditions and for linear homogeneous boundary conditions. The continuity equation for the energy of the field allows us to write this result in the form

$$0 = \int_S S_k n_k \, dS = \frac{\partial H}{\partial t} = \frac{\partial H'}{\partial t} + \frac{\partial E_B}{\partial t}.$$

Thus the total energy, H, of the system is conserved. However, energy may flow from the field into or out of the boundary. That is, neither $\partial H'/\partial t$ nor $\partial E_B/\partial t$ need vanish separately. Essentially the generalization of the Lagrangian density has allowed us to discuss wave fields for which the energy is not conserved. It has done this by allowing a particular type of energy source at the boundary of the field.

The momentum density, G_k, of the complex scalar field may be defined by

$$G_k = -iT_{4k}. \tag{3.19}$$

Then the k-component of the general continuity equation (3.10) is the conservation equation for the k-component of the momentum of the field. The conservation of the angular momentum is, in the usual manner, a direct consequence of the symmetry of $T_{\mu\nu}$.

If the field has linear homogeneous boundary conditions an exchange of momentum or angular momentum may occur between the field and the boundary. The functions defined here include the momentum or angular momentum of both the field and the boundary. However, continuity equations hold for the whole system. The generalized stress–energy tensor has led to all the conservation theorems expected from it. It remains to be shown that a charge conservation theorem can be set up for the generalized formulation. The complex scalar field can be interpreted as a charge carrying field inasmuch as it is possible to define an electric charge density ρ and an electric current density vector, s_k, which satisfy a continuity equation. If we let ϵ be a real constant with the dimensions of electric charge and define:

$$\begin{aligned} \rho &\equiv -i\epsilon(\pi\psi - \pi^*\psi^*) \\ &= -i\epsilon(\psi\dot{\psi}^* - \dot{\psi}^*\psi), \end{aligned} \tag{3.20}$$

$$\text{and } s_k \equiv i\epsilon(\psi\partial_k\psi^* - \psi^*\partial_k\psi)$$

then it follows, as in the usual theory, that

$$\frac{\partial \rho}{\partial t} + \partial_k s_k = 0 \tag{3.21}$$

which expresses the conservation of charge. Since the generalized conjugate momentum fields are identical with the usual conjugate momentum fields, the charge density, ρ, and the current density vector, s_k, are identical with the charge density and the current density vector which are derived from the usual Lagrange function.

4. THE VECTOR FIELD

The equations of the complex vector field are the set

$$\begin{aligned} \partial_\alpha \partial_\alpha \psi_\beta &= \mu^2 \psi_\beta, \\ \partial_\alpha \partial_\alpha \psi^*_\beta &= \mu^2 \psi_\beta \end{aligned} \tag{4.1}$$

with the auxiliary relations—the Lorentz conditions—

$$\partial_\beta \psi_\beta = 0, \qquad \partial_\beta \psi^*_\beta = 0.$$

The field equations as well as the Lorentz conditions are contained in the following equations:

$$\begin{aligned} \partial_\alpha(\partial_\alpha \psi_\beta - \partial_\beta \psi_\alpha) &= \mu^2 \psi_\beta, \\ \partial_\alpha(\partial_\alpha \psi^*_\beta - \partial_\beta \psi^*_\alpha) &= \mu^2 \psi_\beta. \end{aligned} \tag{4.2}$$

For if we take the derivative with respect to x_β of both sides of the first of these equations, for example, then we have

$$\partial_\beta \partial_\alpha(\partial_\alpha \psi_\beta - \partial_\beta \psi_\alpha) = \mu^2 \partial_\beta \psi_\beta.$$

If we interchange dummy indices, the left-hand side vanishes identically so that

$$\mu^2 \partial_\beta \psi_\beta = 0$$

which is the Lorentz condition if $\mu^2 \neq 0$. We shall expect that the action principle will yield both the field equations and the Lorentz conditions, that is, we shall expect the equation (4.2) to be the Euler–Lagrange equations associated with the Lagrange function which we choose for the complex vector field.

The generalized Lagrangian density for the complex vector field may be written

$$\mathscr{L} = -\mu^2 \psi^*_\beta \psi_\beta + \tfrac{1}{2}[\psi_\beta(\partial_\alpha \partial_\alpha \psi^*_\beta - \partial_\alpha \partial_\beta \psi^*_\alpha) + \psi^*_\beta(\partial_\alpha \partial_\alpha \psi_\beta - \partial_\alpha \partial_\beta \psi_\alpha)]. \tag{4.3}$$

The usual Lagrangian density for this field has the form

$$\mathscr{L}' = -\mu^2 \psi_\beta \psi^*_\beta - \tfrac{1}{2}(\partial_\alpha \psi_\beta - \partial_\beta \psi_\alpha)(\partial_\alpha \psi^*_\beta - \partial_\beta \psi^*_\alpha). \tag{4.4}$$

The action principle, with either of these Lagrangian densities, yields in a straightforward manner the field equations in the form (4.2) and a surface condition. Then the Lorentz condition may be invoked to reduce the surface condition to the following form:

$$0 = \int_S \{(\partial_k \psi^*_\beta)\delta\psi_\beta + (\partial_k \psi_\beta)\delta\psi^*_\beta - \psi^*_\beta \partial_k \delta\psi_\beta - \psi_\beta \partial_k \delta\psi^*_\beta\} n_k \, dS \tag{4.5}$$

for the generalized Lagrangian density, and

$$0 = \int_S \{(\partial_k \psi_\beta^* - \partial_\beta \psi_k^*)\delta\psi_\beta + (\partial_k \psi_\beta - \partial_\beta \psi_k)\delta\psi_\beta^*\} n_k \, dS \tag{4.6}$$

for the usual Lagrangian density. Of the set of boundary conditions discussed in the introduction the only ones which satisfy the latter surface condition are the vanishing of the field functions on S or the periodicity of the field functions within S. Thus neither the vanishing of the normal derivatives on S nor linear homogeneous relations on S will serve as boundary conditions with the usual theory. The surface condition derived from the generalized Lagrangian density, $\mathscr{L}$, is satisfied by all the usual boundary conditions and by linear homogeneous boundary conditions.

In the generalized theory the momentum fields, π_β and π_β^*, conjugate to ψ_β and ψ_β^* respectively, and the Hamiltonian density, $\mathscr{H}$, may be defined by:

$$\begin{aligned} &\pi_\beta \equiv \dot{\psi}_\beta, \quad \pi_\beta^* \equiv \dot{\psi}_\beta, \\ &\mathscr{H} \equiv \pi_\beta \pi_\beta^* + \mu^2 \psi_\beta \psi_\beta^* - \tfrac{1}{2}[\psi_\beta(\partial_k \partial_k \psi_\beta^* - \partial_\alpha \partial_\beta \psi_\alpha^*) + \psi_\beta^*(\partial_k \partial_k \psi_\beta - \partial_\alpha \partial_\beta \psi_\alpha)]. \end{aligned} \tag{4.7}$$

It is shown in the Appendix that these field quantities arise naturally from the generalized Lagrangian density.

In the conventional formulation of the vector field the field quantities are constructed from the usual Lagrangian density, $\mathscr{L}'$. Then the usual field quantities, π_β', $\pi_\beta^{*\prime}$, and $\mathscr{H}'$ are defined:

$$\begin{aligned} &\pi_\beta' \equiv \frac{\partial \mathscr{L}'}{\partial \dot{\psi}_\beta} = i(\partial_4 \psi_\beta^* - \partial_\beta \psi_4^*), \\ &\pi_\beta^{*\prime} \equiv \frac{\partial \mathscr{L}'}{\partial \dot{\psi}_\beta^*} = i(\partial_4 \psi_\beta - \partial_\beta \psi_4), \\ &\mathscr{H}' = \pi_\beta' \psi_\beta + \pi_\beta^{*\prime} \psi_\beta^* - \mathscr{L}' - i\partial_j(\pi_j' \psi_4 + \pi_j^{*\prime} \psi_4^*). \end{aligned} \tag{4.8}$$

The terms $-i\partial_j(\pi_j' \psi_4 + \pi_j^{*\prime} \psi_4^*)$ are added to $\mathscr{H}'$ so that the canonical equations with $\mathscr{H}'$ will be the vector field equations. In the usual theory it is assumed that such divergence terms can be added to $\mathscr{H}'$ arbitrarily because the integrated Hamiltonian density, H' ($H' \equiv \int_v \mathscr{H}' dv$), will not be affected by these terms if the field functions vanish at the boundary or if the field functions are periodic within the boundary. $\mathscr{H}'$ is used only for these special boundary conditions.

It is seen on inspection that the generalized π_β, π_β^*, and $\mathscr{H}$ differ in form from the usual π_β', $\pi_\beta^{*\prime}$, and $\mathscr{H}'$. In particular, for the usual formulation both π_4' and $\pi_4^{*\prime}$ vanish identically while for the generalized formulation π_4 and π_4^* do not vanish in general. In the usual development the vanishing of these two field functions introduces difficulties into the theory of vector fields. For example, if the canonical Hamilton equations are to yield the vector field equations then these equations must arise for all the components of ψ and ψ^*, that is, for ψ_1, ψ_2, ψ_3, ψ_4 and ψ_1^*, ψ_2^*, ψ_3^*, ψ_4^*. However, with the usual conjugate momenta, canonical equations would have to be set up involving the identically vanishing π_4' and $\pi_4^{*\prime}$. It is difficult to assign meaning to such a construction. Even otherwise, it is necessary to add divergence terms to $\mathscr{H}'$ in a rather arbitrary manner if the remaining canonical equations are to be the corresponding field equations. Such difficulties are not encountered with the generalized conjugate momenta. It

would be possible, with the usual Lagrangian density, to define the usual conjugate momentum fields to be identical with the generalized conjugate momenta. However, such definitions would not follow naturally from the usual Lagrangian density (see the Appendix).

As in the case of the scalar field, the canonical Hamilton equations may be derived from the action principle using the Hamiltonian density instead of the Lagrangian density. The result, again, may be easily written if we define functional derivatives, $\delta\mathscr{H}/\delta\psi_\beta$, $\delta\mathscr{H}/\delta\psi^*_\beta$, $\delta\mathscr{H}/\delta\pi_\beta$, and $\delta\mathscr{H}/\delta\pi^*_\beta$ of $\mathscr{H}$ in the following way:

$$\frac{\delta\mathscr{H}}{\delta\psi_\beta} \equiv \frac{\partial\mathscr{H}}{\partial\psi_\beta} + \partial_j\partial_j \frac{\partial\mathscr{H}}{\partial(\partial_k\partial_k\psi_\beta)} + \partial_\alpha\partial_\beta \frac{\partial\mathscr{H}}{\partial(\partial_\alpha\partial_\gamma\psi_\gamma)} \tag{4.9}$$

with similar definitions for $\delta\mathscr{H}/\delta\psi^*_\beta$, $\delta\mathscr{H}/\delta\pi_\beta$, and $\delta\mathscr{H}/\delta\pi^*_\beta$. With these definitions of the functional derivatives we may write the canonical equations in the following way:

$$\begin{aligned} \dot{\psi}_\beta &= \frac{\delta\mathscr{H}}{\delta\pi_\beta}, \qquad \dot{\pi}_\beta = -\frac{\delta\mathscr{H}}{\delta\psi_\beta}, \\ \dot{\psi}^*_\beta &= \frac{\delta\mathscr{H}}{\delta\pi^*_\beta}, \qquad \dot{\pi}^*_\beta = -\frac{\delta\mathscr{H}}{\delta\psi_\beta}. \end{aligned} \tag{4.10}$$

It is expected that these canonical equations will be the equations of motion of the vector field. This is readily verified. For example, the first of equations (4.10) yields $\dot{\psi}_\beta = \dot{\psi}_\beta$, an identity, and the second of equations (4.10) yields

$$-\partial_4\partial_4\psi^*_\beta = -\mu^2\psi^*_\beta + \tfrac{1}{2}(\partial_k\partial_k\psi^*_\beta - \partial_\alpha\partial_\beta\psi^*_\alpha) + \tfrac{1}{2}(\partial_k\partial_k\psi^*_\beta - \partial_\alpha\partial_\beta\psi^*_\alpha)$$

which is the field equation for ψ^*_β in the required form (4.2).

It remains to be shown that $\mathscr{H}$ may be interpreted as the energy density of the vector field and that a continuity equation for energy may be set up. In order to do this a stress–energy tensor will be constructed from the definition of $\mathscr{H}$. Using the vector field equations, the generalized Hamiltonian density may be written in the form

$$\mathscr{H} = -(\partial_4\psi_\beta)(\partial_4\psi^*_\beta) + \tfrac{1}{2}(\psi_\beta\partial_4\partial_4\psi^*_\beta + \psi^*_\beta\partial_4\partial_4\psi_\beta). \tag{4.11}$$

A stress–energy tensor, $T_{\mu\nu}$, may now be defined

$$T_{\mu\nu} \equiv \tfrac{1}{2}\{(\partial_\mu\psi_\beta)(\partial_\nu\psi^*_\beta) + (\partial_\nu\psi_\beta)(\partial_\mu\psi^*_\beta) - \psi_\beta(\partial_\mu\partial_\nu\psi^*_\beta) - \psi^*_\beta(\partial_\mu\partial_\nu\psi_\beta)\}. \tag{4.12}$$

It is seen on inspection that $T_{44} = -\mathscr{H}$ as required. The conservation theorems associated with $T_{\mu\nu}$ are of the form

$$\partial_\mu T_{\mu\nu} = 0. \tag{4.13}$$

This equation follows directly from the definition of $T_{\mu\nu}$ and from the vector field equations. The time-component ($\nu = 4$) of (4.13) will be recognized as a continuity equation for energy. The definition of the energy flux vector, S_k, thus follows naturally:

$$S_k = -iT_{k4}. \tag{4.14}$$

Then the time-component of equation (4.13) may be written:

$$\frac{\partial \mathscr{H}}{\partial t} + \partial_k S_k = 0. \tag{4.15}$$

The generalized Hamiltonian density, $\mathscr{H}$, will be identified with the energy density of the vector field through a comparison of $\mathscr{H}$ with the usual Hamiltonian density, $\mathscr{H}'$. Using the definitions of $\mathscr{H}$ and $\mathscr{H}'$ and applying the Lorentz conditions one obtains:

$$\begin{aligned}\mathscr{H} - \mathscr{H}' = \tfrac{1}{2}\partial_k[&- \psi_\alpha \partial_k \psi_\alpha^* - \psi_\alpha^* \partial_k \psi_\alpha + \psi_j \partial_j \psi_k + \psi_j^* \partial_j \psi_k \\ &+ \psi_k \partial_4 \psi_4^* + \psi_k^* \partial_4 \psi_4 - 2\psi_4(\partial_4 \psi_k^* - \partial_k \psi_4^*) - 2\psi_4^*(\partial_4 \psi_k - \partial_k \psi_4)]\end{aligned} \tag{4.16}$$

which is a pure divergence. We identify $\mathscr{H}'$ (and possibly some of the divergence terms) as the energy density of the field. Then we identify the rest of the divergence terms above with the boundary energy density due to the boundary conditions. The generalized Hamiltonian density $\mathscr{H}$ will serve as the energy density of the vector field if we remember that at the boundary $\mathscr{H}$ contains terms which describe a surface energy density. However, the total energy flux through the boundary vanishes, that is,

$$\int_S S_k n_k \, dS = 0$$

which follows readily from the definition of S_k. Therefore the total energy of the system is conserved. As for the scalar field, an exchange of energy may occur between the field and the boundary.

The momentum density vector, G_k, for the vector field may be defined

$$G_k = - iT_{4k} \tag{4.17}$$

from which it follows that the $\nu = k$ component of the general continuity equation (4.13) expresses the conservation of the momentum of the field. The conservation of angular momentum is an immediate consequence of the symmetry of $T_{\mu\nu}$.

By defining a charge density, ρ, and a current density, s_k, in terms of the vector field functions, and by constructing a continuity equation with ρ and s_k, it is possible to interpret the vector field as a charge carrying field. We define:

$$\begin{aligned}\rho &\equiv - i\epsilon(\pi_\beta \psi_\beta - \pi_\beta^* \psi_\beta^*) \\ &= - i\epsilon(\psi_\beta \psi_\beta^* - \psi_\beta^* \psi_\beta), \\ s_k &\equiv - i\epsilon(\psi_\beta \partial_k \psi_\beta^* - \psi_\beta^* \partial_k \psi_\beta)\end{aligned} \tag{4.18}$$

where $\frac{1}{2}\epsilon$ is a real constant with the dimensions of charge. Then, using the vector field equations, it follows that

$$\frac{\partial \rho}{\partial t} + \partial_k s_k = 0 \tag{4.19}$$

which expresses the conservation of charge.

Because the generalized conjugate momentum fields, π_β and π_β^*, are different from those usually employed in the literature, the definitions of charge density

and current density, given above, also differ from the usual definitions of these quantities. Thus usually,

$$\rho' \equiv -\epsilon(\psi_\beta \partial_4 \psi_\beta^* - \psi_\beta \partial_\beta \psi_4^* - \psi_\beta^* \partial_4 \psi_\beta - \psi_\beta^* \partial_\beta \psi_4), \tag{4.20}$$

$$s_k' \equiv -\epsilon(\psi_\beta \partial_k \psi_\beta^* - \psi_\beta \partial_\beta \psi_k^* - \psi_\beta^* \partial_k \psi_\beta - \psi_\beta^* \partial_\beta \psi_k).$$

Then we have

$$\rho - \rho' = \epsilon(\psi_\beta \partial_\beta \psi_4^* - \psi_\beta^* \partial_\beta \psi_4)$$

$$= \epsilon \partial_\beta (\psi_\beta \psi_4^* - \psi_\beta^* \psi_4) \tag{4.21}$$

since $\partial_\beta \psi_\beta = 0$, and $\partial_\beta \psi_\beta^* = 0$. The total charges for ρ and ρ', that is, $\int_V \rho \, dV$ and $\int_V \rho' \, dV$ respectively, then differ only by a quantity which is evaluated at the boundary. This difference vanishes if the field functions vanish at the boundary.

The generalized Lagrange function for the vector field allowed a definition of the conjugate momentum fields for which the time-component of these fields did not vanish identically. It has been shown, in this section, that all the classical field quantities and conservation theorems may be derived along with such definitions of the conjugate momentum fields. The formulation was extended to include fields with linear homogeneous boundary conditions. More than that, the vector field quantities, as derived above, possess a remarkable similarity in form to their analogues in the complex scalar field. As a rule, if any generalized field quantity is defined for the scalar field its analogue in the vector field follows immediately by simply replacing the scalar field functions, ψ, ψ^*, by vector field functions, ψ_β, ψ_β^*, and by replacing products of scalar field functions by inner products of vector field functions. Thus

$$\psi \rightarrow \psi_\beta,$$

$$\psi\psi^* \rightarrow \psi_\beta \psi_\beta^*, \tag{4.22}$$

$$\frac{\partial \psi}{\partial n}\psi^* \rightarrow \frac{\partial \psi_\beta}{\partial n}\psi_\beta^*,$$

etc.

The only exceptions to this rule are the Lagrange function and the Hamiltonian function. These are logical exceptions because we require that the Lagrangian density and also the Hamiltonian density, for the vector field, lead to a Lorentz condition, a condition which has no analogue in the scalar field. The Hamiltonian functions and the Lagrange functions for the vector field are at variance with the rule above only in those terms (that is, mixed-derivative terms), in the vector field quantities, which lead to this Lorentz condition.

The simple rule given above, for the transition in form from the scalar to the vector field, does not apply for any of the field quantities in the usual development of the classical theory for these fields.

5. THE DIRAC FIELD

Because the Dirac equations are of first order the Lagrangian densities for this field may not be generalized to contain second order derivatives. It is possible, for this field also, to show that the boundary conditions arise from the

variational principle. Of the usual boundary conditions the only ones allowed by the action principle for the Dirac field are the vanishing of the field functions on S or their periodicity within S. The vanishing of the normal derivatives on S or linear homogeneous boundary conditions are excluded as possible boundary conditions for the Dirac field.

6. CONCLUSION

It has been shown for the scalar and vector fields how homogeneous linear boundary conditions can be accommodated in a self-consistent theory through the use of Lagrangians containing second order derivatives. Obvious extensions of this work would be the quantization of the classical formulation presented above and a treatment of fields in interaction. Investigation along these lines is now in progress.

APPENDIX
THE CONSTRUCTION OF HAMILTONIANS FROM GENERALIZED LAGRANGIAN DENSITIES

A Hamiltonian function may be defined, for a wave field, if both the field functions and their conjugate momenta may be defined. Usually the conjugate momentum fields are derived from the Lagrangian density in the following way:

$$\pi_\beta \equiv \frac{\partial \mathscr{L}}{\partial \dot{\psi}_\beta}, \quad \pi^*_\beta \equiv \frac{\partial \mathscr{L}}{\partial \dot{\psi}^*_\beta} \tag{A.1}$$

where $\beta = 1,2,3,4$ for the vector field,
$= 1$ for the scalar field.

But the generalized Lagrange functions for neither the complex scalar field nor the complex vector field contain $\dot{\psi}_\beta$ or $\dot{\psi}^*_\beta$ explicitly. Because of the special role played by x_4 in the action principle, it is possible to substitute first derivatives with respect to time for the second order time derivatives occurring in the Lagrangian densities. Thus whenever we have terms of the form $\psi_\beta \partial_\alpha \partial_\alpha \psi^*_\beta$, $\psi^*_\beta \partial_\alpha \partial_\alpha \psi_\beta$ occurring in $\mathscr{L}$ it is possible to replace $\psi_\beta \ddot{\psi}^*_\beta$ by $-\dot{\psi}_\beta \dot{\psi}^*_\beta$, and $\psi^*_\beta \ddot{\psi}_\beta$ by $-\dot{\psi}^*_\beta \dot{\psi}_\beta$, and the action principle remains unchanged under such an interchange. We perform such a transformation on the generalized Lagrangian densities. The transformed generalized Lagrangian densities resulting from such a transformation are:

$$\mathscr{L}_T = -\mu^2 \psi \psi^* + \tfrac{1}{2}(\psi \partial_k \partial_k \psi^* + \psi^* \partial_k \partial_k \psi) - (\partial_4 \psi)(\partial_4 \psi^*) \tag{A.2}$$

for the complex scalar field, and

$$\mathscr{L}_T = -\mu^2 \psi_\beta \psi^*_\beta + \tfrac{1}{2}[\psi_\beta(\partial_k \partial_k \psi^*_\beta - \partial_\beta \partial_\alpha \psi^*_\alpha) + \psi^*_\beta(\partial_k \partial_k \psi_\beta - \partial_\beta \partial_\alpha \psi^*_\alpha)] - (\partial_4 \psi_\beta)(\partial_4 \psi^*_\beta)$$

for the complex vector field.

By employing these transformed Lagrangian densities in the variational procedure it is seen at once that they yield exactly the same Euler–Lagrange equations and the same boundary conditions as the generalized Lagrangian

densities from which they were derived. Therefore $\mathscr{L}_T$ is equivalent to $\mathscr{L}$ in the discussion of either the scalar or the vector field with the action principle. In view of this equivalence, π_β and π^*_β may be defined as

$$\pi_\beta \equiv \frac{\partial \mathscr{L}_T}{\partial \dot{\psi}_\beta}, \quad \pi^*_\beta \equiv \frac{\partial \mathscr{L}_T}{\partial \dot{\psi}^*_\beta} \tag{A.3}$$

where $\beta = 1,2,3,4$, for vector fields,

$= 1$ for scalar fields.

These constitute natural definitions of the conjugate momenta which were stated in the discussion of these fields.

It would be expected that the Hamiltonian function for the wave fields would follow from that form of the Lagrangian density which was employed in defining the conjugate momentum fields. Therefore we define the Hamiltonian density, $\mathscr{H}$, as

$$\mathscr{H} \equiv \pi_\beta \dot{\psi}_\beta + \pi^*_\beta \dot{\psi}^*_\beta - \mathscr{L}_T. \tag{A.4}$$

This is the natural definition of the Hamiltonian density for those wave fields which are described by a generalized Lagrange function. The definitions (3.3) and (4.7) employed in the discussion of the scalar and vector fields follow immediately from (A.3) and (A.4). It is to be noticed, in the generalized vector field theory, that the transformation $\mathscr{L} \rightarrow \mathscr{L}_T$ has not transformed time derivatives occurring in terms of the form $\psi_\beta \partial_\beta \partial_\alpha \psi^*_\alpha$ or $\psi^*_\beta \partial_\beta \partial_\alpha \psi_\alpha$ and therefore these terms are not employed in the definition of the conjugate momentum fields. In order to employ these terms in such definitions it would be necessary to define functional derivatives of $\mathscr{L}$ with respect to $\dot{\psi}_\beta$ or $\dot{\psi}^*_\beta$. However, these terms occur in $\mathscr{L}$ only because they give rise to the Lorentz condition. Thus these terms have an auxiliary role in the variational procedure and their use in extending the definition of π_β and π^*_β need not be expected. It was shown that the definitions (A.3) and (A.4) were completely sufficient for the construction of a Hamiltonian whose canonical equations are the vector field equations in the form which includes the Lorentz conditions. In view of this these definitions are not only natural but also sufficient.

The transformation $\mathscr{L} \rightarrow \mathscr{L}_T$ corresponds to a transformation to a Lagrange function which is not relativistically invariant. This is a qualification of the relativistic invariance of $\mathscr{L}$. It arises because of the special role played by the time coordinate in the action principle. The space derivatives, however, must enter into a generalized $\mathscr{L}$ uniformly.

REFERENCES

1. HEISENBERG, W. and PAULI, W. Z. Physik, 56: 1. 1929.
2. HILL, E. L. Revs. Modern Phys. 23: 253. 1951.
3. PAULI, W. Revs. Modern Phys. 13: 203. 1941.
4. VOGT, E. Thesis, University of Manitoba, Winnipeg, Man. 1952.
5. WENTZEL, G. Quantum theory of fields. Interscience Publishers, Inc., New York. 1949.

A STATISTICAL ANALYSIS OF GRAIN COUNTING IN PHOTOGRAPHIC EMULSIONS[1]

By W. W. Happ,[2] T. E. Hull,[3] and A. H. Morrish[4]

ABSTRACT

Fluctuations in the grain density of tracks of charged particles passing through photographic emulsions are examined in terms of the physical properties of grains and the type of counting convention used. A mathematical model, for one counting convention which takes into account both the frequency distribution of the grains and the frequency distribution of their lengths, yields numerical results in good agreement with experimental data. Other statistical problems of interest in grain counting are discussed.

INTRODUCTION

In recent years the use of sensitive photographic emulsions to record the tracks of particles has led to many new results in nuclear and cosmic-ray physics. Counting grains in the track of a particle is frequently employed to determine one of the characteristics of the particle. Except at very high grain densities, the number of grains per unit length of track is a function of the particle's energy loss by ionization. The ionization of a singly charged particle is, in turn, a function only of its velocity. Therefore, grain density is a measure of a particle's velocity. The observed grain density, together with, for example, a measurement of the momentum or energy, can then lead to a determination of the mass of the particle.

The purpose of this paper is to examine certain statistical aspects of grain counting. We discuss first the formation of grains in nuclear emulsions; the process depends primarily on the following factors:

(1) the sensitivity of the emulsion,

(2) the undeveloped grain size,

(3) the nature of the development process,

as well as

(4) the velocity and charge of the ionizing particles.

The observed frequency distributions, on the other hand, depend on:

(i) the frequency distribution of developed grains,

(ii) the convention used for counting overlapping grains,

(iii) the way in which sections of track are chosen for counting purposes, and

(iv) the distribution of developed grain sizes.

We show how these four factors determine the choice of a mathematical model to describe the statistics of the problem.

[1] *Manuscript received June 10, 1952.*
Contribution from the University of British Columbia, Vancouver, B.C.
[2] *Department of Physics.*
[3] *Department of Mathematics.*
[4] *On temporary duty from the Defence Research Board, Ottawa.*

The distribution of developed grains is generally assumed to follow Poisson's Law. Some grains will overlap and the distribution of *counted* grains will be narrower than the Poisson distribution. Hodgson (8) was able to account for this deviation by assuming that any two grains separated by less than a certain distance are counted as one. (See also Lovera (16).) Thus the observed grain density depends on this distance in the way that the counting rate of a counting mechanism depends on its resolving time. In this investigation analogies between counter theory problems and grain counting problems are used extensively.

The detailed analysis of a more general statistical model is given. Besides accounting for deviations of the distribution of counted grains from Poisson's, this model accounts for variations in the sizes of the counted grains. The results are found to agree satisfactorily with the experimental data.

Other factors which affect the distributions only slightly are discussed.

PROPERTIES OF GRAINS IN NUCLEAR EMULSIONS

It is useful to survey the facts that are known concerning the factors (1), (2), and (3) of the previous section. Except for the initial action, a silver halide grain is made developable in nuclear research plates by a process similar to the action of light on ordinary emulsions (23). Electrons are brought into the silver halide conduction band as a result of the ionizing collisions of the fast particle as it traverses the grain. For particles traveling close to the speed of light the ionization is confined to a cylinder of radius less than 0.01μ. Since the diameter of the undeveloped grain is, on the average, about 0.27μ in Ilford G-5 emulsions (22), this means that usually the ionizing particle must pass through the grain before it may become developable. Mott and Gurney (20) have discussed the way in which the latent image is formed. From the known loss of energy of a particle per unit length, Berriman (2) has calculated that about 15 ion pairs per grain are required to form a latent image in electron sensitive emulsions.

Variations in the sensitivity in different regions of nuclear emulsions have been observed, but in general these variations are small. In any event their effect can be normalized with the aid of suitable calibrations (19). It is convenient to assume the sensitivity to be constant.

The centers of grains traversed by an incident particle will lie in a cylinder whose diameter is D, the mean grain diameter. For spherical grains with their centers on a line Zhdanov (24) has shown that the mean grain spacing (i.e., the average distance between the centers of individual grains) is $2gD/3c$, where g is the density of the silver halide, and c its concentration in the emulsion. Since there is only a small amount of silver iodide present, g may be taken as that for silver bromide, i.e. 6.47 gm. per cc. For Ilford G-5 emulsion $c = 3.25$ gm. per cc. This gives a value of 0.36μ for the mean grain spacing. This means that the average distance between the grain surfaces is less than 0.10μ.

The size of the developed grains depends on the type of developer, but in general is much larger than the undeveloped grain. With the Amidol type

developers now in common use, the mean developed grain diameter is about 0.7 to 0.8μ, whereas with the ID–19 well diluted the diameter is much less.

Mees (17) has taken electron microscope pictures which show that the developed grain consists of many fine silver filaments. He is led to the conclusion that the grain develops by a process of extrusion of the silver.

Grain counting in nuclear emulsions is usually done under a magnification of about 1500 ×. Under these conditions, individual grains can just be resolved if they are separated by about 0.05μ. Since the projection of the track in the plane of the emulsion is observed in the microscope, nearby grains displaced vertically relative to each other will overlap. Further, since developed grains are larger, especially when Amidol is used, two closely spaced, activated grains in the same horizontal plane can overlap on development and be observed as one elongated grain.

GRAIN COUNTING

It is now necessary to discuss possible grain counting conventions. The convention determines the way one counts a portion of track completely covered by overlapping grains. It should be unambiguous, easy to use in practice, and, if possible, capable of being handled theoretically. There are two basically different counting conventions in common use.

Type I

An estimate is made of the number of grains in a completely covered portion of track. Any such estimate is necessarily subjective and even one observer may not perform consistently. Various rules for making estimates have been used: for example, a correction may or may not be made for the amount of overlapping of successive grains.

Generally, such rules do not lend themselves easily to theoretical treatment. If the "nonextended dead time" theory for counters is used as a statistical model, the rule *should* be as follows: a grain is counted if and only if it does not overlap the preceding *counted* grain. Hodgson used this model but, strictly, it does not represent any Type I counting convention.

Type II

A grain is counted if, and only if, it does not overlap any preceding (not necessarily counted) grain and this convention corresponds exactly to the "extended dead time" theory for counters. Here, one counted grain may be many times longer than an individual grain. This convention will be called "extended" or "blob" counting. It can be used easily and consistently and, as we shall see, can be treated theoretically. In addition, the variation of counted grain density with depth in the emulsion is smaller than with many Type I conventions. (Grains near the surface of an emulsion tend to be larger than those near the glass surface because of greater physical development.)

The choice of counting convention will be partly determined by the grain density. Blob counting is usually used only when grain densities are low, i.e. when up to about 25% of the track is covered with grains, corresponding to

grain densities of up to about 1.5 times the minimum value. Such tracks are produced by singly charged particles moving with almost the velocity of light. At higher grain densities (up to about 75% of the track covered by grains) Type I counting is commonly used. It is clear that the relationship between the grain density in the track and the particle's energy loss by ionization depends strongly on the type of counting convention employed. At still higher grain densities, the gaps between blobs or the lengths of blobs may be measured (7). In fact, a thorough analysis of these gap lengths can be made for any grain density, but in practice, because of the time and effort required, this is usually not justified for low grain densities.

There are other methods in use (for example, see (3)) which will not be discussed in this paper. Photometric methods are used to obtain a measure of very high grain densities. Sometimes less sensitive emulsions are employed to reduce the grain density for the same energy loss region but this method necessitates careful calibration. Finally, for particles with $Z \geqslant 2$, δ-ray counting is often employed.

Morrish (19) has shown that particles of charge $|e|$ produce tracks of constant and low grain density at least when their energies E/mc^2 are > 20. Tracks of electrons in this energy region were obtained in Ilford G-5 emulsions exposed to the cosmic radiation. The grain densities were determined by the method of blob counting. Their means were corrected for nonuniform sensitivity of the emulsion with the aid of a previous calibration (19). A histogram for the

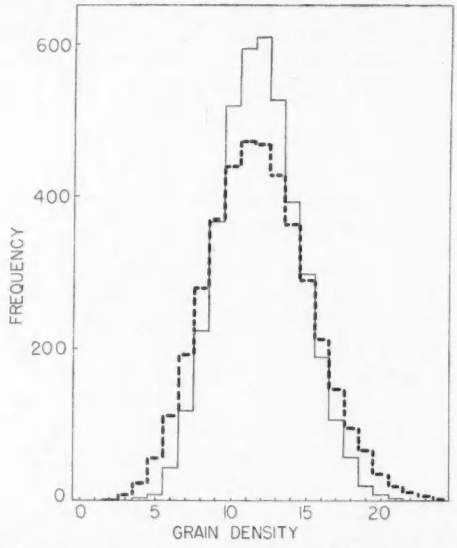

FIG. 1. The solid histogram is the frequency distribution for the number of counted grains per 50.6μ. The tracks were produced by high energy electrons; the blob counting convention was used. The broken histogram is the corresponding Poisson distribution.

number of grains in 4095 cells, each 50.6μ long, is shown in Fig. 1. The mean observed was $M = 11.87$, the variance $B = 7.23$; the ratio of the standard deviation to the square root of the mean ($\sqrt{B/M}$) was then 0.78. Fig. 1 also shows the corresponding Poisson distribution with the same mean; here $\sqrt{B/M} = 1$ and it is clear that the observed distribution is narrower.

To extend the analysis, the lengths of 99 consecutive blobs in two of the tracks were measured. Their histogram is shown in Fig. 2. The mean was $\bar{x} = 0.865\mu$ and the variance $\sigma^2 = 0.0950\mu^2$.

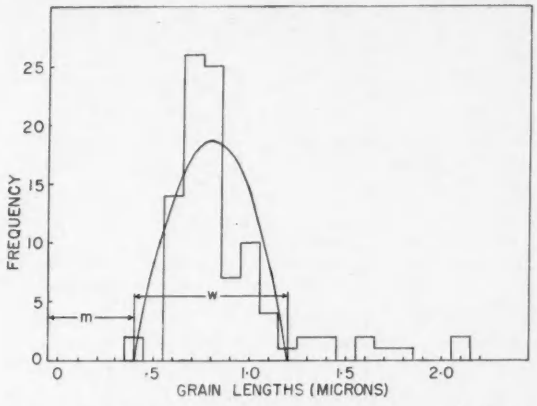

FIG. 2. The parabola is the frequency distribution of grain lengths. The histogram is the observed distribution of *counted* grain (or blob) lengths.

STATISTICAL MODELS OF THE GRAIN COUNTING PROBLEM

An analysis of the distribution of counted grain lengths (Fig. 2) will be postponed to the next section. Here we shall consider only the various known statistical models which might be used to interpret the distribution of counted grains (Fig. 1). These models, such as the one used by Hodgson and previously referred to, are concerned with problems in which each event, in a sequence of random events, is followed by an inactive period in which a certain mechanism does not perform. Examples can be found in the literature of telephone traffic "busy period" (6), the effectiveness of blockading and intercepting (11), the resolving time of mechanical and electrical counting mechanisms (4, 21), the breakdown period of machines (13), and similar problems. During the past 20 years about one hundred papers have been published on the statistics of counting mechanisms alone. A summary of formulas, as they apply to the grain counting problem, has been developed from some of these papers (4, 5, 9, 12, 14, 15) and appears in Table I.

The Distribution of Developed Grains

Assuming that the grains are points and that they occur at random along a track, the probability that n grains appear in a length x is given by the Poisson function*

* *Tabulated by Molina (18).*

TABLE 1*a*

DISTRIBUTION OF NUMBER OF COUNTS IN FIXED INTERVAL x*

Type	Frequency $h(n)$	Mean	Variance	Generating function $\sum_{n=0}^{\infty} e^{-sn} h(n)$
No grain length	$p(n, ax)$	ax	ax	$e^{ax(e^{-s}-1)}$
Nonextended grain length D	$P(n, a(x-nD+D)) - P(n+1, a(x-nD))$	$\sim \frac{ax}{1+aD} + \frac{a^2D^2}{2(1+aD)^2}$	$\sim \frac{ax}{(1+aD)^3}$	
Extended grain length D	$\sum_{i=0}^{\left[\frac{x}{D}-n\right]} (-1)^i \frac{a^{n+i} e^{-(n+i)aD}}{n!\, i!} (x-(n+i)D)^{n+i}$	$ae^{-aD}x + 1 - e^{-aD} - aDe^{-aD}$, $x \geqslant D$	$e^{-aD}(ax - aD - 1) + e^{-2aD}(1 + 3a^2D^2 - 2a^2Dx + 2aD)$, $x \geqslant 2D$	

TABLE 1*b*

DISTRIBUTION OF LENGTH FROM ONE COUNT TO THE n^{th} SUCCEEDING COUNT*

Type	Frequency function $f(x)$	Mean	Variance	Generating function $\int_0^{\infty} e^{-sx} f(x)\, dx$
No grain length	$ap(n-1, ax)$	$\frac{n}{a}$	$\frac{n}{a^2}$	$\left(\frac{a}{a+s}\right)^n$
Nonextended grain length D	$ap(n-1, a(x-nD))$	$\frac{n}{a} + nD$	$\frac{n}{a^2}$	$e^{-nDs}\left(\frac{a}{a+s}\right)^n$
Extended grain length D	$\sum_{i=0}^{\left[\frac{x}{D}-n\right]} (-1)^i \frac{a^{n+i} e^{-(n+i)aD}}{(n-1)!\, i!} (x-(n+i)D)^{n+i-1}$	$\frac{n}{a} e^{aD}$	$\frac{n}{a^2} e^{aD}(e^{aD} - 2naD)$	$\left(\frac{a}{a+se^{(a+s)D}}\right)^n$

* $[k]$ is the greatest integer not exceeding k.

$$p(n, ax) = (ax)^n e^{-ax}/n! \tag{1}$$

where a is the mean number of grains per unit length. Considering x a fixed length, we can now find the mean, variance, and moment generating function for this discrete distribution of n. The results are given in the first row of Table I*a*; for our purposes it is important to notice that the ratio of the standard deviation to the square root of the mean is 1 for this distribution.

Alternatively, although not usually in practice, we can consider the number of grains n to be fixed and study the continuous distribution of the length from one grain to the n^{th} succeeding grain. The probability that this length will be between x and $x + dx$ is equal to the probability that $n - 1$ grains occur in the length x and 1 grain occurs in the interval dx, i.e.

$$p(n - 1, ax)a\,dx.$$

Properties of the continuous frequency function $ap(n - 1, ax)$ are given in the first row of Table I*b*. The formulas of Table I*b* apply even when the origin is chosen arbitrarily, rather than at a grain (4).

The Effect of Finite Grain Length

Because of the finite lengths of the grains, some may overlap so that it is not possible to count them all directly. The distribution of *counted* grains would then be expected to differ from the Poisson distribution discussed above. The counted grains are analogous to the registration times of a counter which does not register all events because of its finite recovery time. However, it should be noted that there is an important difference in magnitude between corrections for recovery time and corrections for finite grain lengths. Under ordinary operating conditions nearly all counting mechanisms have counting losses of less than 1% so that the instrument is inoperative less than 1% of the total time. On the other hand it would be exceedingly difficult to follow a grain track if the grains did not occupy at least 5% of the total track and they frequently cover more than 50%. The effect of such a difference between counters and grain counting is to increase the importance for the latter of higher order corrections to the Poisson Law.

In counter theory two idealized statistical models are usually considered. To describe them in the language of grain counting, we shall use the term "event" to mean the beginning of a grain (as measured from some origin in the track) and the term "count" to mean the beginning of a counted grain. We assume events to be distributed along the track according to Poisson's Law and the problem is to find the distribution of counts which, of course, depends on the counting convention.

The first model is that of the "nonextended grain length" theory. This model is based on the assumption that an event is counted if and only if it is separated from the preceding *count* by more than the grain diameter D. It is convenient to introduce the probability* that at least n events occur in a length x

$$P(n, ax) = \sum_{i=n}^{\infty} p(i, ax).$$

* *Tabulated by Molina (18).*

Then the probability that at least n *counts* occur in the length x is $P(n, a(x - nD + D))$ and the probability that exactly n counts occur in the length x is

$$P(n, a(x - nD + D)) - P(n + 1, a(x - nD)).$$

(Note that the expression $p(n, a(x - nD))$ is the probability that n counted grains, rather than counts, occur in x and so does not consider a grain to be counted unless it lies entirely within the interval x.) Row 2 of Table I*a* contains the properties of this distribution of counts in a fixed interval x.

Row 2 of Table I*b* contains properties of the corresponding distribution of the length from one count up to the n^{th} succeeding count. The probability that this length lies between x and $x + dx$ is the probability that exactly $n - 1$ events occur in the length $x - nD$ and another event occurs in dx, i.e.

$$p(n - 1, a(x - nD))a\,dx.$$

As mentioned previously, the above distributions correspond approximately to a Type I counting convention. However, most Type I conventions lie between the extremes represented by this "nonextended grain length" model and the simpler Poisson model.

On the other hand, the Type II or blob counting convention is well represented by the "extended grain length" model. The corresponding results are given in the third rows of Tables I*a* and I*b*. Details of the calculations will be omitted because they follow readily from a generalization of this model given in the next section.

When the finite grain length is taken into account the ratio of the standard deviation to the square root of the mean is less than 1. The corresponding distributions are therefore narrower than Poisson's. The grain diameter D can be chosen so that the narrowing is that determined experimentally; or D could be taken as the mean measured grain diameter and used to test the suitability of the chosen model.

A GENERALIZED STATISTICAL MODEL

Individual grain lengths (which make up a counted grain length) are not all the same. To analyze the distribution of counted grain lengths in Fig. 2 we must allow for this fact.

Two frequency distributions will now characterize our model. The occurrence of an event will be governed by Poisson's Law (equation 1) while the distribution function for grain lengths will be written

$$G(x) = \Pr\{\text{a grain length} \leqslant x\}. \tag{2}$$

For the moment it will not be necessary to specify $G(x)$ exactly.

We shall consider the grain lengths to be extended so that the model will be based on the blob counting convention used for the data in Figs. 1 and 2. The distribution of extended grain lengths (with constant grain diameter D) considered above is obtained from what follows by putting the frequency function

$$\frac{dG(x)}{dx} = \delta(x - D). \tag{3}$$

The analysis so gained is that given by Feller (5); what follows is therefore a generalization of his method.

We introduce the Laplace transform

$$g(s) = \int_0^\infty e^{-sx}\, dG(x). \tag{4}$$

The plan now is to derive expressions for the mean and variance of the total number of counts in a fixed length of track and the mean and variance of the counted grain lengths. The first two expressions will be used, along with the experimental data, to determine a, the mean number of events per unit length; information about the form of $G(x)$ will then be found from the last two expressions and the experimental data.

Consider first the possibility of two or more grains making up one counted grain. We have

Pr $\{x \leqslant$ length of first grain $\leqslant x + dx\} = dG(x)$,

Pr $\{$second event takes place between 0 and $x\} = 1 - e^{-ax}$.

Therefore

Pr $\{$at least two grains will make up one counted grain$\}$

$$= \int_0^\infty (1 - e^{-ax})\, dG(x)$$

$$= 1 - g(a).$$

Let us put $q = 1 - g(a)$, $p = g(a)$.

The length of a counted grain may be arbitrarily long since a large number of events, separated by short distances, may occur so that only the first is a count. (Of course, with low grain densities there are rarely more than one or two extensions; Fig. 3*a* shows a typical section of track.) We shall now assume that $G'(x)$ has values appreciably different from zero only in an interval which is small compared to its distance from the origin. That is, we allow the grain lengths to vary, but not much from their mean. This assumption enables us to neglect the length of the $(v - 2)$th grain in determining the probability that the vth grain will extend the $(v - 1)$th. In fact, we then have:

Pr $\{v$th event will be a count$\} = p$,

Pr $\{v$th event will not be a count$\} = q$.

The probability that, once a count has occurred, exactly v events will occur before the next count is $q^v p$.

Now let $X^{(i)}$ be the distance between events numbered $i - 1$ and i. If there are v events after a count, the total length of the counted grain up to the last event is (Fig. 3*b*)

$$X = X^{(1)} + X^{(2)} \ldots + X^{(v)}.$$

From equations (1, 2) the function

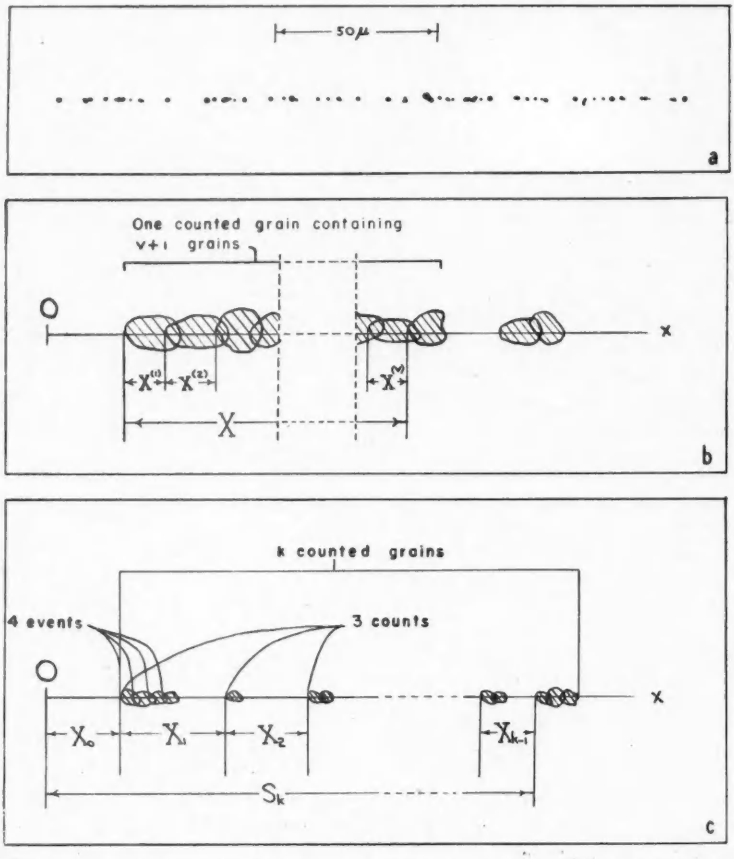

FIG. 3*a*. Section of a track produced by an electron moving close to the velocity of light in an Ilford G-5 emulsion.
FIG. 3*b*. The length of the one counted grain shown is X plus the length of the last grain.
FIG. 3*c*. S_k is the distance from the origin up to the kth count.

$$U(x) = \frac{1}{q}\int_0^x (1 - G(u))\, ae^{-au}\, du \tag{5}$$

is the conditional probability that an event will occur in a distance x if it is known that it occurs near enough to lengthen a grain which starts at $x = 0$. (Here $x = 0$ is not the origin, but is the beginning of the preceding grain.) That is

$$\Pr\{X^{(1)} \leqslant x\} = U(x).$$

Let us put

$$u(s) = \int_0^\infty e^{-sx}\, dU(x). \tag{6}$$

Equations (4, 5, 6) yield

$$qu(s) = \frac{a}{s+a}\,(1 - g(s+a)).$$

Moreover (cf. equation 17 of Elmore (4))

$$\int_0^\infty e^{-sx}\, d\,[\Pr\{X \leqslant x\}] = u^v(s).$$

If we account for the length of the last grain in the counted grain, we find the Laplace transform of the conditional probability distribution of the length of a counted grain (assuming exactly $v + 1$ grains in the counted grain) to be

$$u^v(s)\int_0^\infty e^{-sx}\, dG(x) = u^v(s)\, g(s).$$

The frequency function of counted grain lengths has accordingly the Laplace transform

$$pg(s)\sum_{v=0}^{\infty} (qu(s))^v = \frac{(s+a)\, g(a)\, g(s)}{s + ag(s+a)}. \tag{7a}$$

Let us write this last expression equal to

$$y(s) = \int_0^\infty e^{-sx}\, dY(x). \tag{7b}$$

The frequency function $dY(x)/dx$ should fit the observed distribution in Fig. 2. We shall eventually choose G, and hence g, so that this is the case. Meanwhile we know that

$$y(s) = 1 - \bar{x}a + \tfrac{1}{2}(\sigma^2 + \bar{x}^2)s^2 - \ldots \tag{8}$$

where $\bar{x}$ and σ^2 are the mean and variance of the distribution of counted grain lengths and are therefore the mean and variance found for the distribution in Fig. 2. We proceed to find, in terms of $\bar{x}$ and σ^2, the mean and variance of the number of counts in a fixed interval.

Denote by X_0 the distance from the origin (where there is no grain—see Fig. 3*c*) to the first count and by X_k ($k \geqslant 1$) the distance between the counts numbered k and $k + 1$. Then

$$\Pr\{X_0 \leqslant x\} = 1 - e^{-ax}$$

and for $k \geqslant 1$

$$\Pr\{X_k \leqslant x\} = F(x)$$

say, where (6)

$$\int_0^\infty e^{-sx}\, dF(x) = \frac{a}{a+s}\, y(s). \tag{9}$$

Now (Fig. 3*c*)

$$S_k = X_0 + X_1 + \ldots X_{k-1}$$

is the distance up to the kth count. If we write

$$\Pr\{S_k \leqslant x\} = F_k(x)$$

we obtain for p_k, the probability that the number of counts in x is exactly k,

$$p_k = F_k(x) - F_{k+1}(x)$$

so that

$$M(x) = \sum_{k=1}^{\infty} kp_k$$

$$= \sum_{k=1}^{\infty} F_k(x).$$

It can be shown that (5)

$$\int_0^{\infty} e^{-sx}\, dF_k(x) = \frac{a}{a+s}\left[\int_0^{\infty} e^{-sx}\, dF(x)\right]^{k-1}$$

so that, using equation (9), we obtain finally

$$\int_0^{\infty} e^{-sx} M(x)\, dx = \frac{a}{a+s}\frac{1}{s}\frac{1}{1 - \dfrac{a}{a+s}y(s)}. \tag{10}$$

Expanding this last expression in powers of s and using equation (8) we obtain

$$\frac{a}{1+a\bar{x}}\frac{1}{s^2} + \frac{a^2\sigma^2 + a^2\bar{x}^2}{2(1+a\bar{x})^2}\frac{1}{s} + 0(1)$$

so that, asymptotically,

$$M(x) = \frac{ax}{1+a\bar{x}} + \frac{a^2\sigma^2 + a^2\bar{x}^2}{2(1+a\bar{x})^2} + o(1). \tag{11}$$

Similarly we obtain for the variance $B(x)$ of the number of counts in the length x

$$B(x) = \sum_{k=1}^{\infty} k^2 p_k - M^2(x)$$

$$= 2\sum_{k=1}^{\infty} kF_k(x) - M(x) - M^2(x). \tag{12}$$

But

$$\int_0^{\infty} e^{-sx}\, 2\sum_{k=1}^{\infty} kF_k(x)\, dx = \frac{2a}{s(s+a)}\left[\frac{1}{1 - \dfrac{a}{a+s}y(s)}\right]^2 \tag{13}$$

so that, finally,

$$B(x) = \frac{a + a^3\sigma^2}{(1+a\bar{x})^3}x + 0(1) \tag{14}$$

asymptotically.

It should be remarked in passing that the special choice (equation 3) for $G'(x)$ leads through equations (4, 7, 10) to the mean and equations (12, 13) to the variance in row 3 of Table 1*a* in agreement with the results given by Feller (5).

Formulas (11, 14) will be used in the next section along with the observed values of $\bar{x}$, σ^2, M, and B to determine a.

To study the distribution of counted grain lengths in Fig. 2 it is necessary to postulate a distribution for the individual grain lengths. The choice is somewhat arbitrary but the following has proved satisfactory:

$$G'(x) = \begin{cases} \frac{6}{w^3}(x - m)(m + w - x), & m \leqslant x \leqslant m + w, \\ 0, & \text{otherwise.} \end{cases} \tag{15}$$

That is, we assume that the grain lengths have a parabolic distribution with a minimum length m and a maximum length $m + w$. The graph of $9.9\ G'(x)$, with the values $m = 0.4\mu$ and $w = 0.8\mu$ found in the next section, is the parabola in Fig. 2. (The factor 9.9 normalizes the parabola to the observed distribution since 99 observations are there plotted against a scale divided into units of 0.1μ.) As expected the distribution of *counted* grain lengths is smaller for small x and larger for large x.

Using equations (4, 15) in (7) and comparing with (8) we can find $\bar{x}$ and σ^2 in terms of the unknown parameters m and w. The calculations are laborious but straightforward. (They are simplified if the numerator and denominator in $y(s)$ are expanded in powers of s only *after* each is multiplied by e^{ms}.) The results are

$$\begin{cases} \bar{x} = m + \frac{w}{2} + \left(\frac{m^2}{2} + \frac{mw}{2} + \frac{3w^2}{20}\right)a + \left(\frac{m^3}{6} + \frac{m^2w}{4} + \frac{mw^2}{10} + \frac{w^3}{120}\right)a^2 \\ \qquad + \ldots, \\ \sigma^2 = \frac{w^2}{20} + \left(\frac{m^3}{3} + \frac{m^2w}{2} + \frac{3mw^2}{10} + \frac{w^3}{15}\right)a \\ \qquad + \left(\frac{-2m^4}{3} + \frac{2m^3w}{3} + \frac{m^2w^2}{2} + \frac{mw^3}{6} + \frac{157w^4}{8400}\right)a^2 + \ldots. \end{cases} \tag{16}$$

With the observed values of $\bar{x}$ and σ^2 and the calculated value of a these formulas will be used to find the values m and w used above.

COMPARISON OF THEORY WITH EXPERIMENT

The mean of the distribution in Fig. 1 was 11.87 and the length of the interval 50.6μ. Without allowing for the overlapping of grains the mean number of grains per micron would then be 0.23.

On the other hand, if the experimental values of $\bar{x}$ and σ^2 as well as M are used with equation (11), we obtain the "true" mean

$$a = 0.29 \text{ grains per micron}$$

and from the value of B with equation (14) we obtain

$$a = 0.26 \text{ grains per micron.}$$

The discrepancy can be explained as follows: in finding equations (11, 14) it was assumed that one could neglect the possibility of one grain overlapping the second preceding grain without overlapping the immediately preceding one. The chance of this happening compared to the chance of two succeeding grains overlapping their predecessors is less than 1 in 10—as a rough calculation using the values of m and w found below will show. The resulting theoretical mean then turns out to be too high by less than 1%. The value of a calculated from equation (11) is then too low by less than 1%. The theoretical value of the variance is however more seriously affected by the assumption. The value of a calculated from equation (14) should therefore be lower than that from equation (11).

The basic Poisson distribution is itself only an approximation since the finite size of the undeveloped grains tends to prevent the appearance of two very closely spaced developed grains. The theoretical mean and especially the variance used above are again too large. The required correction is analogous to that for a counter with a nonextended recovery time. The "recovery length" was found to be approximately 0.27 compared to the mean counted grain length 0.865 accounted for in the theory; moreover, because some grains can be vertically displaced, the effective "recovery length" is less than 0.27. The error in assuming the basic Poisson distribution is therefore probably less than 20% of the overlapping effect considered in this paper.

Altogether, then, it appears that the "true" mean number of grains per micron is between 0.29 and 0.30.

Neglecting higher order terms in equations (11, 14) appears to be justified when the cell size x is as large as used here.

With $a = 0.29$ and the observed $\bar{x}$ and σ^2 we now use equation (16) to obtain

$$m = 0.4\,\mu,\ w = 0.8\,\mu.$$

As remarked earlier, these values appear to be consistent with the observed distribution of counted grain lengths in Fig. 2. In principle the theoretical distribution of blob lengths (it is the inverse transform of equation (7), using (4, 15)) could now be found and compared with that observed.

Further refinement in the values of m and w is not justified since only 99 observations were used for Fig. 2 and the value of a is so large that more terms would be needed in equation (16). Finally, it would probably be more satisfactory to postulate a normal rather than parabolic distribution. Altogether a more refined analysis of the counted grain lengths would appear to require machine methods for the computations involved.

FURTHER CONSIDERATIONS

The narrowness of the distribution in Fig. 1 compared to Poisson's has been accounted for. There are factors which apparently lead to distributions broader than Poisson's. These include inhomogeneities in the emulsion or the developing process and variations in sensitivity of the emulsion due to changes in temperature, humidity, or time.

Fading will also broaden the distribution. If a plate is exposed over a long period of time, tracks produced at the beginning of the period may have lower grain densities than those produced at the end under otherwise similar conditions (1). Thus, in a given emulsion, not all tracks are equally prone to fading. Similar situations have been considered theoretically in connection with, for example, industrial accidents (10). The resulting distributions are broader than Poisson's.

To test grain densities for fading, 57 tracks, each containing about 500 counted grains so that each has equal weight, were chosen. The deviations of their means from the over-all mean is plotted on probability paper (Fig. 4).

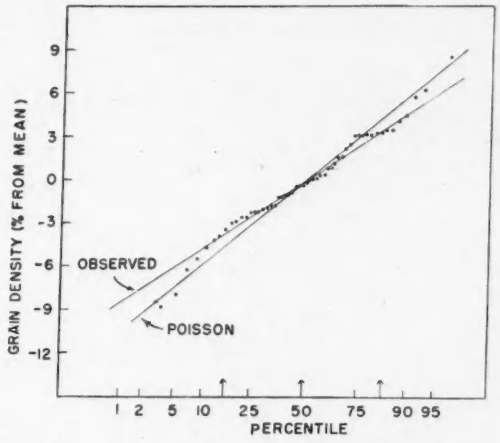

FIG. 4. The deviations from the over-all mean of the means of 57 electron tracks are plotted on probability paper. The line marked OBSERVED has $\sqrt{B/M} = 0.78$ and that marked POISSON has $\sqrt{B/M} = 1$.

(For large samples the Poisson distribution is practically normal and is therefore a straight line on such a graph.) The observed distribution is seen to lie close to the line with $\sqrt{B/M} = 0.78$, the same ratio found for Fig. 1. If there is any fading, the *individual* tracks (considered as groups of cells) will have ratios which average *less* than 0.78; the over-all ratio would be larger than the average of the individual ratios because of the broadening effect of the fading. The individual tracks were, in fact, found to have ratios ranging from 0.71 to 0.86 and averaging 0.78. We conclude that the effect of fading was negligible in these tracks.

CONCLUSIONS

The technique of counting grains in nuclear emulsions had reached a stage where further refinements in theory were needed to interpret the data. We have constructed a statistical model which accounts for the distribution of

counted grain lengths as well as the distribution of counted grains. This model is characterized by three parameters (the grain density, the minimum grain length, and the maximum variation in grain length) and values of these parameters have been found so that the theory is consistent with the experimental results. Grain size would therefore appear to dominate those factors which might be expected to mask the underlying distribution of random events.

This model might also be applied to problems such as droplet counting in a Wilson cloud chamber as well as to those mentioned earlier.

ACKNOWLEDGMENTS

We are grateful to K. Gottstein (Göttingen) and D. T. King (Washington) for assistance with some of the experimental measurements.

REFERENCES

1. ALBOUY, G. and FAREGGI, H. Fundamental mechanisms of photographic sensitivity. Butterworth Scientific Publications, London. 1951. p. 290.
2. BERRIMAN, R. W. Phot. J. Sec. B, 89: 121. 1949.
3. CECCARELLI, M. and ZORN, G. T. Phil. Mag. 43: 356. 1952.
4. ELMORE, W. C. Nucleonics, 6 (No. 1): 26. 1950.
5. FELLER, W. Courant anniversary volume. Interscience Publishers, Inc., New York. 1948.
6. FELLER, W. An introduction to probability theory and its applications. John Wiley and Sons, Inc., New York. 1950.
7. HODGSON, P. E. Phil. Mag. 41: 725. 1950.
8. HODGSON, P. E. Brit. J. Applied Phys. 3: 11. 1952.
9. JOST, R. Helv. Phys. Acta, 20: 172. 1947.
10. KENDALL, M. G. The advanced theory of statistics. Charles Griffin & Co., London. 1943. p. 124.
11. KOSTEN, L. Elek. Nachr. Tech. 14: 5. 1937.
12. KOSTEN, L. Physica, 10: 749. 1943.
13. KRONIG, R. Physica, 10: 215. 1943.
14. KURBATOV, J. D. and MANN, H. B. Phys. Rev. 68: 40. 1945.
15. LEVERT, C. and SCHEEN, W. Physica, 10: 225. 1943.
16. LOVERA, G. Ricerca Sci. 13: 677. 1942.
17. MEES, C. K. Nature, 150: 720. 1942.
18. MOLINA, E. C. Poisson's exponential binomial limit. D. Van Nostrand Company, Inc., New York. 1947.
19. MORRISH, A. H. Phil. Mag. 43: 533. 1952.
20. MOTT, N. F. and GURNEY, R. W. Electronic processes in ionic crystals. 2nd ed. Oxford at the Clarendon Press. 1948.
21. SCHIFF, L. I. Phys. Rev. 50: 88. 1936.
22. WALLER, C. Private communication.
23. WEBB, J. H. Phys. Rev. 74: 511. 1948.
24. ZHDANOV, A. J. phys. radium, 6: 233. 1935.

LETTERS TO THE EDITOR

Under this heading brief reports of important discoveries in physics may be published. These reports should not exceed 600 words and, for any issue, should be submitted not later than six weeks previous to the first day of the month of issue. No proof will be sent to the authors.

A Determination of the Multipole Character of the 637 and 722 kev. γ-ray Transitions in Xe^{131}*

Verster *et al.* (5) and more recently D. Rose *et al.* (2) have reported that the 637 kev. γ-ray transition in Xe^{131} following β decay of I^{131} (eight days) is electric dipole, $E1$, in character on the basis of its measured K conversion coefficient α_K. Because of the rare occurrence of $E1$ transitions between low-lying nuclear states this finding is of some interest. However, Bell and Graham (1), also on the basis of the measured α_K, find that the radiation is electric quadrupole, $E2$, in character. D. Rose *et al.* agree with Bell and Graham as to the $E2$ character of the 722 kev. γ-ray transition, but use Thulin's value (4) for the γ-ray intensity. This value, however, is lower than Bell and Graham's by a factor of 2.4. The results of an experiment performed to resolve these discrepancies are given here, and support the conclusions of Bell and Graham.

The method used involved the determination of the relative intensities of the 364, 637, and 722 kev. γ rays, and of their K internally converted lines. From these measurements values of α_K for the 637 and 722 kev. γ rays were obtained using the calculated value of M. E. Rose *et al.* (3) of α_K for the 364 kev. γ transition, which was taken to be $E2$ in character. There is little doubt that this assignment is correct. The γ ray and its internally converted K line are both intense and hence easily measured, and the measurements of Verster *et al.*, D. Rose *et al.*, and Bell and Graham all support this assignment.

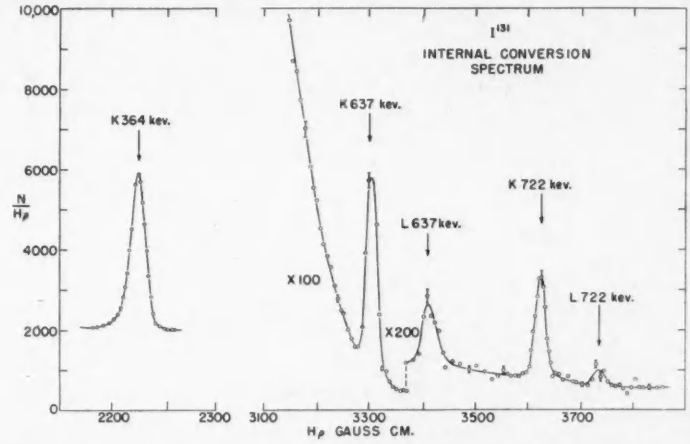

FIG. 1. Internal conversion spectrum of I^{131}. The ordinates are proportional to the counting rate per unit momentum interval. Standard deviations are represented by vertical bars on a few sample points. For the 364 K line the standard deviations are less than the radii of the circles.

Two β-ray spectrometers were used in the investigation. The internal conversion spectrum shown in Fig. 1 was obtained with one of these spectrometers adjusted for a line width of 0.63% in momentum at half maximum intensity. The source, $\sim$ 1.5 mm. in diameter, was made by precipitating 25 μc. of silver iodide from a solution of sodium iodide on to a backing of mica 2 mgm. per cm.^{2} thick. The source thickness was estimated to be about 0.3 mgm. per cm.^{2} A layer of grounded aluminum 0.2 mgm. per cm.^{2} thick covered the rear surface of the mica and prevented source charging. The second spectrometer was used to obtain the secondary electron spectrum shown in Fig. 2. A source of 2.5 mc. was used with a gold radiator 4.9 mgm. per cm.^{2} thick. Sufficient aluminum to stop all primary β rays was placed between the source and radiator. The spectrometer line width as defined above was 1.6%.

**Issued as A.E.C.L. No. 6.*

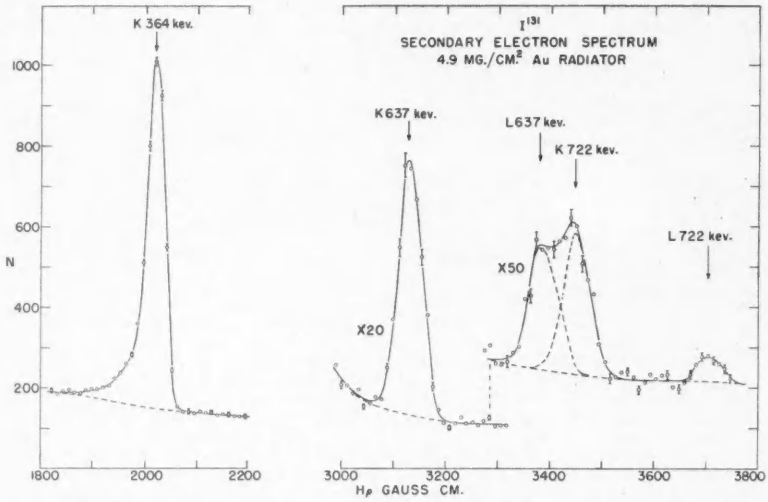

FIG. 2. Secondary electron spectrum of I^{131}. The ordinates are the observed counting rates. The relative intensities of the photoelectron lines are given by the line areas divided by their corresponding momenta. Standard deviations are represented by vertical bars on a few sample points. The dashed curve gives the shape of the Compton distribution under the lines.

The K line areas of the internal conversion spectrum give directly the relative intensities of the respective K internal conversion groups. The relative intensities of the quanta are obtained from the intensities of the corresponding photoelectron lines of the secondary electron spectrum, after correction for the variation with energy in the cross section for photoelectric absorption. As shown in Fig. 2, the 722 K line is not well resolved from the 637 $(L + M)$ lines. However, the ratio of $(L + M)$ to K line areas for a γ ray in this energy region was found to be 0.23 ± 0.01 using the same spectrometer arrangement. Since the area of the 637 K line was known, this added information enabled the areas of the 637 $(L + M)$ and 722 K lines to be obtained separately.

The results are given in Table I.

TABLE I

γ-ray energy (kev.)	Relative γ-ray intensities	Calculated values for α_K (3)			Experimental value	Multipole character
		$E1$	$E2$	$M1$		
364	1.00	—	0.019	0.024	—	$E2$ (Assumed)
637	0.102 ± 0.012	0.0015	0.0042	0.0059	0.0040 ± 0.0006	$E2$
722	0.028 ± 0.004	0.0012	0.0031	0.0044	0.0031 ± 0.0007	$E2$

It is indicated that both the 637 and 722 kev. γ rays are predominantly $E2$ in character with perhaps some admixture of $M1$. The results are however inconsistent with assignment of $E1$ character to either transition.

The author is indebted to Dr. R. E. Bell for suggesting that these measurements be made, and to A.E.C.L. Isotopes Branch for supplying the sources.

1. BELL, R. E. and GRAHAM, R. L. Phys. Rev. 86:212. 1952.
2. ROSE, D., HINMAN, G., and LANG, L. G. Phys. Rev. 86:863. 1952.
3. ROSE, M. E., GOERTZEL, G. H., and PERRY, G. L. Oak Ridge National Laboratory Report No. 1023. 1951.
4. THULIN, S. Phys. Rev. 83:860. 1951.
5. VERSTER, N. F., NIJGH, G. J., VAN LIESHOUT, R., and BAKKER, C. J. Physica 17:637. 1951.

RECEIVED SEPTEMBER 11, 1952.
J. L. WOLFSON
PHYSICS DIVISION,
ATOMIC ENERGY OF CANADA LIMITED,
CHALK RIVER, ONTARIO.

Angular Distribution of the Gamma Rays from the Reaction $N^{15}(p,\alpha\gamma)C^{12}$

The excitation function of the reaction $N^{15}(p,\alpha\gamma)C^{12}$ shows sharp resonances at proton bombarding energies of 429, 898, and 1210 kev. (3). In order to determine the spins and parities of the excited states of C^{12} and O^{16} involved in this reaction, we have measured the angular distributions of the gamma radiation from these three resonances.

Evaporated targets of potassium nitrate (enriched to 60% N^{15}) on silver backings were bombarded with protons from the University of British Columbia Van de Graaff generator. The 4.47 Mev. gamma rays were detected in a 1 in. long × 1 in. diameter sodium iodide crystal, mounted on a R.C.A. 5819 photomultiplier tube, which was rotated about the target in a plane containing the proton beam. Since the targets (approximately 30 kev. stopping power for protons) deteriorated with bombardment, it was necessary to monitor the gamma-ray intensity with a fixed sodium iodide scintillation counter. Background counting rates were measured by reversing the target and bombarding the clean silver for equal times. These background rates were less than 20% of the counting rate from the N^{15} layer. Since the yield of this reaction is small it was necessary to employ appreciable solid angles for the detector. The angle subtended at the target by the sodium iodide crystal was ± 15° for the 898 and 1210 kev. resonances, and ± 30° for the 429 kev. resonance.

The measured angular distributions, normalized to unity at $\theta = 90°$, are:

$$1 - (1.14 \pm 0.04)\cos^2\theta + (1.66 \pm 0.06)\cos^4\theta \text{ at 429 kev.,}$$
$$1 - (0.53 \pm 0.02)\cos^2\theta + (1.05 \pm 0.04)\cos^4\theta \text{ at 898 kev.,}$$
$$1 + (2.15 \pm 0.07)\cos^2\theta - (1.54 \pm 0.05)\cos^4\theta \text{ at 1210 kev.}$$

A typical run at 898 kev. is shown in Fig. 1.

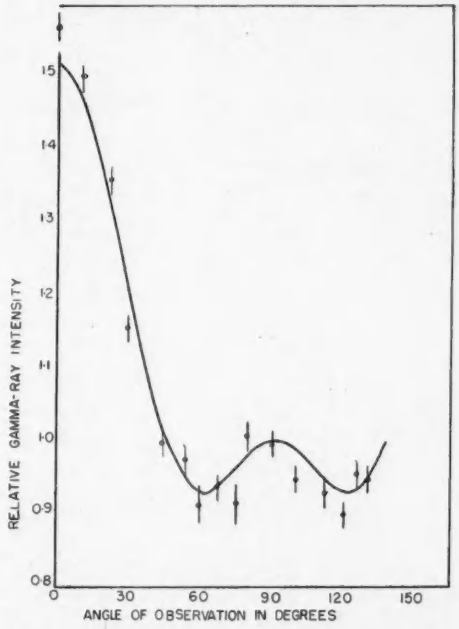

FIG. 1. The angular distribution of the gamma rays from $N^{15}(p,\alpha\gamma)C^{12}$ at 898 kev. The experimental points shown are the average values of readings taken symmetrically about 0°. The solid curve corresponds to $1 - 0.53\cos^2\theta + 1.05\cos^4\theta$.

After the effect of the finite solid angles is computed, the distributions are;

$$1 - (2.62 \pm 0.09)\cos^2\theta + (3.40 \pm 0.11)\cos^4\theta \text{ at 429 kev.,}$$
$$1 - (0.70 \pm 0.03)\cos^2\theta + (1.29 \pm 0.05)\cos^4\theta \text{ at 898 kev.,}$$
$$1 + (2.45 \pm 0.08)\cos^2\theta - (1.87 \pm 0.06)\cos^4\theta \text{ at 1210 kev.}$$

Assuming (2)that N^{15} has spin 1/2 and odd parity, and that the ground state of C^{12} and the alpha particle have zero spin and even parity, the assignments of spin and parity, shown in Table I, are consistent with the observed distributions.

TABLE I

Resonance energy, kev.	Total spin and parity of $N^{15}+p$	Orbital angular momentum of proton capture	Spin and parity of O^{16} state	Orbital angular momentum of α-emission
(*a*) 429	0, odd, and 1, odd	2	2, odd	1 only
(*b*) 429	0, odd, only	2	2, odd	1 and 3
(*c*) 898	0, odd, and 1, odd	2	2, odd	1 only
(*d*) 1210	1, odd, only	2	3, odd	1 and 3
(*e*) 1210	1, odd, only	3	4, even	2 only

In each case the excited state in carbon has spin 2, and even parity, and the gamma-ray transition is electric quadrupole.

It is possible that the distribution at the 1210 kev. resonance might be fitted with still higher angular momentum for the O^{16*} state. We are investigating the angular distribution of the competing long range alpha particle transition to the C^{12} ground state at 1210 kev., to eliminate uncertainty in the O^{16*} spin assignment.

These assignments are in agreement with similar work at the Cavendish Laboratory and at California Institute of Technology (1).

The absolute cross sections quoted by Schardt *et al.* (3) should be corrected for these angular distributions.

We are indebted to the National Research Council of Canada for support during the course of this research.

1. French, A. P. Private communication.
2. Hornyak, W. F., Lauritsen, T., Morrison, P., and Fowler, W. A. Revs. Modern Phys. 22: 291. 1950.
3. Schardt, A. W., Fowler, W. A., and Lauritsen, C. C. Phys. Rev. 86: 527. 1952.

Received September 29, 1952.
University of British Columbia,
Vancouver, B.C.

C. A. Barnes
D. B. James
G. C. Neilson

CONTENTS OF VOLUME 30

ATOMIC ENERGY OF CANADA LTD. TECHNICAL RELEASE—Nuclear constants for reactor studies, 624.
BARNES, C. A., JAMES, D. B., and NEILSON, G. C.—Angular distribution of the gamma rays from the reaction $N^{15}(p, \alpha\gamma)C^{12}$, 717 (L).
BELL, R. E.—See Graham, R. L.
BELL, R. E., GRAHAM, R. L., and PETCH, H. E.—Design and use of a coincidence circuit of short resolving time, 35.
BETTS, D. D.—See MacDonald, A. D.
BRECKON, S. W.—See Martin, W. M.
BUCKMASTER, H. A.—Radial matrix element for the quadrupole transition with the Morse potential, 314.
CAMERON, A. G. W.—See Haslam, R. N. H.
CARMICHAEL, H.—Design and performance of a fused silica microbalance, 524.
CHALMERS, B.—See Teghtsoonian, E.; Weinberg, F.; Winegard, W.C.
COLLADAY, G. S.—See Falkoff, D. L.
COOKE, J. A.—See Haslam, R. N. H.
CORMACK, D. V.—See Johns, H. E.
CRAWFORD, M. F.—See Welsh, H. L.
CRAWFORD, M. F., WELSH, H. L., and HARROLD, J. H.—Rotational wings of Raman bands and free rotation in liquid oxygen, nitrogen, and methane, 81.
CROSBY, E. H.—See Haslam, R. N. H.
DAYKIN, P. N.—An analysis of the self-energy problem for the electron in quantum electrodynamics, 70.
DE GRANDPRÉ, J-L.—See Demers, P.
DEKKER, A. J.—See Lipsett, F. R.
DEMERS, P. ET DE GRANDPRÉ, J-L.—Ballons de matière plastique fabriqués par un nouveau procédé, 235.
DENESUK, S. A.—See Johns, H. E.
DIXON, W. R. and WHYTE, G. N.—Search for anomalous absorption of Ra(B + C) γ rays, 438.
DOUGLAS, A. E.—The near ultraviolet bands of N_2^+ and the dissociation energies of the N_2^+ and N_2 molecules, 302.
DUCKWORTH, H. E.—See Hogg, B. G.
DUNN, A. F.—See Romanowski, M.
DYNE, P. J.—A new band system excited in acetylene, 79.
FALKOFF, D. L., COLLADAY, G. S., and SELLS, R. E.—Transformation amplitudes for vector addition of angular momentum; $(j3mm' \mid j3JM)$, 253.
GRAHAM, R. L.—See Bell, R. E.
GRAHAM, R. L., WOLFSON, J. L., and BELL, R. E.—The disintegration of Tm^{170}, 459.
GRAYSON-SMITH, H. and STURROCK, R. F.—Dielectric behavior at the second-order transitions in chromium sulphate, chromium nitrate, and nickel nitrate, 26.
GREENBERG, L. H. and HAPP, W. W.—Design and operation of a 'mean deviation meter',317.
GRUENBERG, H.—Symmetrically placed inductive posts in rectangular wave guide, 211.
GUPTILL, E. W. and MACDONALD, A. D.—The acoustical field near a circular transducer, 119.
HAPP, W. W.—See Greenberg, L. H.; Keeping, E. S.
HAPP, W. W., HULL, T. E., and MORRISH, A. H.—A statistical analysis of grain counting in photographic emulsions, 699.
HARROLD, J. H.—See Crawford, M. F.
HASLAM, R. N. H.—See Horsley, R. J.
HASLAM, R. N. H., CAMERON, A. G. W., COOKE, J. A., and CROSBY, E. H.—Alpha particles from the photodisintegration of silver and bromine, 349.
HASLAM, R. N. H., SUMMERS-GILL, R. G., and CROSBY, E. H.—The measurement of photonuclear cross sections in isotopes leading to short-lived decay products, 257.
HENRY, W. G. and RAYNOR, G. V.—Superlattice studies in the systems silver–magnesium–tin and silver–magnesium–zinc, 412.
HERZBERG, G.—Forbidden transitions in diatomic molecules. II. The $^3\Sigma_u^+ \leftarrow {}^3\Sigma_g^-$ absorption bands of the oxygen molecule, 185.
HESS, F. G.—Some directional correlation functions for successive nuclear radiations, 130.
HINES, C. O.—Electromagnetic energy density and flux, 123.
HOGG, B. G. and DUCKWORTH, H. E.—Some atomic masses for tellurium, 628 (L). A mass spectrographic determination of the decay energies of Rh^{102} and Rh^{104}, 637.
HORSLEY, R. J., HASLAM, R. N. H., and JOHNS, H. E.—Gamma–neutron reactions in O^{16} and N^{14}, 159.

HULL, T. E.—See Happ, W. W.
JAMES, D. B.—See Barnes, C. A.
JOHNS, H. E.—See Horsley, R. J.
JOHNS, H. E., CORMACK, D. V., DENESUK, S. A., and WHITMORE, G. F.—Initial distribution of Compton electrons, 556.
KATZ, L., PEASE, L., and MOODY, H.—The photoneutron cross sections for the reactions $Br^{81}(\gamma,n)Br^{80}$ and $Br^{81}(\gamma,n)Br^{80*}$ and an analysis of the ratio between these cross sections, 476.
KATZMAN, J.—See Rose, D.C.
KEEPING, E. S. and HAPP, W. W.—Statistics of the mean deviation meter, 329.
KERWIN, L.—Note on the resolving power of mass spectrometers, 503.
KUSHNERIUK, S. A.—Efficiency of the long boron counter for fast neutrons, 402.
LAIRD, E. R.—Dielectric properties of some solid proteins at wave lengths 1.7 meters and 3.2 centimeters, 663.
LEVY, M.—Sur quelques problèmes posés par les méthodes d'analyse des graphiques par le calcul, 147.
LIPSETT, F. R. and DEKKER, A. J.—Fluorescent spectra of some organic solid solutions, 165.
LOVE, G. R.—See Welsh, H. L.
MCDIARMID, I. B.—The energy spectrum of the X rays from a 70-Mev. synchrotron, 670.
MACDONALD, A. D.—See Guptill, E. W.
MACDONALD, A. D. and BETTS, D. D.—High frequency gas discharge breakdown in neon, 565.
MCKAY, C. D.—See Scheidegger, A. E.
MCLAUCHLAN, T. A.—See Sennett, R. S.
MARTIN, W. M. and BRECKON, S. W.—The new radioactive isotopes vanadium 46, manganese 50, cobalt 54, 643.
MEI, J. Y.—Size distribution of cosmic ray stars in photographic emulsions, 453.
MEI, J. Y. and PICKUP, E.—Slow π-mesons in cosmic-ray stars and the negative–positive π-meson ratio, 430.
MONTALBETTI, R.—Nomogram of lifetime–energy–spin for gamma-ray transitions, 660.
MOODY, H.—See Katz, L.
MORRISH, A. H.—See Happ, W. W.
NEAMTAN, S. M. and VOGT, E.—Boundary conditions in the mechanics of fields, 684.
NEILSON, G. C.—See Barnes, C. A.
NEWTON, T. D.—The collision matrix for the compound nucleus, 53.
OSBORNE, F. J. FITZ.—A simple activation for BeCu multipliers, 658.
PAGHIS, I.—Surface losses in electromagnetic cavity resonators, 174.
PASHLER, P. E.—See Welsh, H. L.
PEASE, L.—See Katz, L.
PETCH, H. E.—See Bell, R. E.; Volkoff, G. M.
PICKUP, E.—See Mei, J. Y.
POPE, N. K.—The theory of neutron diffraction by gases. I, 597.
PRESTON-THOMAS, H.—The superconductive transition in lead, 626 (L).
RAYNOR, G. V.—See Henry, W. G.
REDHEAD, P. A.—A linear radio-frequency mass spectrometer, 1.
ROMANOWSKI, M.—Modified bridge method for absolute determination of ohm, 631.
ROMANOWSKI, M. and DUNN, A. F.—A note on the sensitivity of electrical bridge networks, 342.
ROSE, D. C. and KATZMAN, J.—Radioactive deposits found at Ottawa after the atomic explosions of January and February 1951, 111.
ROSE, D. C. and VOISIN, A. G.—The low energy spectrum of cosmic-ray mesons at sea level at high geomagnetic latitudes, 373.
SCHEIDEGGER, A. E.—Physical aspects of the contraction hypothesis of orogenesis, 14.
SCHEIDEGGER, A. E. and MCKAY, C. D.—On the thermodynamics of wave fields, 117.
SCOTT, G. D.—See Sennett, R. S.
SELLS, R. E.—See Falkoff, D. E.
SENNETT, R. S., MCLAUCHLAN, T. A., and SCOTT, G. D.—Electron microscope studies of evaporated cadmium and zinc, 370.
SHANMUGADHASAN, S.—The dynamical theory of magnetic monopoles, 218. Spinors in the dynamical theory of spinning particles, 226.
SMELLIE, D. W. L.—See Volkoff, G. M.
STOICHEFF, B. P.—See Welsh, H. L.
STURROCK, R. F.—See Grayson-Smith, H.
SUMMERS-GILL, R. G.—See Haslam, R. N. H.
TEGHTSOONIAN, E. and CHALMERS, B.—Further observations on the macromosaic structure of tin single crystals, 388.
THOMAS, T. R.—See Welsh, H. L.
VOGT, E.—See Neamtan, S. M.
VOISIN, A. G.—See Rose, D. C.

VOLKOFF, G. M., PETCH, H. E., and SMELLIE, D. W. L.—Nuclear electric quadrupole interaction in single crystals, 270.
WAIT, J. R.—Mutual inductance of circuits on a two layer earth, 450. Electromagnetic fields of current-carrying wires in a conducting medium, 512.
WEINBERG, F. and CHALMERS, B.—Further observations on dendritic growth in metals, 488.
WELSH, H. L.—See Crawford, M. F.
WELSH, H. L., CRAWFORD, M. F., THOMAS, T. R., and LOVE, G. R.—Raman spectroscopy of low pressure gases and vapors, 577.
WELSH, H. L., PASHLER, P. E., and STOICHEFF, B. P.—Density effects in the Raman spectrum of carbon dioxide, 99.
WHITMORE, G. F.—See Johns, H. E.
WHYTE, G. N.—On the γ-ray spectrum of Ra(B + C), 442. See Dixon, W. R.
WINEGARD, W. C. and CHALMERS, B.—Self-diffusion at silver surfaces, 422.
WOLFSON, J. L.—A determination of the multipole character of the 637 and 722 kev. γ-ray transitions in Xe^{131}, 715 (L). See Graham, R. L.
WU, TA-YOU.—The intensities of harmonic bands of the HD molecule, 291.

ADDITIONS AND CORRECTIONS

Vol. 29, pp. 470-479. 1951. The author of this paper has submitted the following changes:

"(1) On p. 473, at the end of the second line after equation (22), for $J^5cF_{45}/i \equiv cq$, write J^5cF_{45}/i; i.e., omit $\equiv cq$.

(2) Prior to p. 475, for ξ write ξ^1. Otherwise write ξ which, of course, is the physically significant parameter.

(3) On p. 475, to the line containing equation (42) add $(\tilde{\delta}^4 \equiv iq)$, $(\xi \equiv -i\xi')$.

None of the conclusions of the paper are affected by these changes in the symbolism."

Vol. 30, p. 1. In the **Abstract**, Line 2, "tin ions" should read "the ions".

CANADIAN JOURNAL OF PHYSICS

Notice to Contributors

GENERAL: Manuscripts should be typewritten, double spaced, and the **original and one extra copy** submitted. Style, arrangement, spelling, and abbreviations should conform to the usage of this Journal. Names of all simple compounds, rather than their formulas, should be used in the text. Greek letters or unusual signs should be written plainly or explained by marginal notes. Superscripts and subscripts must be legible and carefully placed. Manuscripts should be carefully checked before being submitted, to reduce the need for changes after the type has been set. If authors require changes to be made after the type is set, they will be charged for changes that are considered to be excessive. **All pages, whether text, figures, or tables, should be numbered.**

ABSTRACT: **An abstract of not more than about 200 words, indicating the scope of the work and the principal findings, is required.**

ILLUSTRATIONS:

(i) *Line Drawings:* All lines should be of sufficient thickness to reproduce well. Drawings should be carefully made with India ink on white drawing paper, blue tracing linen, or co-ordinate paper **ruled in blue only**; any co-ordinate lines that are to appear in the reproduction should be ruled in black ink. Paper ruled in **green, yellow, or red should not be used** unless it is desired to have all the co-ordinate lines show. Lettering and numerals should be neatly done in India ink preferably with a stencil (**do not use typewriting**) and be of such size that they will be legible and not less than one millimeter in height when reproduced in a cut three inches wide. All experimental points should be carefully drawn with instruments. Illustrations need not be more than two or three times the size of the desired reproduction, but the ratio of height to width should conform with that of the type page. **The original drawings and one set of small but clear photographic copies are to be submitted.**

(ii) *Photographs:* Prints should be made on glossy paper, with strong contrasts; they should be trimmed to remove all extraneous material so that essential features only are shown. Photographs should be submitted **in duplicate**; if they are to be reproduced in groups, one set should be so arranged and mounted on cardboard with rubber cement; the duplicate set should be unmounted.

(iii) *General:* **The author's name, title of paper, and figure number should be written in the lower left hand corner (outside the illustration proper) of the sheets on which the illustrations appear.** Captions should not be written on the illustrations, but typed together at the end of the manuscript. All figures (including each figure of the plates) should be numbered consecutively from 1 up (arabic numerals). **Each figure should be referred to in the text.** If authors desire to alter a cut, they will be charged for the new cut.

TABLES: Each table should be typed on a separate sheet. Titles should be given for all tables, which should be numbered in Roman numerals. Column heads should be brief and textual matter in tables confined to a minimum. **Each table should be referred to in the text.**

REFERENCES: **These should be listed alphabetically by authors' names, numbered in that order, and placed at the end of the paper.** The form of literature citation should be that used in this Journal. **Titles of papers should not be given.** The first page only of the references cited should be given. **All citations should be checked with the original articles.** Each citation should be referred to in the text by means of the key number.

REPRINTS: A total of 50 reprints of each paper, without covers, are supplied free to the authors. Additional reprints will be supplied according to a prescribed schedule of charges. On request, covers can be supplied at cost.

Approximate charges for reprints may be calculated from the number of printed pages, obtained by multiplying by 0.6 the number of manuscript pages (double-spaced typewritten sheets, 8½ in. by 11 in.) and making allowance for space occupied by line drawings and half-tones (not inserts). The cost per page is tabulated at the back of the reprint request form sent with the galley.

Contents

Page

Modified Bridge Method for Absolute Determination of Ohm—*M. Romanowski* - - - - - - - - - - - - - - - - - - - 631

A Mass Spectrographic Determination of the Decay Energies of Rh^{102} and Rh^{104}—*Benjamin G. Hogg and Henry E. Duckworth* - - 637

The New Radioactive Isotopes Vanadium 46, Manganese 50, Cobalt 54—*W. M. Martin and S. W. Breckon* - - - - - - - - - - 643

A Simple Activation for BeCu Multipliers—*F. J. Fitz Osborne* - - 658

Nomogram of Lifetime–Energy–Spin for Gamma-ray Transitions—*R. Montalbetti* - - - - - - - - - - - - - - - - - - - 660

Dielectric Properties of Some Solid Proteins at Wave Lengths 1.7 Meters and 3.2 Centimeters—*Elizabeth R. Laird* - - - - - 663

The Energy Spectrum of the X Rays from a 70-Mev. Synchrotron—*I. B. McDiarmid* - - - - - - - - - - - - - - - - - - 670

Boundary Conditions in the Mechanics of Fields—*S. M. Neamtan and E. Vogt* - 684

A Statistical Analysis of Grain Counting in Photographic Emulsions —*W. W. Happ, T. E. Hull, and A. H. Morrish* - - - - - - - 699

Letters to the Editor:

A Determination of the Multipole Character of the 637 and 722 Kev. γ-Ray Transitions in Xe^{131}—*J. L. Wolfson* - - - - 715

Angular Distribution of the Gamma Rays from the Reaction $N^{15}(p,\alpha\gamma)C^{12}$—*C. A. Barnes, D. B. James, and G. C. Neilson* 717

Contents of Volume 30 - - - - - - - - - - - - - - - - - - 719

Printed in Canada *by* University of Toronto Press